REPORT DOCUMENTATION PAGE

Form Approved
OMB No. 0704-0188

Public reporting burden for this collection of information is estimated to average 1 hour per response, including the time for reviewing instructions, searching existing data sources, gathering and maintaining the data needed, and completing and reviewing this collection of information. Send comments regarding this burden estimate or any other aspect of this collection of information, including suggestions for reducing this burden to Department of Defense, Washington Headquarters Services, Directorate for Information Operations and Reports (0704-0188), 1215 Jefferson Davis Highway, Suite 1204, Arlington, VA 22202-4302. Respondents should be aware that notwithstanding any other provision of law, no person shall be subject to any penalty for failing to comply with a collection of information if it does not display a currently valid OMB control number. **PLEASE DO NOT RETURN YOUR FORM TO THE ABOVE ADDRESS.**

1. REPORT DATE *(DD-MM-YYYY)* 12 January 2017	2. REPORT TYPE Conference Paper with Briefing Charts	3. DATES COVERED *(From - To)* 17 November 2016 – 12 January 2017

4. TITLE AND SUBTITLE	5a. CONTRACT NUMBER
2D and 3D Modeling Efforts in Fuel Film Cooling of Liquid Rocket Engines (Conference Paper with Briefing Charts)	
	5b. GRANT NUMBER
	5c. PROGRAM ELEMENT NUMBER
6. AUTHOR(S) Kevin C. Brown, Edward B. Coy, Venkateswaran Sankaran	5d. PROJECT NUMBER
	5e. TASK NUMBER
	5f. WORK UNIT NUMBER Q0VZ

7. PERFORMING ORGANIZATION NAME(S) AND ADDRESS(ES) AND ADDRESS(ES)	8. PERFORMING ORGANIZATION REPORT NO.
Air Force Research Laboratory (AFMC) AFRL/RQRC 10 E. Saturn Blvd. Edwards AFB, CA 93524-7680	

9. SPONSORING / MONITORING AGENCY NAME(S) AND ADDRESS(ES)	10. SPONSOR/MONITOR'S ACRONYM(S)
Air Force Research Laboratory (AFMC) AFRL/RQR 5 Pollux Drive Edwards AFB, CA 93524-7048	
	11. SPONSOR/MONITOR'S REPORT NUMBER(S) AFRL-RQ-ED-TP-2016-359

12. DISTRIBUTION / AVAILABILITY STATEMENT

Approved for Public Release; Distribution Unlimited. PA Clearance Number: 16569 Clearance Date: 12/02/2016 The U.S. Government is joint author of the work and has the right to use, modify, reproduce, release, perform, display, or disclose the work.

13. SUPPLEMENTARY NOTES

For presentation at 2017 AIAA SciTech conference; Grapevine, TX; January 12, 2017 Conference Paper with Briefing Charts

14. ABSTRACT

Two- and three-dimensional simulations of slot injection of fuel film cooling have been carried out using an unsteady detached eddy simulation (DES) turbulence model at operating conditions relevant to liquid rocket engine (LRE) thrust chambers. The aim of this study is to determine what parameters drive unsteadiness in fuel films, and how these parameters affect wall temperature profiles. Parametric studies performed in 2D suggest that a Helmholtz resonator exists for simple slot geometries. Frequencies in 3D were observed to be of a lower frequency, with a rich mix of modes driving unsteadiness. Changing the shape of the inlet had a strong impact on both unsteadiness and wall temperature profile. These simulations do not capture trends seen in experimental results, but do provide insight into the complex nature of fuel film cooling.

15. SUBJECT TERMS
N/A

16. SECURITY CLASSIFICATION OF:			17. LIMITATION OF ABSTRACT	18. NUMBER OF PAGES	19a. NAME OF RESPONSIBLE PERSON E. Coy
a. REPORT Unclassified	b. ABSTRACT Unclassified	c. THIS PAGE Unclassified	SAR	77	19b. TELEPHONE NO *(include area code)* N/A

Standard Form 298 (Rev. 8-98)
Prescribed by ANSI Std. 239.18

2D and 3D Modeling Efforts in Fuel Film Cooling of Liquid Rocket Engines

Kevin C. Brown,[*] Edward B. Coy,[†] and Venkateswaran Sankaran[‡]

Air Force Research Laboratory, Edwards AFB, CA 93524

Two- and three-dimensional simulations of slot injection of fuel film cooling have been carried out using an unsteady detached eddy simulation (DES) turbulence model at operating conditions relevant to liquid rocket engine (LRE) thrust chambers. The aim of this study is to determine what parameters drive unsteadiness in fuel films, and how these parameters affect wall temperature profiles. Parametric studies performed in 2D suggest that a Helmholtz resonator exists for simple slot geometries. Frequencies in 3D were observed to be of a lower frequency, with a rich mix of modes driving unsteadiness. Changing the shape of the inlet had a strong impact on both unsteadiness and wall temperature profile. These simulations do not capture trends seen in experimental results, but do provide insight into the complex nature of fuel film cooling.

I.   Introduction

Advanced hydrocarbon boost engines with an oxygen-rich staged-combustion (ORSC) cycle require fuel film cooling (FFC) of the thrust chamber in order to maintain wall temperatures within design limits. However, film coolant flow must also be minimized or the specific impulse will be negatively impacted. Fuel films may be introduced in the subsonic section of the chamber upstream of the nozzle throat through circumferential slots. Figure 1 shows some of the features of the flow field for a simple FFC inlet geometry. With small amounts of fuel coolant being added relative to the flow rate of the hot chamber gases, this geometry resembles flow over a cavity, a case that has been studied and modeled extensively.[1][2] Previous work has shown that flow over rectangular cavities can have complex instabilities driven by vortex shedding, Kelvin-Helmholtz instabilities and acoustic resonance.[3] Such instabilities have been shown[2][3] to have a large impact on the cooling effectiveness of a fuel film, as these instabilities may expose the chamber walls to higher temperatures than would steady flows wherein the film remains attached to the wall.

Thus, it is important to capture these physical effects to better characterize the effectiveness of a given fuel film cooling (FFC) geometry. This paper covers recent modeling efforts to extend the computational fluid dynamics (CFD) model to include unsteady dynamics of the film and investigate the effects of density, mass flow ratio, momentum flux ratio (J), and other factors on the adiabatic wall temperature of the fuel film. The effect of various inlet shapes is also discussed, as well as the effects of 3D simulation on predicted wall temperatures.

Fuel film cooling flows in ORSC engines are characterized by large density gradients, complex chemistry, supercritical fluid behavior, thermal radiation, and the formation of soot and carbonaceous wall deposits.[5] Experiments performed in the laboratory have shown that the reductions in heat flux that can be achieved with FFC depend primarily on the conditions of the gas flow.[5] Specifically, the variables found to be most significant are the heat flux driving potential of the flow as measured on an uncooled wall, and the momentum flux of the flow. Other significant variables are the distance downstream of the injection slot and the time elapsed since the start of the run. In addition, the geometry of the injector slot, the mixture ratio and the mixture ratio biasing are found to have a minor effect on film cooling effectiveness. In general, the heat flux exhibits complex trends and did not scale well with chamber pressure.

---

[*]Aerospace Engineer, Combustion Devices Branch.
[†]Mechanical Engineer, Combustion Devices Branch.
[‡]Senior Scientist, Aerospace Systems Directorate.
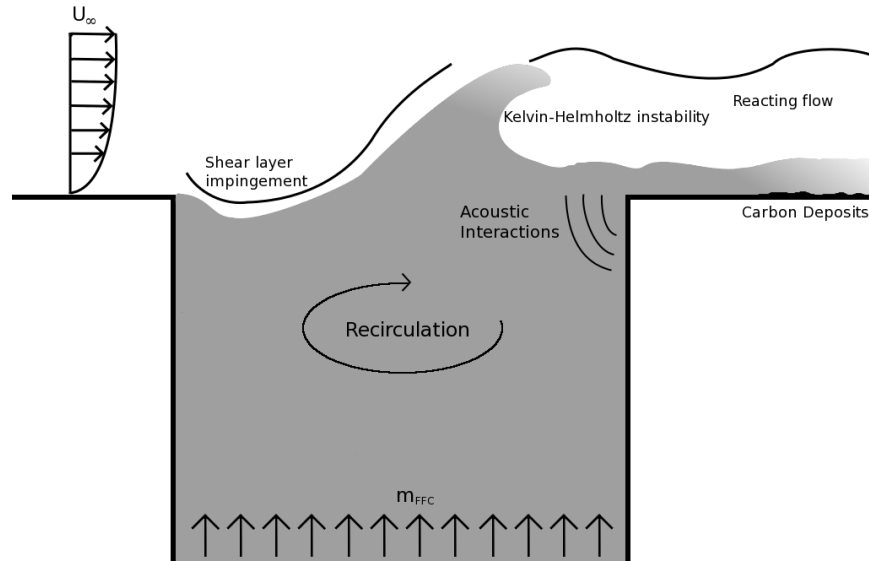
Figure 1. Film cooling with a liquid hydrocarbon fuel.

There have been several attempts to model film cooling flow under liquid rocket engine (LRE) conditions. A common method has been to develop a model that predicts the intact length of the liquid film. This approach assumes that the wall must be shielded from the hot gas by an intact liquid film, and when the film has been consumed another injection slot is needed. This has been implemented using experimental correlations,[67] and a steady state Reynolds-Averaged Navier Stokes (RANS) code.[8] This method assumes that the liquid film is in a subcritical thermodynamic state and possesses surface tension and a heat of vaporization. These assumptions are not valid for the operating conditions of ORSC engines.

Himansu et al.[4] reported on an FFC simulation using a 2D steady state Reynolds-Averaged Navier Stokes (RANS) code that approximated the fuel film coolant issued from a slot as a dense, high molecular weight ideal gas. Chemical reactions were modeled using an equilibrium mixture fraction approach and heat transfer was handled using a conjugate conduction model. The heat flux predictions were compared with the results of experiment and it was found that the steady state RANS model over-predicted film cooling effectiveness immediately downstream of the inlet slot and under-predicted heat flux further downstream. The model also did not predict the insensitivity to film coolant flow rate that had been observed in the experiments.[5] Recent work by Brown et al.[23] has shown that unsteady simulations offer improved predictions of film cooling effectiveness compared to steady state RANS, although unsteadiness does not fully account for the discrepancies between experimental results and simulations.

One focus of recent research has been to determine the significance of unsteadiness in the film coolant flow as a possible cause of disagreement. It is hypothesized that momentary periods of low flow in the film coolant are associated with increased heat transfer, while high flow is associated with effective but inefficient cooling, which leads to reduced effectiveness of the cooling further downstream. Consider a hot chamber wall protected by a constant fuel film of mass flow rate $\dot{m}$. Experiments have shown that doubling the mass flow rate to $2\dot{m}$ will not have a large effect on wall temperature, but removing this fuel film entirely will raise the temperatures to that of an uncooled wall. If instead we allow the mass flow rate of the fuel film to vary from 0 to $2\dot{m}$ with an average value of $\dot{m}$, the wall temperature should be close to the average of the two extremes. In a liquid rocket engine with chamber temperatures in the thousands of degrees and a low FFC mass flow rate, this can produce a result far removed from that of a steady state simulation. Unsteadiness in fuel film cooling has been examined before by Rutledge,[9] who found that a coolant film with a pulsed mass flow rate resulted in a decreased net heat flux reduction versus a case with constant mass flow rate.

The computations in this paper focus on several parametric studies which seek to determine the effect of unsteadiness in the flow field on film cooling effectiveness. The first parametric study varies the momentum ratio of the fuel film with respect to the main chamber by changing one or both of the mass flow rates for

the main chamber and the fuel film. A second parametric study focuses on the effects of density ratio on the unsteadiness of the flow field. This is accomplished by changing the molecular weight of the film coolant and modifying the slot width such that the mass flow and momentum of both the main chamber and the coolant remains the same for all cases. Additional cases are run at the highest and lowest molecular weight cases of this parametric study to ensure that the observed patterns of the first parametric study are not density-dependent. A third parametric study is run to determine if varying the width of the FFC slot has an impact on flow stability, with the mass flow ratio and density ratio being held constant. In addition to determining the effects on cooling effectiveness, the parametric studies also serve to provide a better understanding of the physics driving the unsteadiness in a fuel-film cooled configuration. This understanding in turn sheds light on the observed frequencies and amplitudes of the unsteady simulations.

Two additional parametric studies are discussed in this paper, which build on the results of earlier studies to address additional variables. One study uses a range of different inlet geometries to better understand how unsteadiness develops in FFC inlets, with several inlets modeled from existing experimental setups. The other study is focused on three-dimensional effects, and how the presence of sidewalls may impact the wall temperature profiles and unsteadiness observed in two-dimensional simulations. Due to the increased computational cost of more complex geometries, these studies are not as expansive as the first few parametric studies. However, they do provide insight into some elements of fuel film cooling that the simpler geometry could not address.

This research expands on previous work in the field by adding a few new features to simulations of FFC LREs. Unlike previous work done in-house on thermal management systems, these studies are entirely performed using unsteady, time-accurate simulations. Previous work[23] has shown that unsteadiness can have a significant impact on predictions of film cooling effectiveness, so time-accurate solutions are prioritized rather than steady state solutions. In addition, a more detailed turbulence model is found in Detached Eddy Simulations (DES), which has been incorporated into all cases. This allows for more of the turbulent structures in the flow field to be captured, producing a more accurate result. Finally, the molecular weight of the fuel can be varied. The ideal gas law, which is used in both this study and previous work in-house, under-predicts density for the fuel film by a factor of three. This results in a flow field that does not capture the same density gradients as has been observed experimentally. By modifying the molecular weight, one can capture the correct density ratio without the additional complications of a real gas equation of state.

Several additional factors were not considered for this study. One potentially important factor is a soot deposition model. Experimental results show a much higher film cooling effectiveness in the region far downstream of the slot than simulations, where a layer of soot had been observed on the walls post-experiment. This soot could be acting as a thermal barrier coating, insulating the wall as the fuel film begins to dissipate. Another important physical factor could be radiative heat transfer, which is not currently modeled. Experimental results have shown that there is a higher heat flux immediately downstream of the FFC inlet than are observed in simulations, perhaps due to the lack of a developed soot barrier and a fuel film with high transmissivity. Since the code used in these simulations cannot handle radiative heat transfer, it is currently not being investigated.

As these features are vital for a truly predictive FFC simulation, the goal of these studies was not to reproduce experimental results, but rather to determine within the bounds of fluid dynamics how this system responds to various parameters. By varying mass flow rates, fuel density, inlet geometry and the number of dimensions of the problem, a better understanding of the driving phenomena can be obtained.

II.   Numerical Models

The simulations in this study are run using the general equation and mesh solver or GEMS, a finite volume CFD code developed by Purdue University.[10][11][12] GEMS couples equations for species with the Navier-Stokes equations and the energy equation, and is second-order accurate in time and space. Implicit dual time-stepping is used to allow higher aspect ratio cells near the wall.[13]

The ideal gas law is used to model combustion products and the film coolant. The simplification of using an ideal gas equation of state (EOS) makes for more stable calculations, at the cost of accuracy with regards to some fluid properties. Turbulence is computed using the k-ω model.[14] For each case the flow field is first initialized using a steady state Reynolds-Averaged Navier-Stokes (RANS) approach. The main, unsteady simulations use a DES approach, which approximates Large Eddy Simulations (LES) in the core flow and RANS near the walls[15].[16]

The two-reaction, five-species global chemical kinetics model developed by Westbrook and Dryer[17] is used in all tested cases. The free stream gas is assumed to be composed of the combustion byproducts downstream of the injector, with a mixture of gaseous oxygen, carbon dioxide, carbon monoxide and water vapor. The liquid fuel coolant is modeled as dodecene ($C_{12}H_{24}$), as a simplification of RP-2 for simulation purposes.

In the interest of performing large parametric studies, conjugate heat transfer is not used in the simulations in this paper. While heat transfer to the wall is an important feature in LREs, in a convection heat transfer calculation involving film cooling, the adiabatic wall temperature replaces the freestream temperature as the thermodynamic driving potential.[24] Neglecting conjugate heat transfer allows for a greater number of cases to be run using the same computational resources. Conjugate heat transfer will be an important inclusion in future higher-fidelity simulations of FFC systems.

III. Validation Cases

In the course of these modeling efforts, several parametric different studies are completed. The overarching goal of these efforts is to characterize the flow field of a fuel film cooling system into a combustion chamber, and attempt to determine which factors drive film cooling effectiveness. Previous steady state RANS models of FFC LREs have shown a perfectly monotonic heat flux profile downstream, with almost no heat flux immediately downstream of the FFC inlet and an asymptotic approach to the heat flux of an unshielded wall as one looks further downstream. Experimentally a more complex result has been observed: heat flux to a cool wall increases slightly immediately downstream of a FFC inlet, with the decreased heat flux one would expect in this setup having a delayed start and persisting further downstream than the steady state RANS models.

Three separate parametric studies are first completed using a slightly modified geometry and flow conditions from Himansu et al.,[4] shown in Figure 3. Additionally, several flow variables are recorded as a function of time near the FFC inlet. This data is used to characterize the behavior of the flow field, in particular oscillations in density and temperature. This case is useful in that there is experimental data on this particular setup which can be compared with these results.[5]
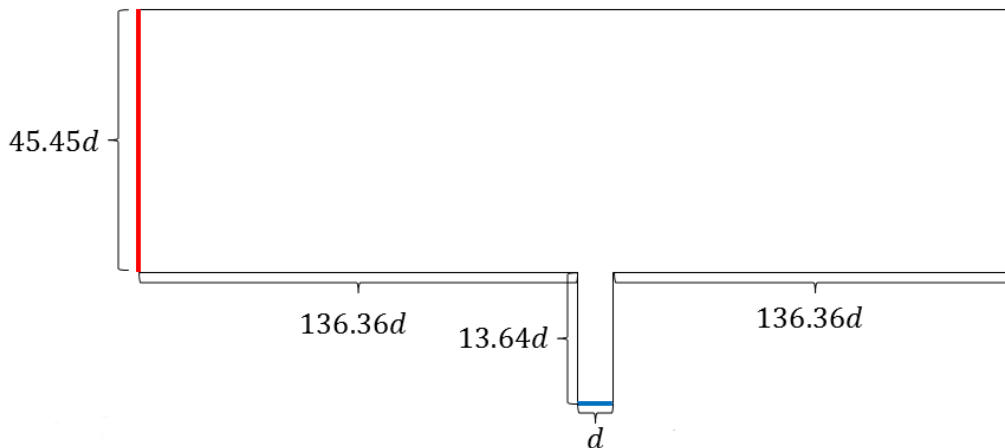
Figure 2. Domain of first validation case. Red specifies main chamber inlet, blue specifies FFC inlet, and green specifies outlet.

Initial and boundary conditions are specified to match experimental data. The baseline case has a FFC mass flow rate that is 1.6% of the main chamber mass flow rate. The hot gas in the main chamber has a Reynolds number on the order of 10^5, while the fuel coolant has a Reynolds number on the order of 10^4. Table 1 shows the flow conditions for the baseline case. From this focal point, a few parameters are varied to determine their impact on the effectiveness of the film cooling. Initial parameters of interest are mass flow ratio, momentum ratio, fuel density, and the width of the FFC inlet. It was determined that by performing three parametric studies, these variables can be isolated and studied in more detail.

In the first parametric study, all walls are set to adiabatic boundary conditions and the mass flow rates of the FFC inlet and main chamber are varied. By varying the mass flow ratio of either the fuel film, the hot

Table 1. Flow conditions for baseline case.

Pressure (MPa)	5.2	Slot width (m)	5.6×10^{-4}
FFC temperature (K)	350	Main chamber temperature (K)	3680
FFC mass flow rate (kg/s)	0.41	Main chamber mass flow rate (kg/s)	25.64
FFC density (kg/m^3)	638	Main chamber density (kg/m^3)	4.4
Density ratio	145	Momentum ratio	7.9×10^{-5}
Mass flow ratio	0.015	Main chamber Mach number	0.2

gases in the combustion chamber, or both, a range of different conditions could be compared to determine the impact of mass flow ratio and momentum ratio on fuel film cooling effectiveness. A number of cases were also run at the same mass flow ratio and momentum ratio, with varying total mass flow rates, to ensure that the cooling effects were linked to ratio and not total throughput. A grid size of 17,000 cells is used in the first parametric study, with $y^+ = 1$ at the center of wall-bounding cells. The upper wall is treated as a symmetry boundary condition to decrease grid size. The adiabatic wall temperatures upstream and downstream of the inlet are recorded, and the frequency and amplitude of any downstream oscillations of density are recorded at points in the flow as a function of time. All cases are run for 100,000 time steps with a time step of 10^{-6} s.

A second study focuses on the impacts of coolant density on adiabatic wall temperature. By varying the molecular weight of the RP-2 substitute gas and varying the slot width, the density of the fuel can be varied without impacting the mass flow ratio of the system. Since an ideal gas equation of state is used in these simulations, and since the ideal gas equation of state underpredicts density in the transcritical operating conditions of an ORSC engine, a more dense fuel film may have a sufficiently different flow profile to affect adiabatic wall temperatures. By performing this study at a wide range of densities, any trends in fuel film cooling effectiveness should be more visible. This study uses grid sizes of 300,000 cells with $y^+ = 0.25$ at the center of wall-bounding cells. The upper wall is again treated as a symmetry boundary condition to decrease grid size. For consistency this study uses the same time step, run time, and measurement points as the first parametric study.

A third study covered the effect of slot width on adiabatic wall temperature. The third study is also helpful in closing the system for the first and second parametric studies; by varying slot width but holding density constant, the effects of slot width can be examined independently of density variations or mass flow ratio variations. This also helped to isolate momentum ratio effects when examined in conjunction with previous cases. This study also uses grid sizes of 300,000 cells with $y^+ = 0.25$ at the center of wall-bounding cells. For consistency this study uses the same time step, run time, and measurement points as the first parametric study. A description of the differences between these three linked studies can be found in Table 2.

A fourth study looks at the impact of three-dimensional modeling on predictions of wall temperature and system unsteadiness. In the two-dimensional studies, a strong Helmholtz resonator effect is observed in the FFC inlets in most cases. It is believed that this resonator, which has a significant impact on downstream wall temperature profiles, might not persist in a three-dimensional simulation. Transverse waves and additional walls could prevent this strong resonance from dominating the flow field, leading to different adiabatic wall temperatures and unsteady flow features. Due to increased computational cost, only two 3D cases are run: one that matches the baseline conditions in the experimental setup, and one that has periodic walls in the z-direction over a comparably-sized domain. The experiment-matching case (referred to as the Full case) has 9.5 million cells, while the periodic case has 3.3 million cells. Both cases have wall-bounding cells with $y^+ = 1$ at cell centers. The periodic case is designed to see if effects observed in 2D simulations are recovered in an infinitely long FFC inlet. By extension, this tests whether the width of the inlet has a significant impact on the flow features of the coolant. Figure 3 shows a sketch of the 3D domain.

Table 2. Cases in parametric studies.

Parametric study	Constant density and slot width, varying mass flow rates and momentum	Constant mass flow rates and momentum, varying density and slot width	Constant density, varying slot width and momentum
Reynolds number	$\approx 10^5 - 10^6$	$\approx 10^5$	$\approx 10^5$
Slot width (m)	5.6×10^{-4}	$3.8 - 11 \times 10^{-4}$	$3.8 - 11 \times 10^{-4}$
Main chamber density (kg / m^3)	$4.31 - 4.44$	4.42	4.42
Main chamber velocity (m/s)	$50 - 273$	233	233
Fuel density (kg / m^3)	638	$146 - 432$	295
Fuel velocity (m/s)	$0.7 - 5.4$	$1.2 - 1.6$	$1 - 3$
Momentum thickness (m)	$1.5 - 2.4 \times 10^{-4}$	1.6×10^{-4}	1.6×10^{-4}
Mass flow ratio	$0.01 - 0.075$	0.014	0.014
Density ratio	145	$33 - 97$	67
Momentum ratio	$10^{-4} - 10^{-3}$	$\approx 10^{-4}$	$\approx 10^{-4}$
Mach number	$0.05-0.33$	0.2	0.2
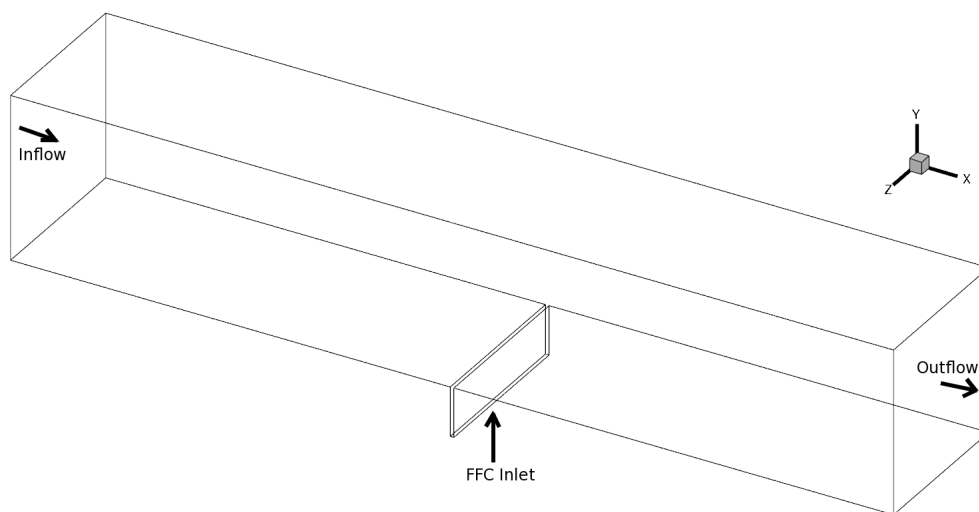
Figure 3. Domain of three dimensional cases. Periodic case is periodic on the two faces in xy-plane.

Finally, a study looking at how different inlet shapes effect film cooling effectiveness is completed in 2D. Other work in this paper focuses on a generic inlet design that would not be used in a production engine, and as a consequence may be capturing phenomena that other geometries do not experience. Three inlet geometries are chosen to match experimental setups used at the Air Force Research Lab for FFC testing, shown in Figure 4. While these three geometries do not cover the diverse range of inlet designs used for FFC in the liquid rocket community, matching the profiles of in-house experiments should help close the gap between experimental results and simulations. The first case (Thin slot) has 141,000 cells, the second case (Wide slot) has 196,000 cells, and the third case (Bent slot) has 231,000 cells. All three cases have wall-bounding cells with $y^+ = 0.5$ at cell center.

(a) Thin slot   (b) Wide slot   (c) Bent slot
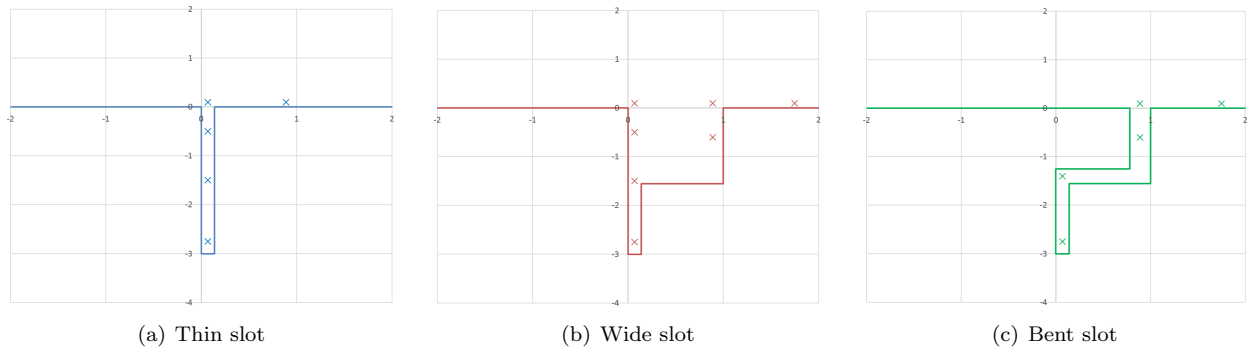
Figure 4. Inlet geometries for parametric study. (a) Simple straight inlet, (b) Inlet with wide entrance cavity, (c) Inlet with bend. Markers indicate points of unsteady frequency measurement.

IV.   Results

IV.A.   Results of Baseline Case

Figure 5 shows a series of instantaneous flow fields from the baseline case. The color contours represent the fuel mass fraction, while the black lines are contours of iso-vorticity. A plot of pressure as a function of time is also shown, to establish where in the unsteady cycle each flow field is taken. In all of the cases in this parametric study, a recirculation region is observed within the FFC inlet. In the lower momentum ratio cases this region of recirculation and intrusion is most visible in the upstream portion of the FFC inlet as predicted by Salazar et al.,[18] which changes the effective size of the FFC inlet and may be partially responsible for driving the instabilities observed.

(a)   (b)

(c)   (d)
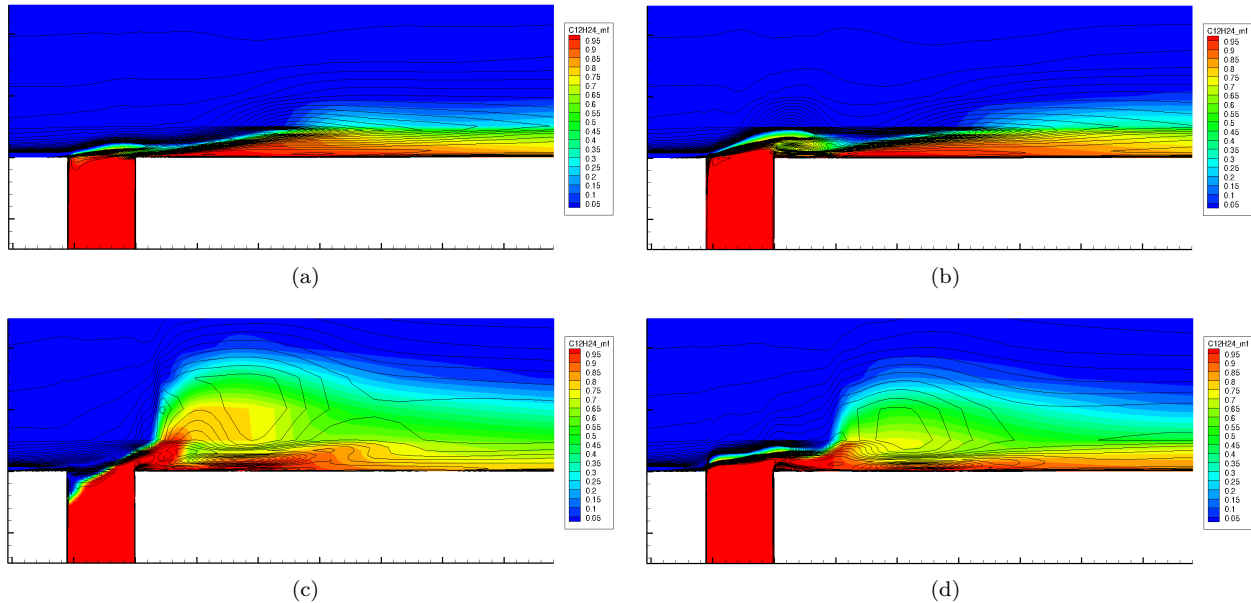
Figure 5. Instantaneous flow patterns (fuel mass fraction of flow field with contours of constant vorticity superimposed) of the baseline case.

For all cases tested, simulations predict that these oscillations will persist tens of slot widths downstream of the FFC inlet. By measuring the adiabatic wall temperature as a function of time, it is possible to obtain some information on the frequency of oscillations in wall temperature, and see how these oscillations change as a function of distance downstream of the FFC inlet. The power spectral density (PSD) of these temperature variations is calculated at each point along the wall downstream of the FFC inlet, and projected onto a heat map as shown in Figure 6. Flow variables are also monitored at several points throughout the flow field downstream of the FFC inlet. The velocity used to calculate nondimensional parameters is the convection velocity U_c, which is defined by Dimotakis[20] as:

$$U_c = \frac{U_1 \rho_1^{1/2} + U_2 \rho_2^{1/2}}{\rho_1^{1/2} + \rho_2^{1/2}}$$

While originally formulated for single phase flow, this convection velocity term was validated by Wegener et al.[21] for similar conditions to these simulations. By monitoring the oscillations of the density, there appears to be a relationship between the convection velocity U_c and the frequency of oscillation. In an effort to find the driving frequency for these oscillations, the power spectral density of the flow field is calculated at a point downstream of the inlet (the black x in Figure 3).

(a) PSD of wall temperature

(b) PSD of flow field
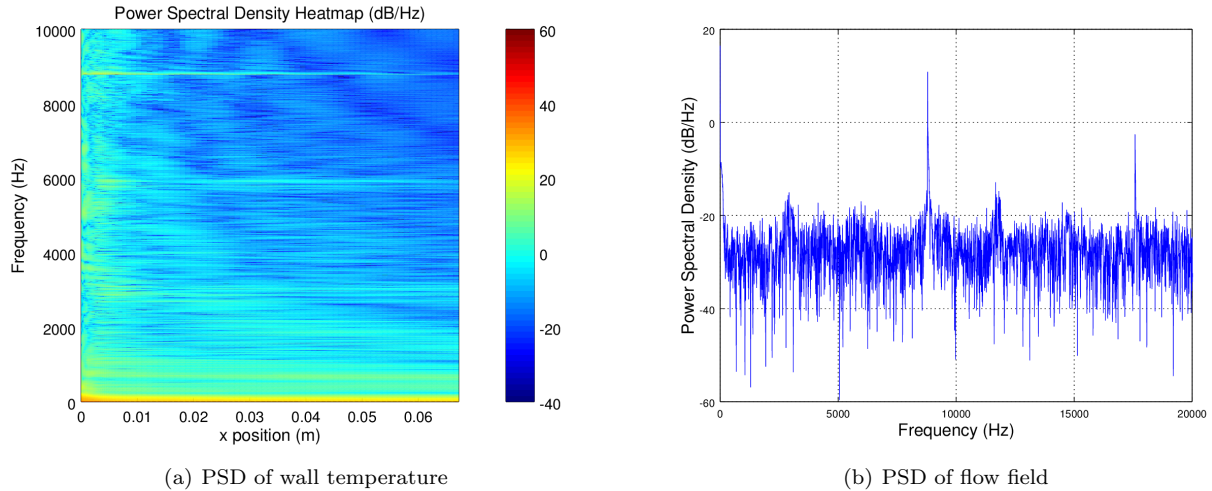
Figure 6. Power spectral density of baseline case.

IV.B. Parametric Study 1: Constant Density and Slot Width, Varying Mass Flow Rates and Momentum

By looking at the same calculations for other cases in the first parametric study, one can see how these fluctuations persist as a function of momentum ratio and main chamber velocity. Figure 7 shows how the PSD based on wall temperature changes as either the main chamber velocity or FFC flow velocity are varied. Cases are listed in terms of their momentum ratio (J), as well as whether the FFC mass flow rate or main chamber mass flow rate were varied relative to the baseline case. Of interest is the fact that varying the main chamber mass flow rate has a larger impact on the dominant frequencies than varying the FFC mass flow rate.

(a) J=0.13%, FFC Varies

(b) J=0.13%, Main chamber Varies

(c) J=7.89%, FFC Varies

(d) J=7.34%, Main chamber Varies
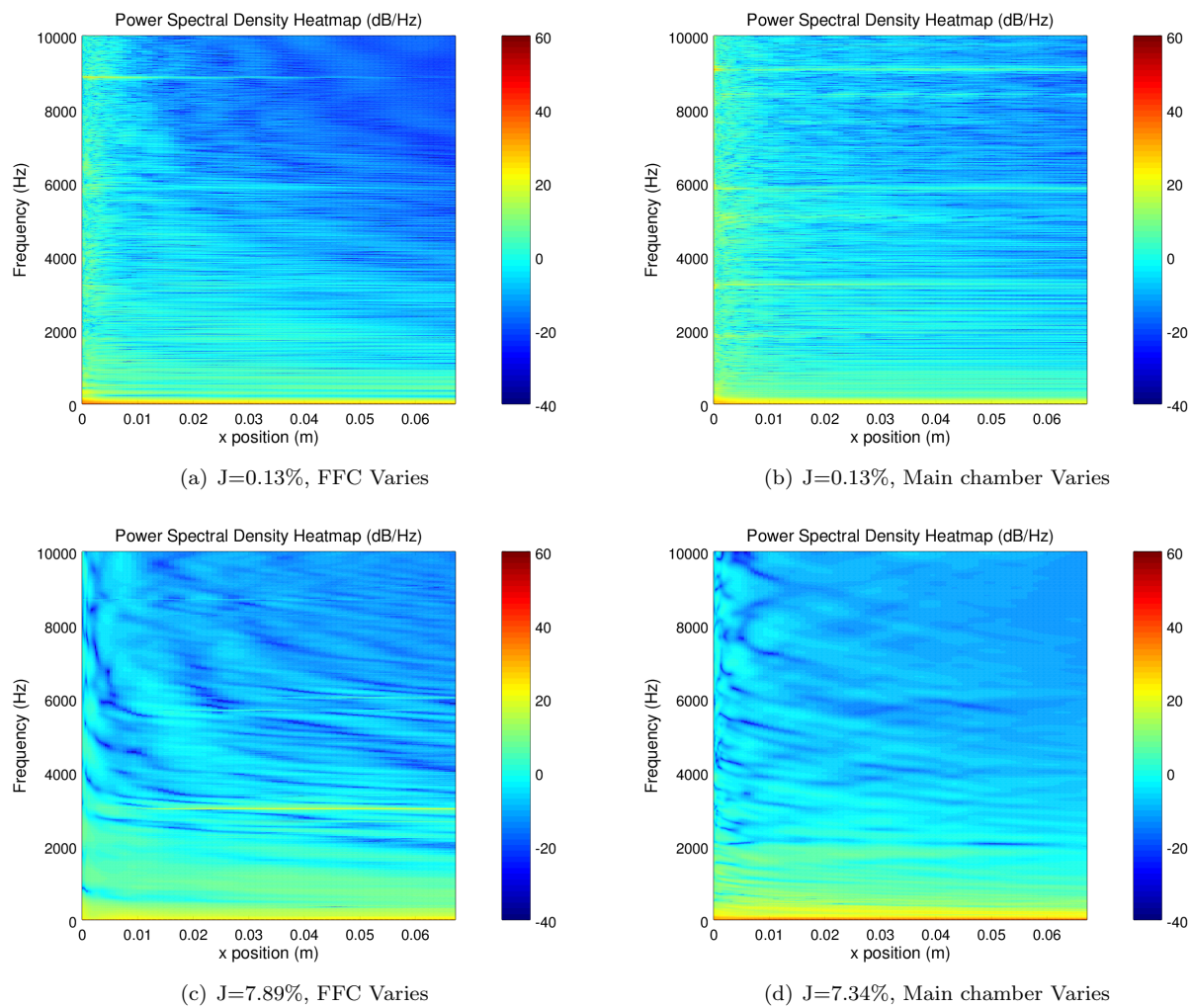
Figure 7. Power Spectral Density of Various Cases.

These heat maps show several trends. Of note is that as the main chamber velocity decreases, higher frequency oscillations are damped out and lower frequencies dominate. There is also a clear distinction between the frequencies present depending on whether the FFC mass flow rate or the main chamber mass flow rate is changed. This shows that while the temperature profiles in Figure 11 do not show significant difference between cases with similar momentum ratios, there are still noticeable differences in how the flow interacts with the wall. As a point of comparison, Figure 8 shows the PSD calculated using the density of the flow field under the same inlet conditions.

(a) J=0.13%, FFC Varies

(b) J=0.13%, Main Varies

(c) J=1.23%, FFC Varies

(d) J=1.18%, Main Varies

(e) J=7.89%, FFC Varies

(f) J=7.34%, Main Varies
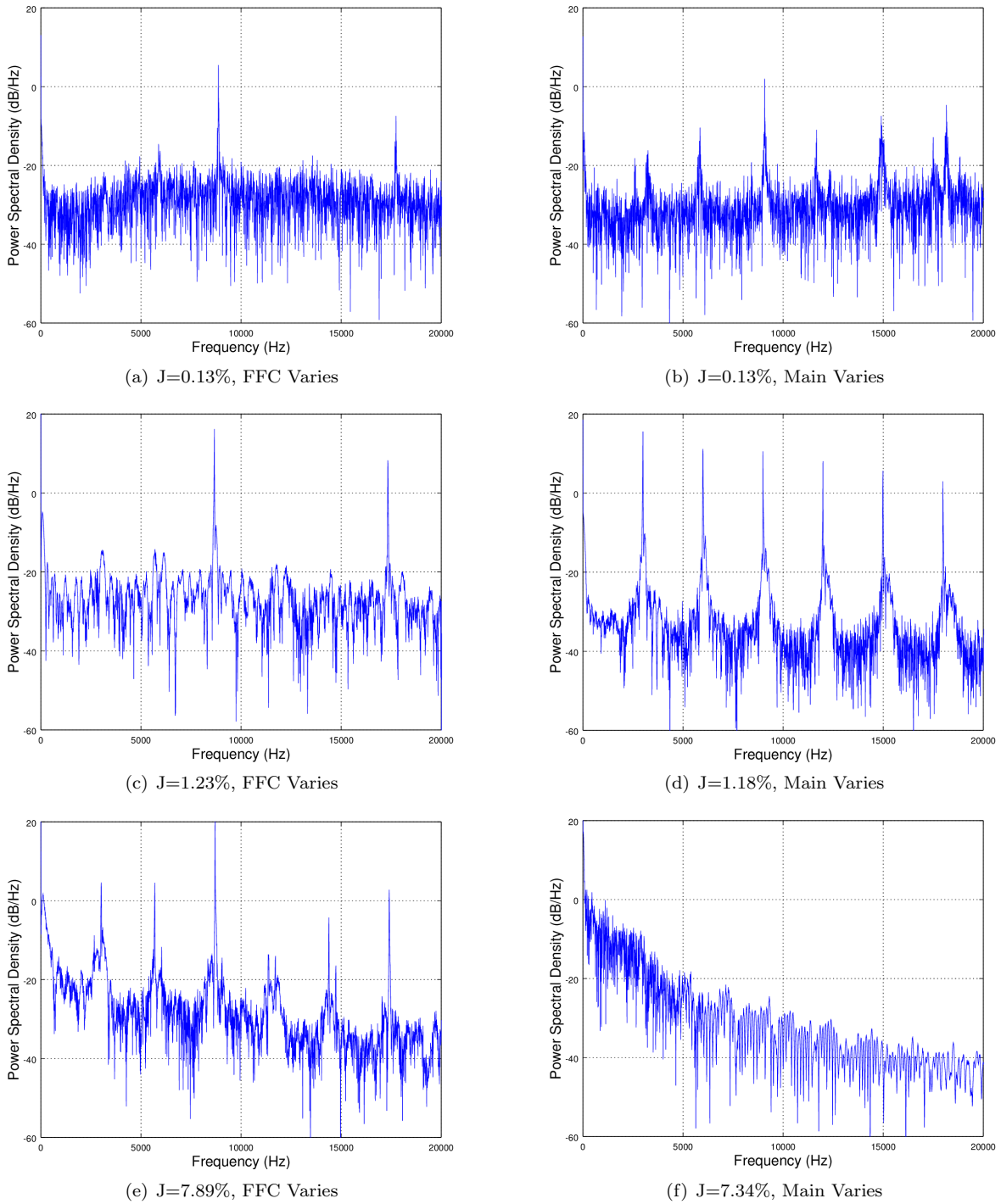
Figure 8. Power Spectral Density data from flow field.

As the momentum ratio increases, the stronger frequencies are damped out and the overall frequency response is diminished. This is consistent with the work of Sarohia,[19] which showed that introducing mass flow to a cavity in cross flow caused a decrease in cavity noise.

These frequencies can be nondimensionalized as a Strouhal number to better describe the mechanisms behind these oscillations in the flow field. The frequency of oscillations in density is measured at the far field point in Figure 3. The length scale used is the width of the FFC inlet d, and the velocity used is the convection velocity U_c. The Strouhal number can be calculated using this velocity:

$$St_c = \frac{fd}{U_c}$$

Figure 9 shows the relationship between the Strouhal number and Mach number for the first three dominant frequencies for all the cases simulated in this study. A filled in marker represents the strongest frequency in the flow field at a given Mach number.
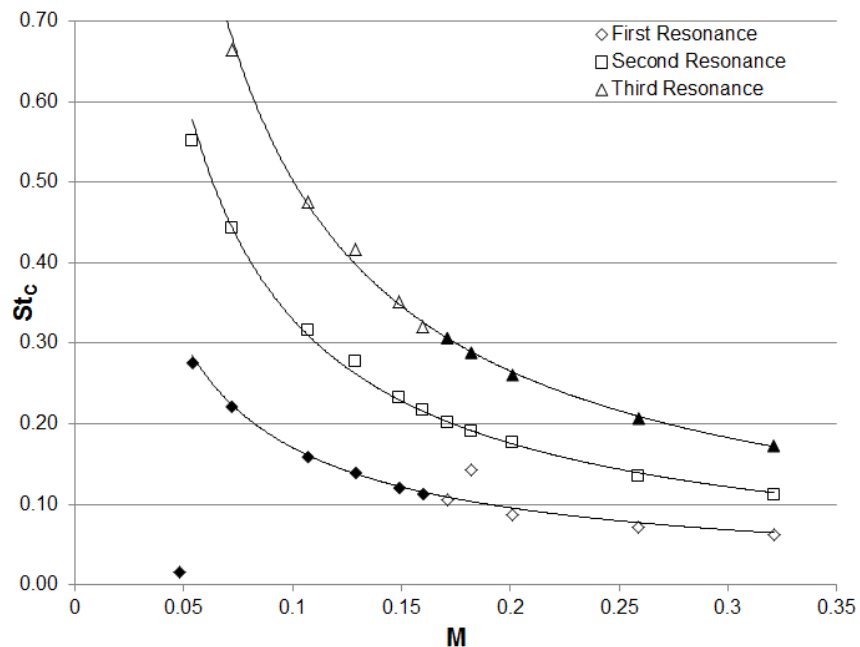
Figure 9. Strouhal number as a function of Mach number for the three dominant frequencies in each simulation. Filled points represent the strongest frequency for that simulation.

An important consideration in this study of frequency is that the inlet duct of the fuel film functions as a cavity resonator. This can be seen by calculating the Helmholtz number:

$$He = \frac{2\pi f d}{a}$$

where f is frequency, d is the depth of the cavity, and a is the speed of sound in the fluid (in this case dodecene). A Helmholtz number that approaches unity indicates that the cavity is functioning as a Helmholtz resonator, while higher integers correspond to higher resonances. When He is calculated using the dominant frequencies found in the flow fields of each case, the results show that these frequencies are aligned with that of a Helmholtz resonator. Figure 10 shows the relationship between Mach number and Helmholtz number.
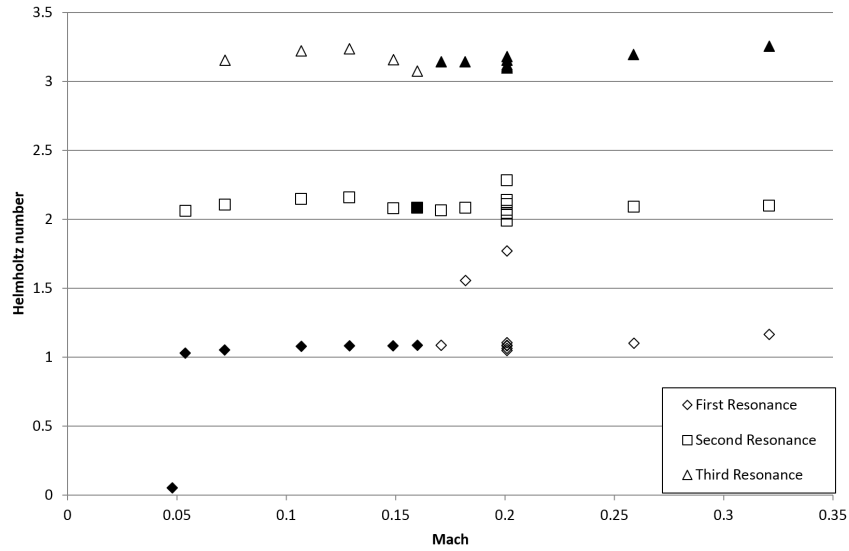
Figure 10. Helmholtz number as a function of Mach number for the three dominant frequencies in each simulation. Filled points represent the strongest frequency for that simulation.

4

    While this comparison gives a clear answer for why the first dominant frequency exists where it does, it does not explain the jump from the first harmonic to the third harmonic as the Mach number increases. At M≈0.17, the strongest frequency switches from the first frequency ($St_c \approx 0.11$) to the third frequency ($St \approx .30$), skipping over the second frequency entirely. The frequency of oscillation triples given a very slight difference in operating conditions, indicating a change in the driving mechanisms behind the oscillations. Colonius[3] suggests that flow over a cavity transitions from a mode driven by shear layer interaction and vortex shedding to a wake-driven mode as the Mach number is increased and the acoustic interactions of the flow with the back wall of the cavity reflect upstream and interact with the flow. It is possible that the increase in frequency of the higher Mach flows in this study are an indication that interactions between the fuel film and the freestream are causing this jump in resonant modes. The geometry of these simulations is different from that of Colonius (and indeed from most studies of flow over cavities), but given the sharp jump in frequency there is basis for comparison with his work. Colonius predicts a shift in modes when $\sqrt{Re_0}d/\theta_0 \geq 800$, where Re_0 is the Reynolds number based on momentum thickness θ_0, with d corresponding to the width of the cavity. The switch in modes of this more complex system occurs at $\sqrt{Re_0}d/\theta_0 \approx 200$. This may be driven by the difference in density between the fluid in the main chamber and that in the FFC slot.

    The fluctuations exist not only in the flow field far downstream, but in the adiabatic wall temperature as well. Figure 11 shows these fluctuations for a range of different operating conditions. Here, the black line represents the time-averaged adiabatic wall temperature, with the red line representing a sample of the wall temperatures at one instance in time and the blue lines representing the bounds of these fluctuations to two standard deviations. Note that two different approaches for varying the momentum ratio are presented - one by varying the FFC mass flow rate, and the other by varying the main chamber mass flow rate.

(a) J=0.13%, FFC Varies

(b) J=0.13%, Main Varies

(c) J=2.79%, FFC Varies

(d) J=2.64%, Main Varies

(e) J=7.89%, FFC Varies

(f) J=7.34%, Main Varies
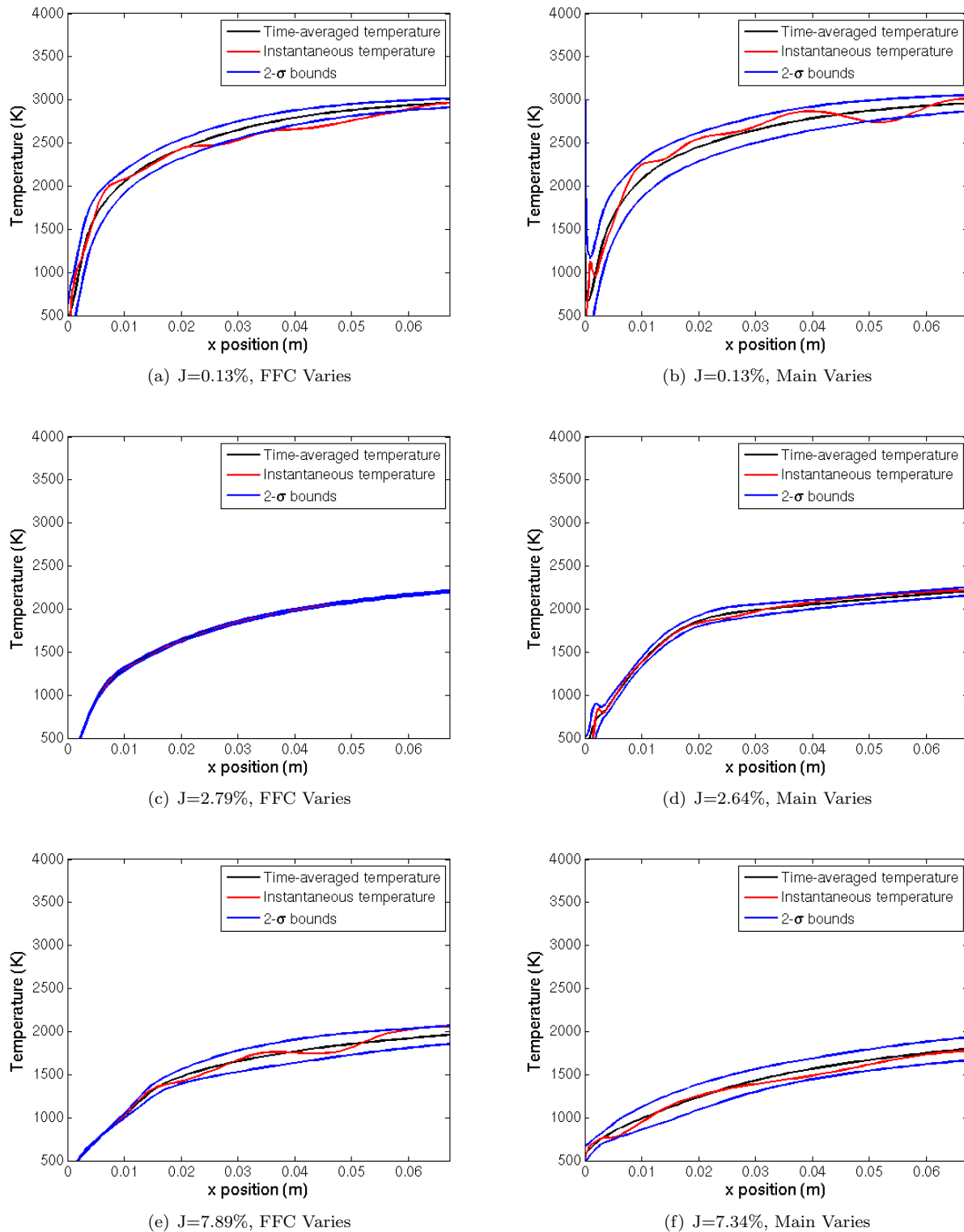
Figure 11. Wall temperatures for varying inlet conditions.

An interesting trend is present in the wall temperature plots: as the momentum ratio increases the wall temperatures and the amplitude of oscillations both decrease, with the exception of the highest momentum ratio case where the variation in temperature is higher than almost all other cases in the far downstream region. In spite of this difference in the amplitude of oscillations, the adiabatic wall temperature does decrease monotonically with increasing momentum ratio. Figure 12 shows how these amplitudes change

with momentum ratio. The relationship is not simple; although the amplitude decreases downstream in most cases, the relationship with mass flow ratio does not follow a consistent trend. This suggests that baroclinic torque may be driving the oscillations in higher momentum ratio cases. In some cases, the flow seemed to switch between two modes, with either no fuel on the wall or the wall having a thick layer of cooled fuel driving the adiabatic wall temperature down.

(a) FFC Varies   (b) Main Varies
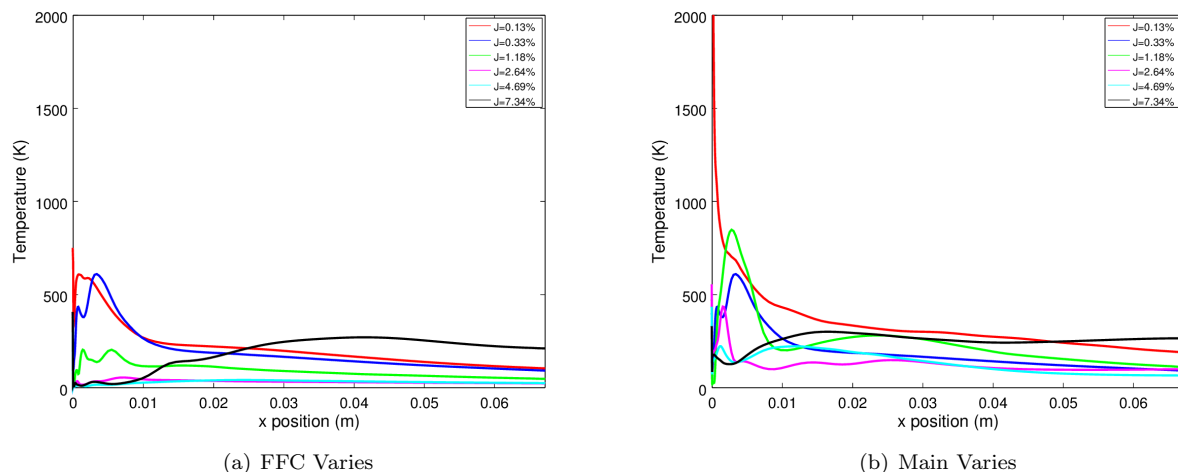
Figure 12. Amplitude measurements.

Temperature profiles can be defined non-dimensionally in terms of an adiabatic effectiveness η, which can be calculated using the freestream temperature of the hot flow T_h, the adiabatic wall temperature T_{aw} and the temperature of the coolant T_c as:

$$\eta = \frac{T_h - T_{aw}}{T_h - T_c}$$

Adiabatic wall temperature data is taken from all of the cases in this parametric study, and can be arranged into three separate series to showcase how different variables affect the flow. Figures 13 through 15 show how modifying the flow results in significant changes in the adiabatic effectiveness.
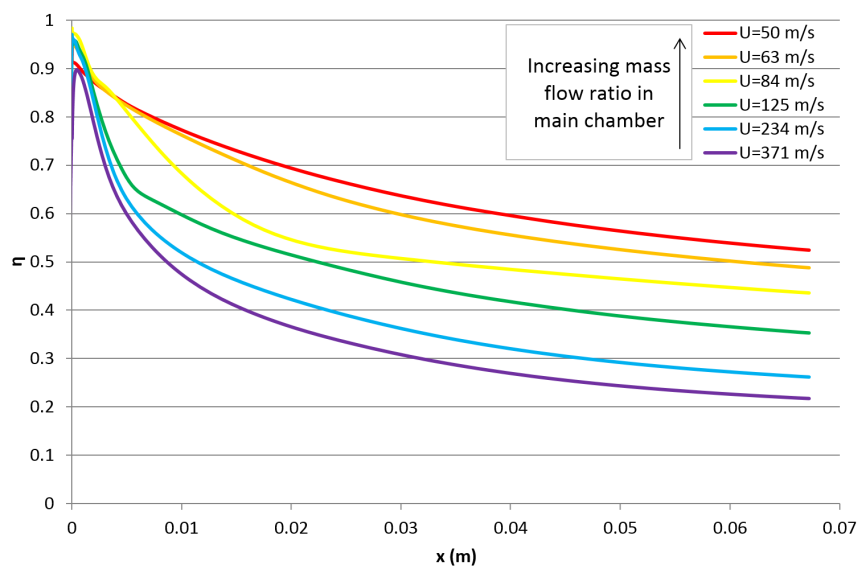
Figure 13. Adiabatic effectiveness with varying main chamber mass flow rate. Constant density and slot width.

FFC Velocity (m/s)	≈ 1.15	Main Velocity	$50 - 371$	Convection Velocity	$4.9 - 29.7$
FFC Density (kg/m^3)	638	Main Density	4.4	Density Ratio	145
FFC Mass flow rate (kg/s)	≈ 0.41	Main mass flow rate	$5.5 - 41$	Mass flow ratio	$1.0 - 7.5 \times 10^{-2}$
FFC Reynolds	3.8×10^4	Main Reynolds	$5.1 \times 10^4 - 3.8 \times 10^5$	Momentum ratio	$3.1 \times 10^{-5} - 1.7 \times 10^{-3}$
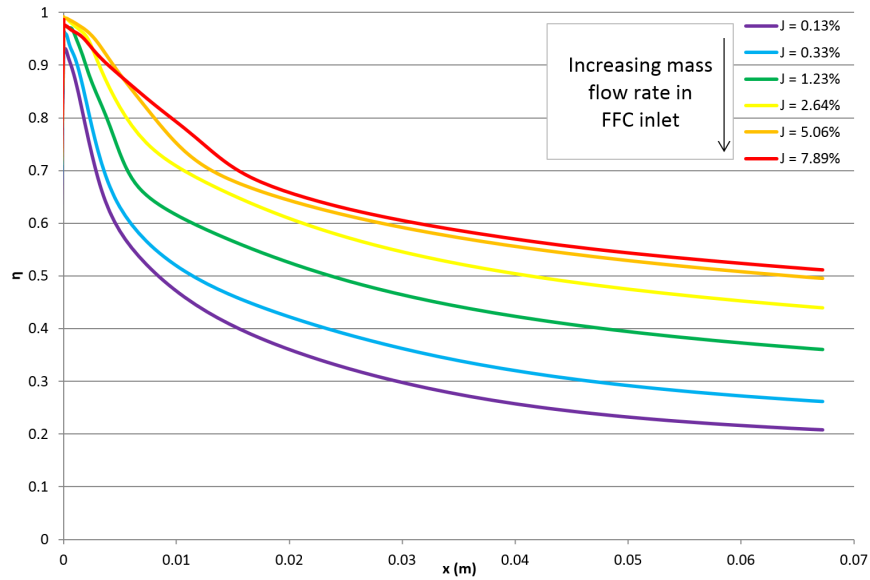
Figure 14. Adiabatic effectiveness with varying FFC mass flow rate. Constant density and slot width.

FFC Velocity (m/s)	$0.7 - 5.4$	Main Velocity	234	Convection Velocity	$18.5 - 22.9$
FFC Density (kg/m^3)	638	Main Density	4.4	Density Ratio	145
FFC Mass flow rate (kg/s)	$\approx 0.3 - 1.9$	Main mass flow rate	25.6	Mass flow ratio	$1.0 - 7.5 \times 10^{-2}$
FFC Reynolds	$2.4 \times 10^4 - 1.8 \times 10^5$	Main Reynolds	2.4×10^5	Momentum ratio	$3.0 \times 10^{-5} - 1.7 \times 10^{-3}$
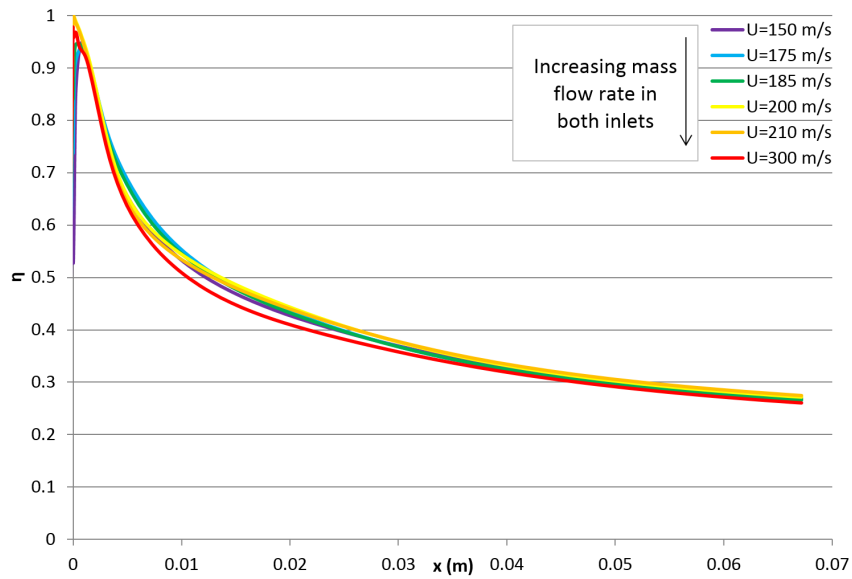
Figure 15. Adiabatic effectiveness with varying FFC and main chamber mass flow rates. Constant density, slot width, mass flaw ratio and momentum ratio.

FFC Velocity (m/s)	$0.7 - 1.4$	Main Velocity	$150 - 300$	Convection Velocity	$12.2 - 24.3$
FFC Density (kg/m^3)	638	Main Density	4.4	Density Ratio	145
FFC Mass flow rate (kg/s)	$\approx 0.3 - 0.5$	Main mass flow rate	$16.5 - 33.0$	Mass flow ratio	1.6×10^{-2}
FFC Reynolds	$2.4 \times 10^4 - 4.8 \times 10^4$	Main Reynolds	$1.5 \times 10^5 - 3.0 \times 10^5$	Momentum ratio	7.9×10^{-5}

In each of these three series, one of three interlinked variables (main chamber mass flow rate, FFC mass flow rate, and mass flow ratio) are held constant while the other two vary. The mass flow ratio appears to be the primary driver of adiabatic wall temperature, as the only case to not show significant variation was that in which the mass flow ratio was held constant.

IV.C. Parametric Study 2: Constant Mass Flow Rates and Momentum, Varying Slot Width and Density

The second parametric study builds upon the findings of the first parametric study to determine if density has a significant impact on film cooling effectiveness. As before, unsteady results will be discussed before wall temperature plots. Changing the density of the flow did in fact have a significant impact on the flow field. While the cases close in density to the baseline case recover a consistent driving frequency, the outermost cases on both ends produce much different results. The PSD of each case in Figures 16 through 20 shows how the strength of the frequencies drops by many orders of magnitude in the outer cases; the resulting primary frequency is effectively noise.
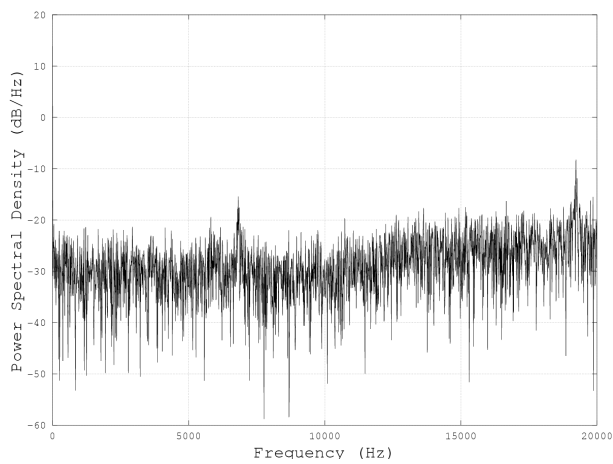
(a) 50% Density flow field PSD
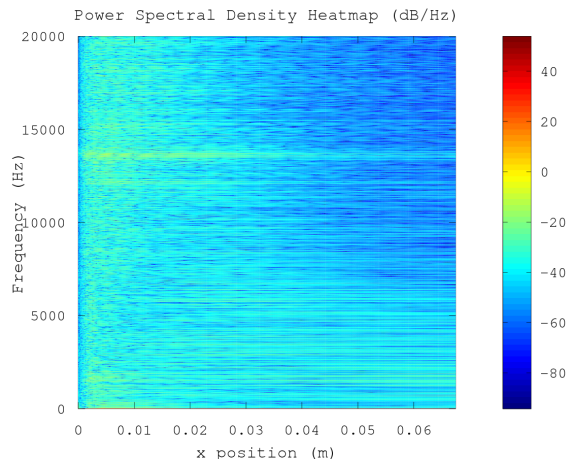
(b) 50% Density wall temperature PSD

Figure 16. Power Spectral Density plots for flow field and wall temperature oscillations in the lowest density case.
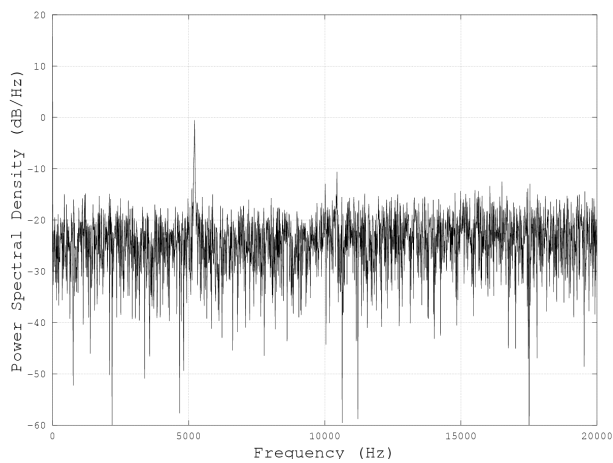
(a) 75% Density flow field PSD
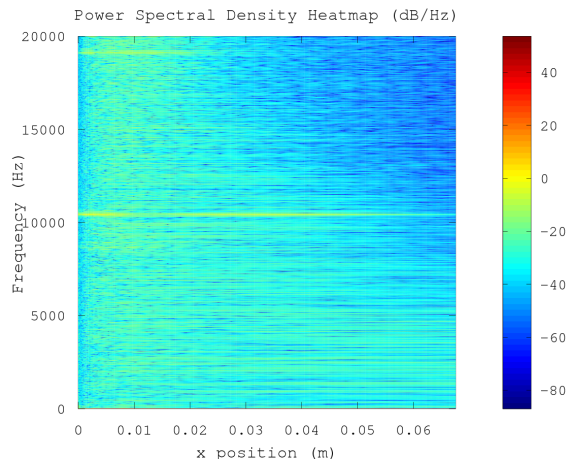
(b) 75% Density wall temperature PSD

Figure 17. Power Spectral Density plots for flow field and wall temperature oscillations in a low density case.
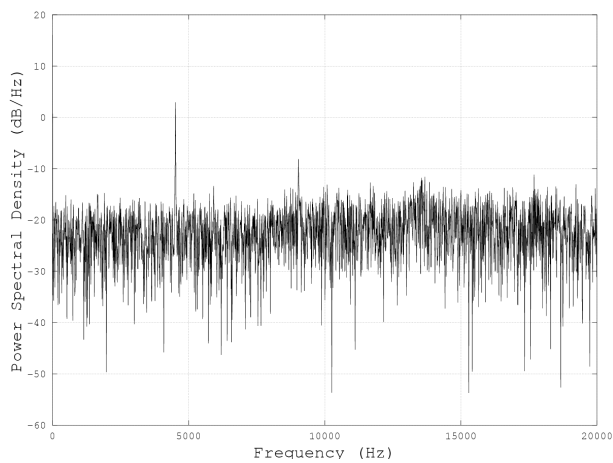
(a) Baseline flow field PSD
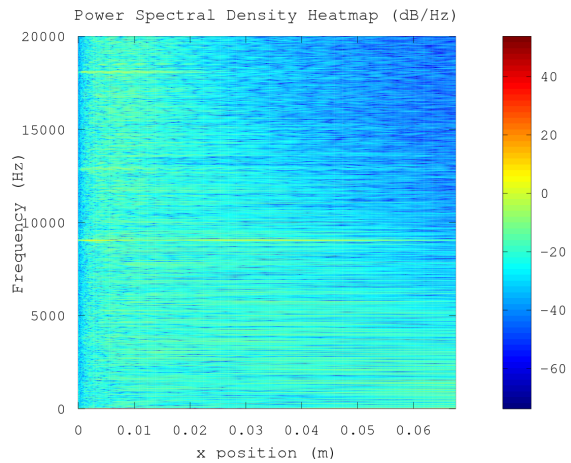
(b) Baseline wall temperature PSD

Figure 18. Power Spectral Density plots for flow field and wall temperature oscillations in the baseline density case.

(a) 125% Density flow field PSD

(b) 125% Density wall temperature PSD
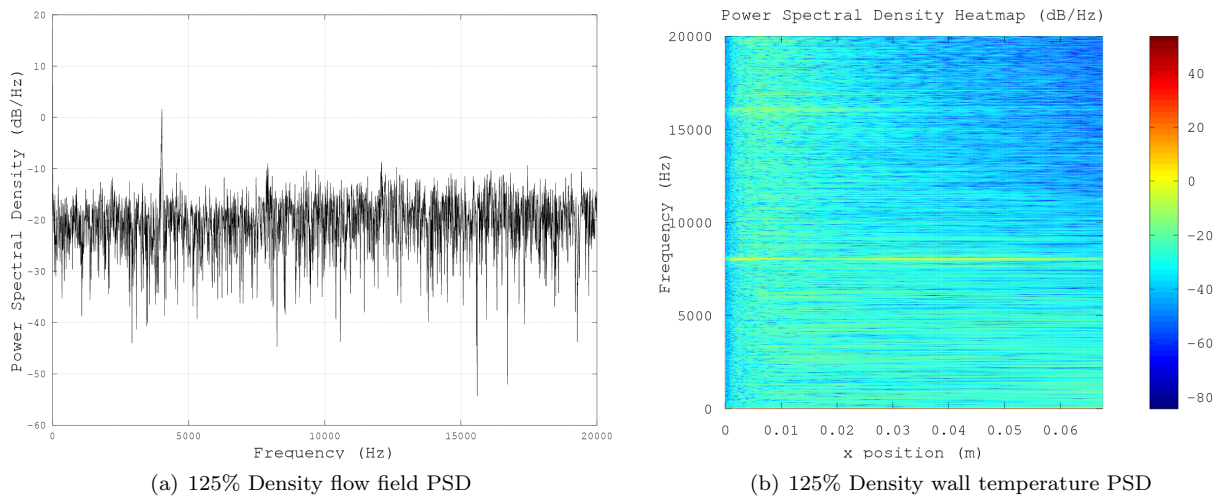
Figure 19. Power Spectral Density plots for flow field and wall temperature oscillations in a high density case.

(a) 150% Density flow field PSD

(b) 150% Density wall temperature PSD
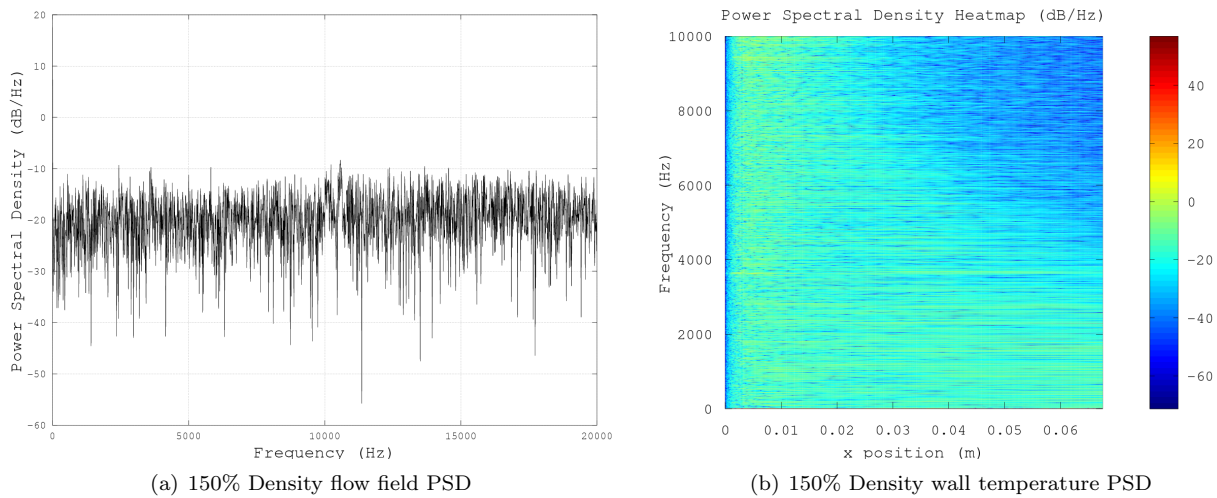
Figure 20. Power Spectral Density plots for flow field and wall temperature oscillations in the highest density case.

There is one large discrepancy between this parametric study and the first: the driving frequency of the baseline case appears to be half the frequency. This discrepancy is related to how the methodologies differed between the two studies. When calculating the density of a fluid, GEMS looks at the state of the primitive variables, and calls a chemical database to determine the correct molecular weight and other parameters. In the first parametric study, the molecular weight of the gas is artificially inflated to match the density ratio predicted by the Peng-Robinson equation of state. Since the study uses an ideal gas equation of state and this is known to produce incorrect values, it was decided to model a denser fuel to better match experimental conditions. In the second parametric study this is not a concern, so the correct molecular weight is used. It is important to note that even the highest molecular weight tested in this study does not match the density that a real gas equation of state would predict, so there is not a direct overlap between the two studies in terms of density. However, there are still important conclusions that can be drawn from this study.

When one examines the Strouhal numbers for these cases, there seems to be a slight scaling with density for cases where there is a strong driving frequency. A similar trend is recovered in the third parametric study, to be discussed in more detail later. All cases with a strong driving frequency have a Helmholtz number of unity, and no oscillatory mode switching is observed. These results can be found in Table 3

When time-averaged, the adiabatic effectiveness profiles for all these cases are nearly identical. Figure 21 shows differences too small to draw meaningful trends. However, there is something subtle not captured in this figure. As with the driving frequencies, the significant drop in density between the two studies has a significant impact on the adiabatic wall temperature profile. As Figure 22 shows, the results are

Table 3. Frequency Response in Varying Density Study

Density	50%	75%	Baseline	125%	150%
Frequency (kHz)	19.32	5.22	4.52	4.02	10.58
Convection Velocity (m/s)	36.47	30.72	27.30	25.62	23.37
Strouhal Number	0.60	0.13	0.09	0.08	0.17
Helmholtz Number	3.06	1.02	1.01	1.02	2.93
Slot Width (m)	1.14×10^{-3}	7.46×10^{-4}	5.59×10^{-4}	4.79×10^{-4}	3.83×10^{-4}

most apparent in far downstream. While the artificial molecular weight produce an adiabatic effectiveness trending towards 0.25, the lighter molecular weights trend toward 0.45 instead. This suggests that there is some dependence on density in the adiabatic wall temperature response. It is worth noting that the temperatures do not vary significantly across the second parametric study, just between the two parametric studies themselves. Hence, there is either a weak dependence of density on wall temperature, or there exists a jump to a higher mode between these two studies.
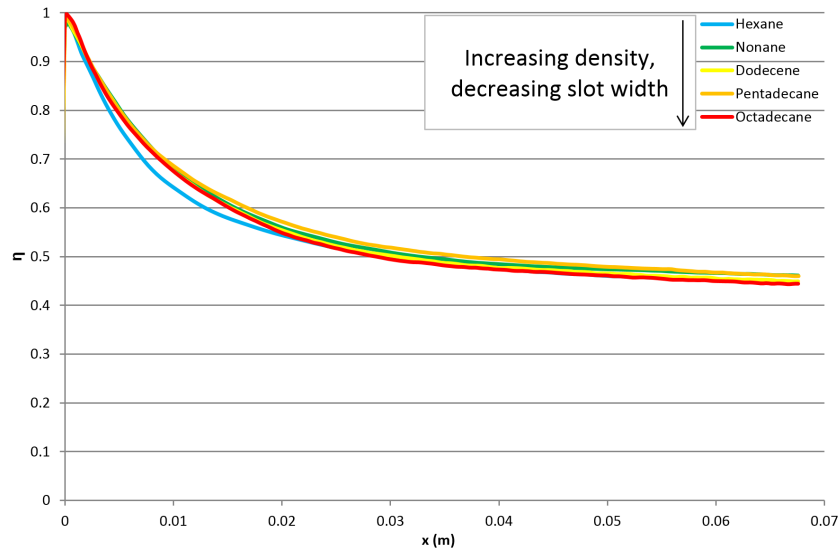
Figure 21. Adiabatic effectiveness with varying densities. Constant mass flaw ratio and momentum ratio.

FFC Velocity (m/s)	2.1	Main Velocity	234	Convection Velocity	$23.3 - 36.5$
FFC Density (kg/m^3)	$145 - 430$	Main Density	4.4	Density Ratio	$33 - 98$
FFC Mass flow rate (kg/s)	≈ 0.3	Main mass flow rate	25.6	Mass flow ratio	1.4×10^{-2}
FFC Reynolds	3.2×10^4	Main Reynolds	6.5×10^5	Momentum ratio	1.2×10^{-4}
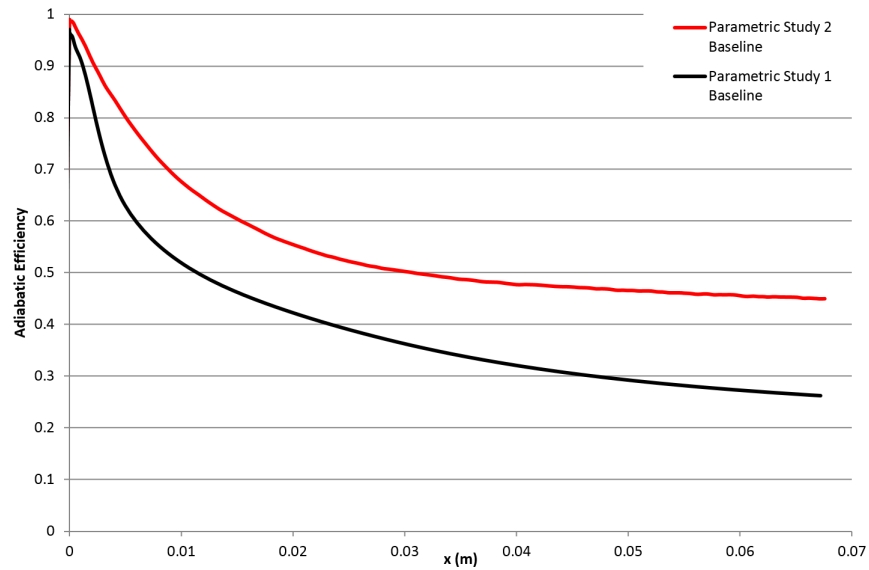
Figure 22. Difference in baseline adiabatic effectiveness between first and second parametric study.

IV.D. Parametric Study 3: Constant Density and Mass Flow Ratio, Varying Slot Width and Momentum

Parametric study three seeks to close the loop along with studies one and two, varying the slot width and momentum but holding density and mass flow ratio constant. The slot widths are exactly the same as those used in the varying density parametric study, so the effects of slot width can be examined independently of density variations. Mass flow ratio is held constant, but momentum ratio is allowed to vary. These results can be found in Figures 23 through 27.

(a) Flow field PSD

(b) Wall temperature PSD
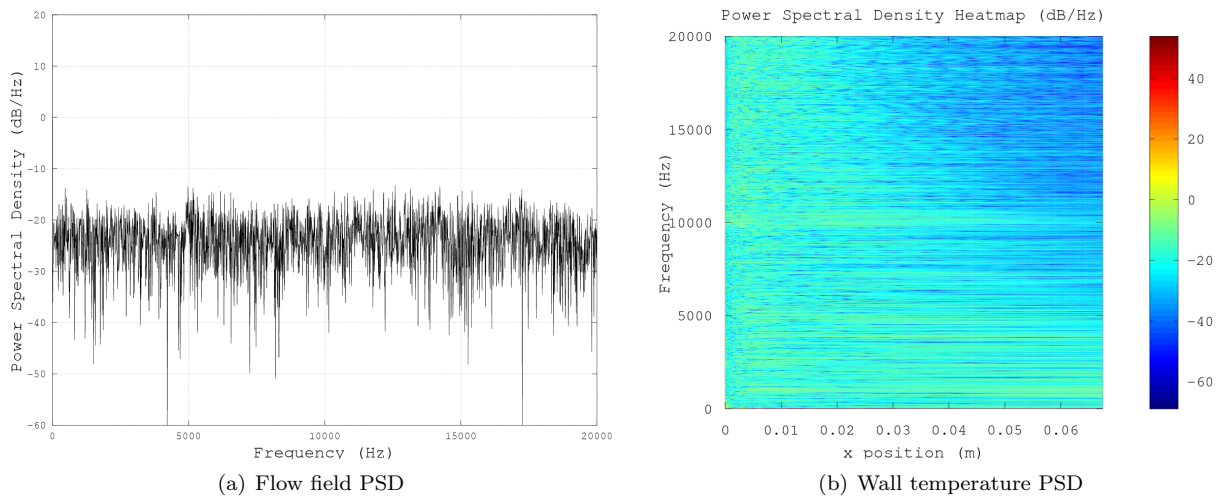
Figure 23. Power Spectral Density plots for flow field oscillations in the widest slot.
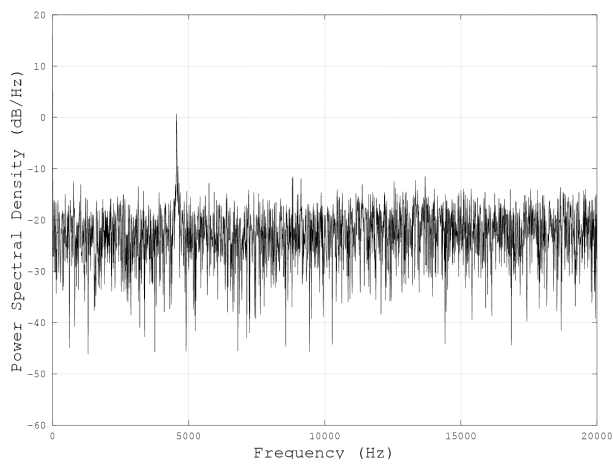
(a) Flow field PSD
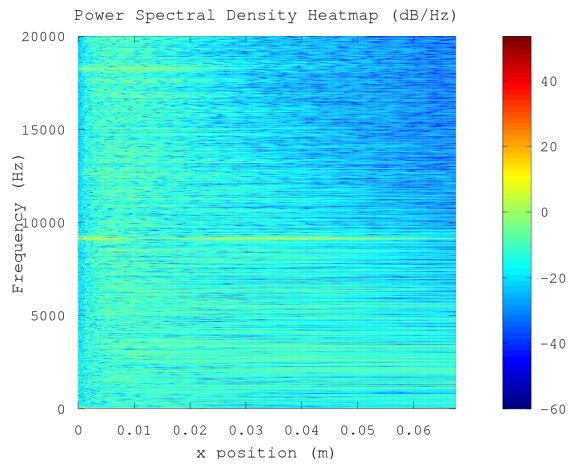
(b) Wall temperature PSD

Figure 24. Power Spectral Density plots for flow field oscillations in a wide slot.
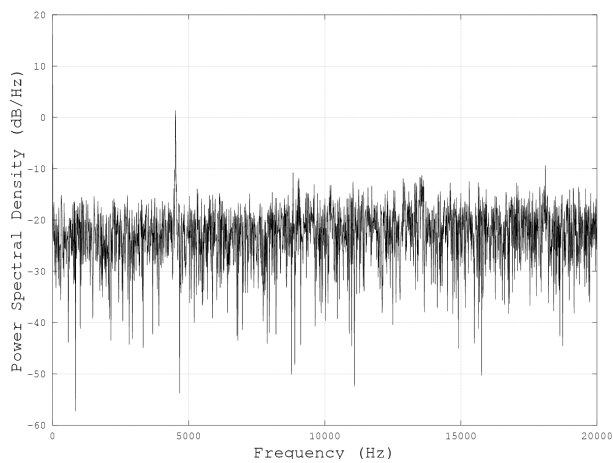
(a) Flow field PSD
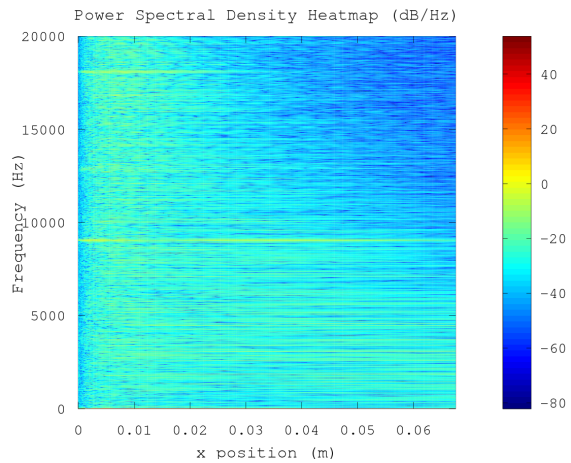
(b) Wall temperature PSD

Figure 25. Power Spectral Density plots for flow field oscillations in the baseline slot.
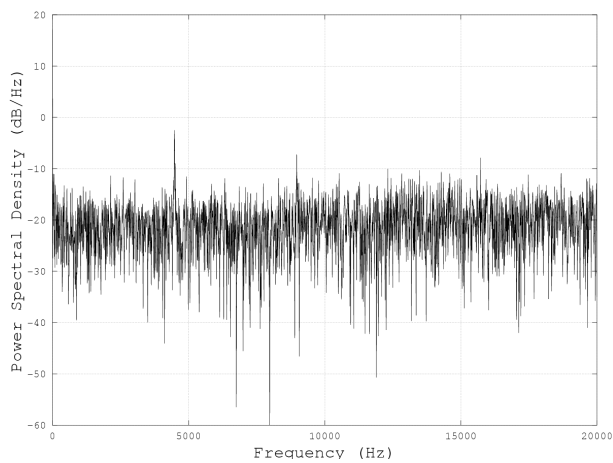
(a) Flow field PSD
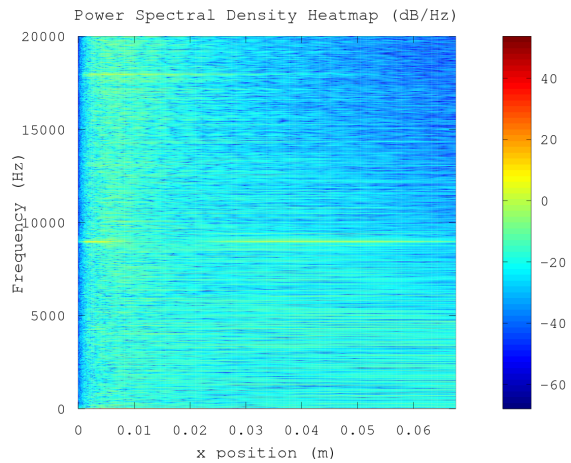
(b) Wall temperature PSD

Figure 26. Power Spectral Density plots for flow field oscillations in a thin slot.

(a) Flow field PSD

(b) Wall temperature PSD
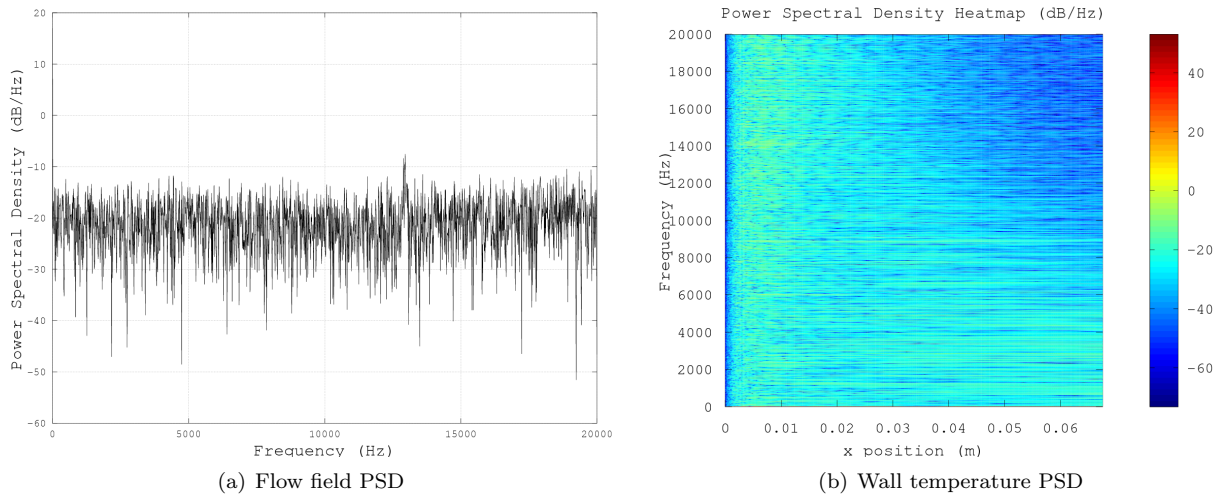
Figure 27. Power Spectral Density plots for flow field oscillations in the thinnest slot.

The driving frequencies line up almost exactly with the previous parametric study. As the frequency remain largely unchanged for the central cases, this suggests that the width of the slot does not have a strong impact on the frequency of oscillation. Table 4 lists some of the same parameters as parametric study 2 for direct comparison. It should be noted that the density used in this parametric study was identical to that of the second parametric study, allowing for direct comparison.

Table 4. Frequency Response in Slot Width Study

Slot Width (m)	1.14×10^{-3}	7.46×10^{-4}	5.59×10^{-4}	4.79×10^{-4}	3.83×10^{-4}
Frequency (kHz)	12.58	4.56	4.52	4.49	19.29
Convection Velocity (m/s)	26.34	26.83	27.30	27.62	28.12
Strouhal Number	0.54	0.13	0.09	0.08	0.26
Helmholtz Number	2.82	1.02	1.01	1.00	4.32

This table reinforces the findings of the previous parametric study. The frequencies of the second parametric study varied on the order of 500 Hz between cases, but varying only the grid produces differences in frequency between cases on the order of 50 Hz. Hence, varying density is shown to have a stronger impact on the frequency of oscillation than varying the slot width alone. However, Strouhal numbers for the two cases scale identically. This is because the slot width is varying much faster than the frequency across these cases, which are weighted equally in the equation for the Strouhal number.

The adiabatic wall temperature plots suggest that slot width does not play an important role in wall temperature determination. Figure 28 shows how adiabatic wall temperatures change with slot width.
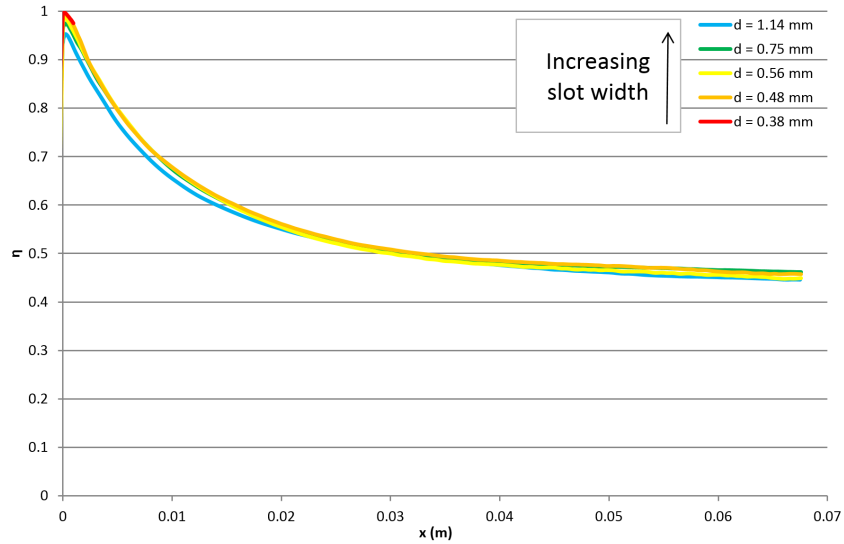
Figure 28. Adiabatic effectiveness with varying slot width. Constant density and mass flow ratio.

FFC Velocity (m/s)	$1.0 - 3.1$	Main Velocity	234	Convection Velocity	$26.3 - 28.2$
FFC Density (kg/m^3)	295	Main Density	4.4	Density Ratio	67
FFC Mass flow rate (kg/s)	≈ 0.3	Main mass flow rate	25.6	Mass flow ratio	1.4×10^{-2}
FFC Reynolds	3.2×10^4	Main Reynolds	6.5×10^5	Momentum ratio	$6.0 \times 10^{-5} - 2.0 \times 10^{-4}$

Between the three discussed parametric studies there is a lot of information, but the clear trend is that the mass flow ratio is closely linked to adiabatic effectiveness and by extension the adiabatic wall temperature. Varying both flow rates did not cause a significant change in adiabatic effectiveness, nor did changing the density or slot width. In all series shown except Figures 13 and 14, the differences in adiabatic wall temperature are small and do not vary monotonically with the independent parameter. This finding supports existing literature that links the effectiveness of a FFC system to the mass flow ratio.[22]

IV.E.   Parametric Study 4: Three-Dimensional Effects

The main objective of the three dimensional study is to determine whether the effects seen in two dimensional simulations are comparable to these more expensive and time-consuming 3D simulations. Two cases are run: A case that matches the experimental setup used in-house, and a version with periodic boundary conditions. The case matching the experimental conditions (referred to as the Full case) addresses some of the limitations of earlier 2D simulations: no-slip walls on the side and boundary layer thickening at the corners may have a large impact on the flow field, and a transverse wave in the FFC inlet could disrupt the Helmholtz resonator effect. The periodic case is designed to see if these effects disappear for a sufficiently long FFC inlet. In an LRE combustion chamber, having an FFC inlet that wraps around the entire circumference of the combustion chamber is not uncommon, and such an inlet is well suited to being modeled with periodic boundary conditions. Figures 29 and 30 show instantaneous flow fields from the two cases. Iso-contours of fuel mass fraction are used to display the spread of the fuel film, while the color represents the speed at which that part of the film is moving (blue is slow, green is fast).
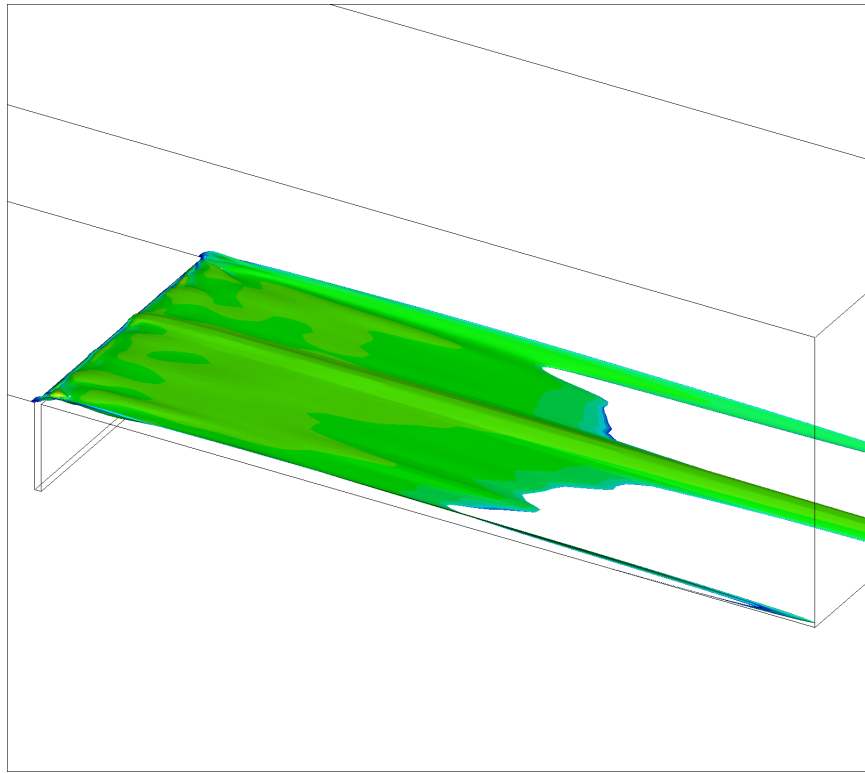
Figure 29. Fuel iso-contour of Full case. Contour surface is colored with total velocity.
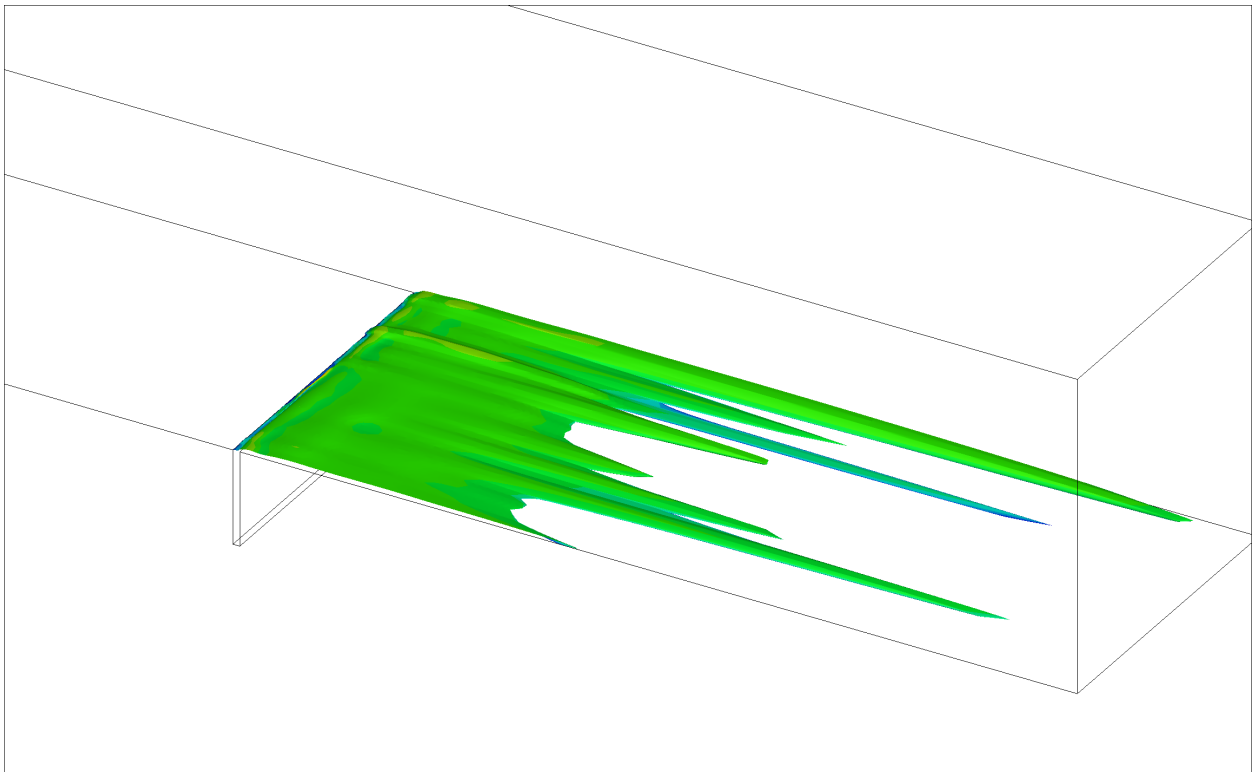
Figure 30. Fuel iso-contour of Periodic case. Contour surface is colored with total velocity.

In the Full case, strong 3D effects can be observed. The outer walls dramatically slow the fuel film, with the film failing to persist as far downstream outside of the central region. The center maintains a much thicker film, and as a consequence has lower wall temperatures than parts of the duct closer to the walls. It is also worth nothing that a rich mixture of oscillatory modes is present in the Full case. A transverse wave appears to interact with longitudinal waves, and generates a response that seems cyclical, although not as simple as those observed in 2D. The transverse wave is at a much lower frequency than the longitudinal wave, but has a stronger amplitude. This results in a less variable fuel film than that observed in 2D simulations, and the resulting wall temperature is almost steady.

The periodic case is interesting in that it reproduces several of the effects seen in 2D. While there are some 3D features in the flow field, no transverse waves form, and a standing longitudinal wave forms in the FFC inlet. The power spectral density plots of the flow field are shown for both cases in Figure 31.

<div style="text-align:center">(a) Full Case   (b) Periodic Case</div>
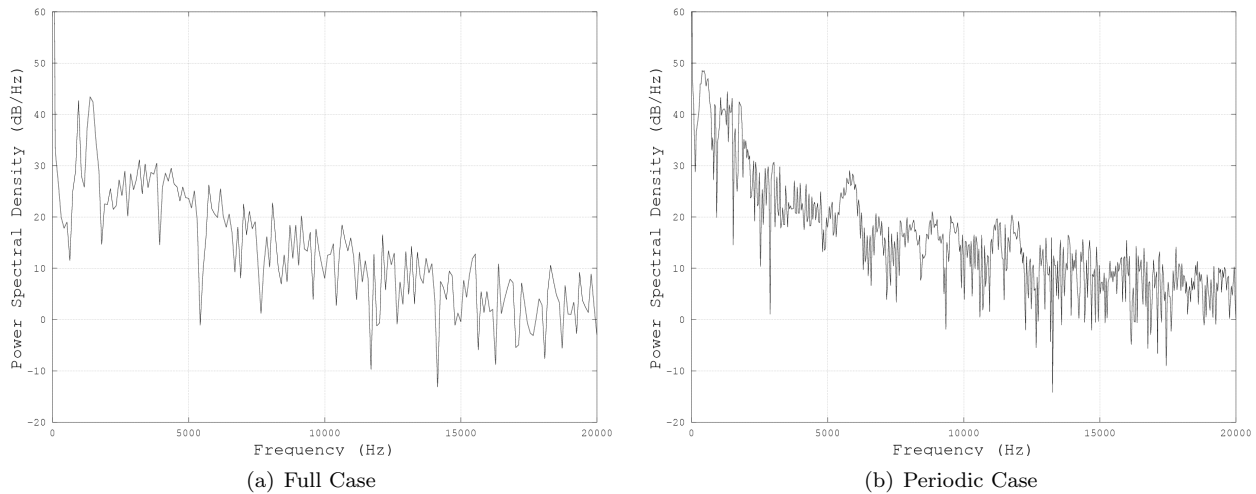
Figure 31. PSD of flow fields for (a) Full case and (b) Periodic case.

Both of these cases have a very low driving frequency compared to 2D simulations. And while the periodic case does reproduce qualitatively the resonation mode seen in 2D, the unsteadiness is not as pronounced in 3D simulations. This suggests that 3D effects are still driving an infinitely long or circumferential slot, and 2D alone is not capturing these features. However, this lost information does not appear to have a large impact on wall temperature profiles. When examining wall temperatures in the 3D cases, a problem arises: Neither case is uniform in the z-direction, so wall temperature profiles vary depending on where the line is drawn. The wall temperature of the Full case is shown in Figure 32, while the temperature of the periodic case is shown in Figure 33.
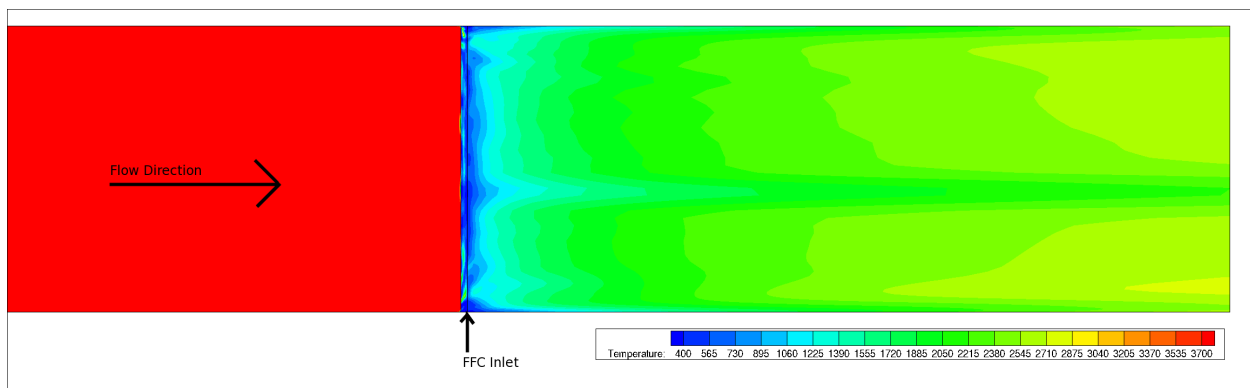
Figure 32. Wall temperature of Full case. View is from above the domain, looking down.
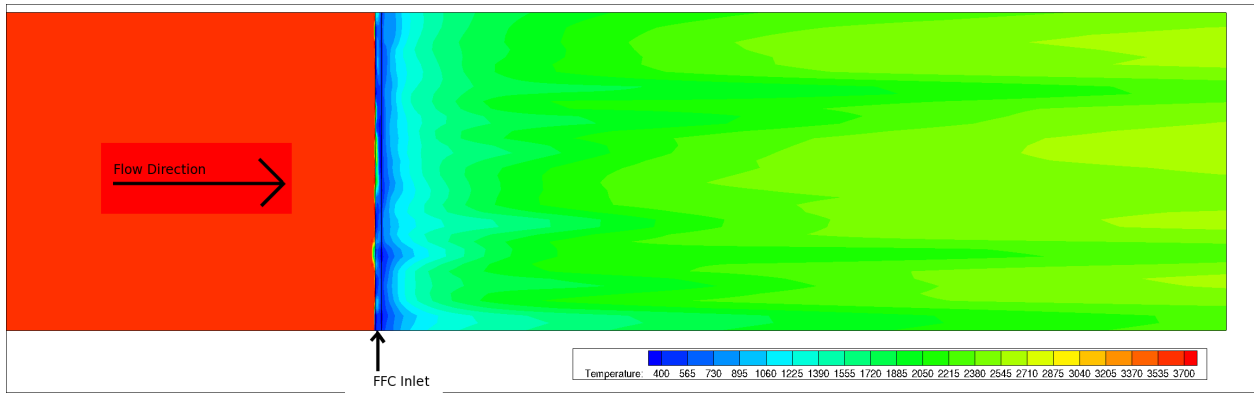
Figure 33. Wall temperature of periodic case. View is from above the domain, looking down.

The Full case has an almost symmetrical fuel distribution. While there is a thick and consistent fuel film down the center of the domain, this film tapers off significantly on either side, with the areas close to the wall having the lowest coverage. By comparison, the periodic case also has regions of thick film and thin film, but the distribution appears to be more random in nature.

As a consequence of these varying fuel film thicknesses, the wall temperature profile and adiabatic effectiveness can vary significantly depending on where the measurements are made. To put bounds on this, Figure 34 shows the adiabatic effectiveness along the line of highest effectiveness (the center line), as well as the results along the line of lowest effectiveness for both cases. The 2D baseline effectiveness is shown for comparison.
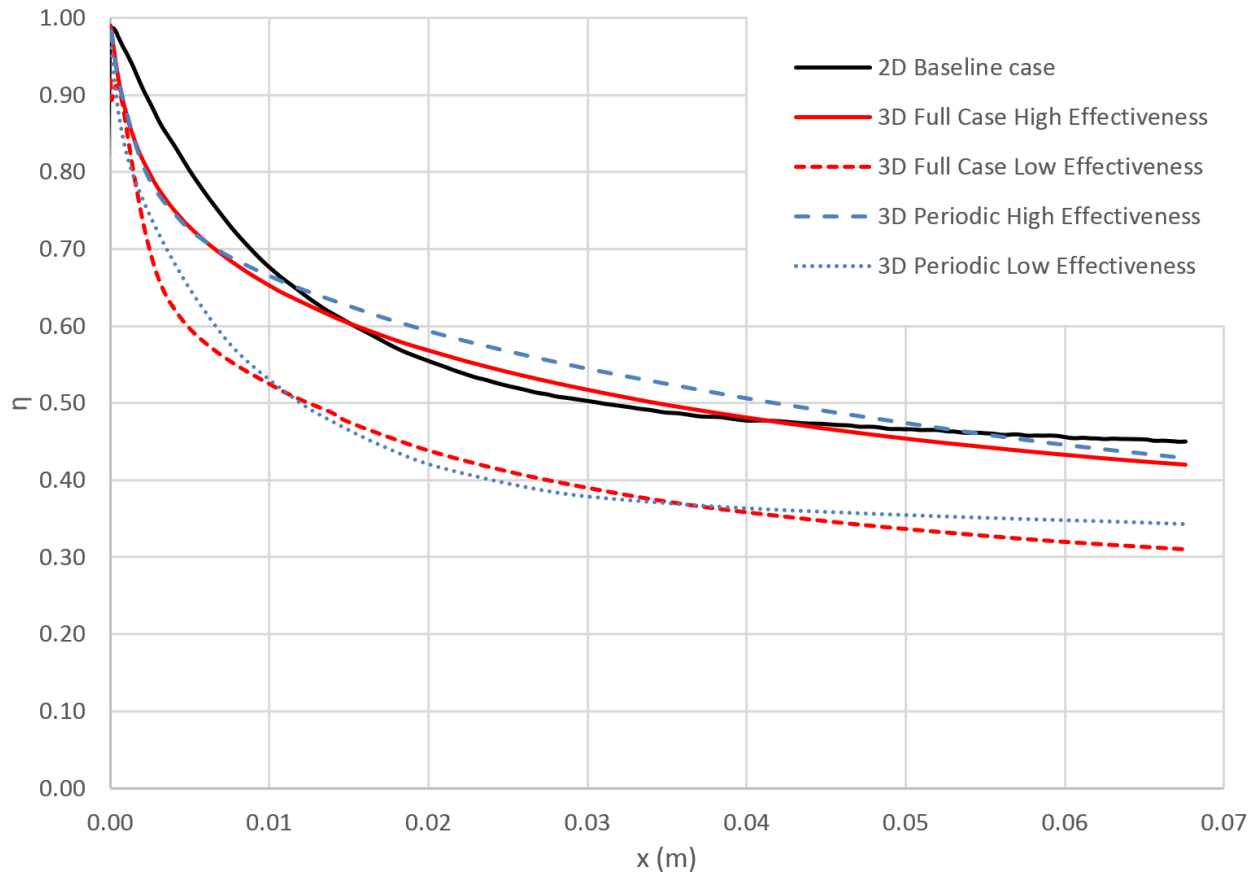
Figure 34. Adiabatic effectiveness of Full 3D case at center line versus 2D baseline case.

What is perhaps surprising is how well the Full and periodic cases agree in terms of the possible range of wall temperature values. While the distribution of these values is quite different for the two cases, the highs and lows follow similar trend lines and approach similar values in the far field. This suggests that a bounded slot as used in local experiments should produce similar film cooling effectiveness numbers to a circumferential slot.

While the 2D simulations are close in effectiveness to the center line of the Full case, they fail to capture the much lower effectiveness elsewhere along the panel. Yet a fully periodic case also produces regions of thick and thin fuel film, so this behavior is not only limited to narrow FFC inlets. However, one cannot discount the results of a 2D simulation. It did reproduce several features seen in the periodic case such as the presence of a Helmholtz resonator and highly unsteady fuel films, which may play a larger role in very wide or circumferential FFC inlets. Further research is needed to determine whether the inlet effects studied in the last parametric study (detailed in the next subsection) would carry over into 3D simulations.

IV.F.   Parametric Study 5: Varying Inlet Shape

For the last parametric study, the effect of inlet shape on flow unsteadiness and wall temperature profile is recorded. The first case (referred to as the Thin slot for simplicity) is a simple slot similar to the other 2D cases, but at a skinnier width. This is for direct comparison against the second case (hereafter the Wide slot), where a narrow FFC inlet opens to a cavity region before entering the hot flow. The lower half of the Wide slot geometry is the same width as the Thin slot. The final case (Bent slot) features a bent inlet, mimicking an experimental setup used for in-house experiments. While the Bent slot is not capturing all the elements of the experimental setup's 3D geometry, it does inform how resonance waves and recirculation regions are affected by sharp turn in the geometry. Figure 35 shows a few instantaneous snapshots of the normalized temperature, compared to that of the baseline case.

(a) Baseline

(b) Thin slot

(c) Wide slot

(d) Bent slot
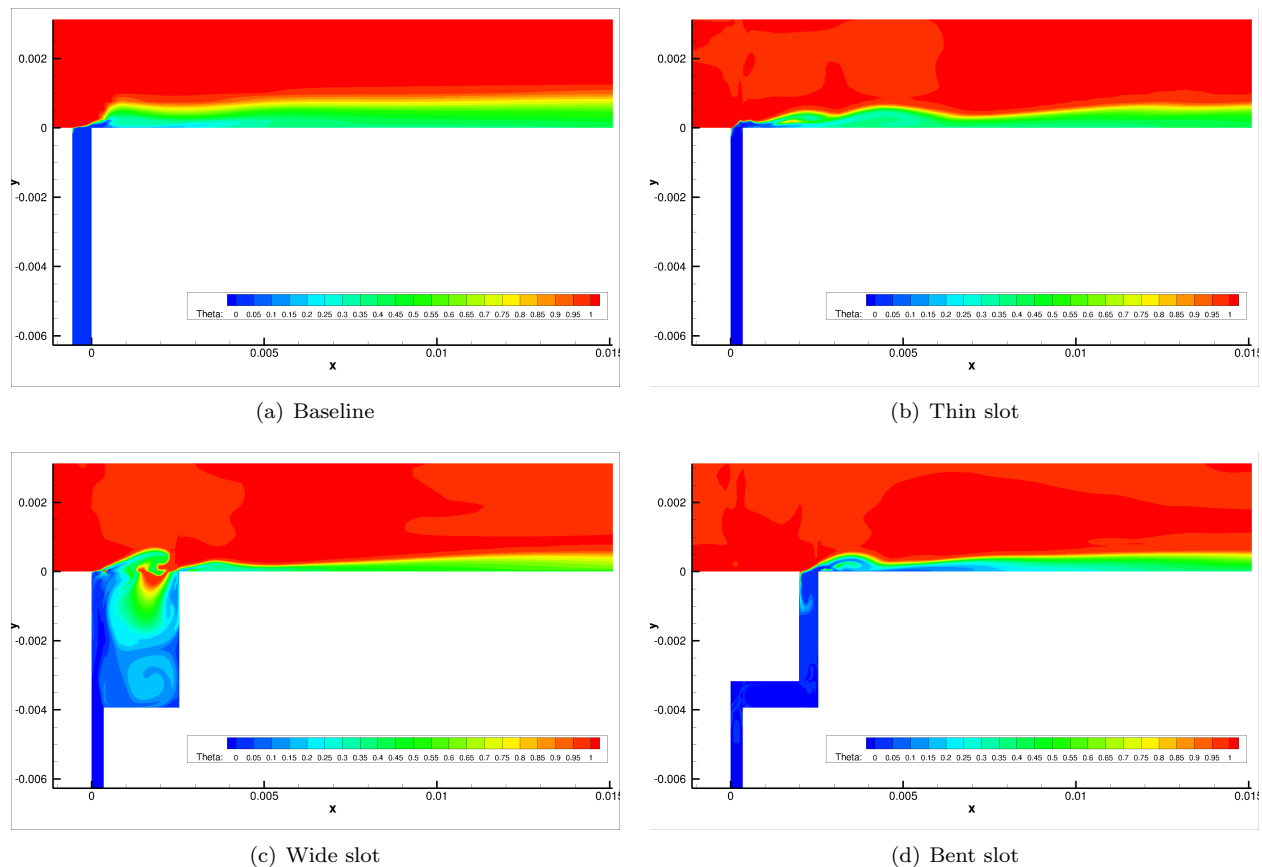
Figure 35. Instantaneous flow fields showing normalized temperature in varying inlet geometry study.

There are a few interesting features in these snapshots. In the Wide slot, there exists a strong recirculation region inside the FFC inlet, but a thick fuel film is still present downstream. In the Bent slot, the results

appear at first glance very similar to the Thin slot. However, the unsteady response is much different; while pressure waves form a resonance along the entire length of the Thin slot case, in the Bent slot all unsteadiness is damped out almost entirely after the first bend. Interactions with the main chamber are less pronounced in the Bent slot, and there does not appear to be a strong resonance.

Figure 36 shows the PSD of both the flow field and the wall temperatures for all three cases. It is notable that there is no primary frequency evident in any of these cases. The Thin slot closely mirrors the results from the thinnest slot in the third parametric study, where there did not appear to be a strong resonance established. Given the strong recirculation zone in the Wide slot, it is surprising that there does not appear to be a strong driving frequency observed downstream.
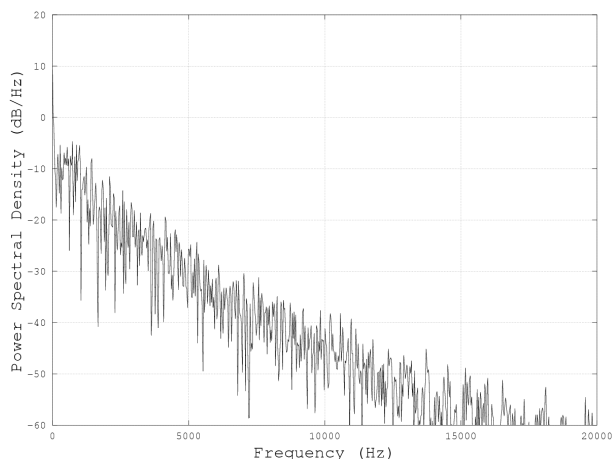
(a) Thin slot Flow field PSD
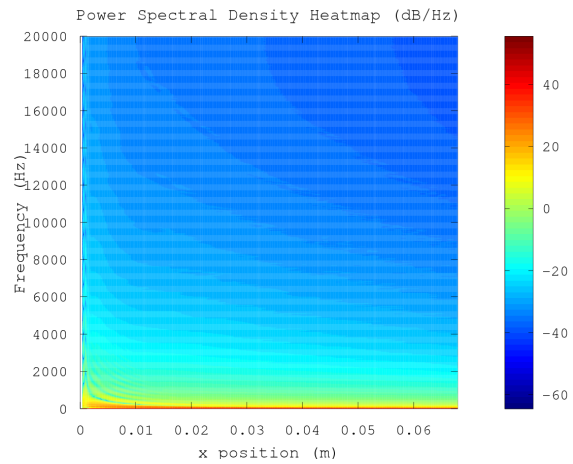
(b) Thin slot Wall Temp PSD
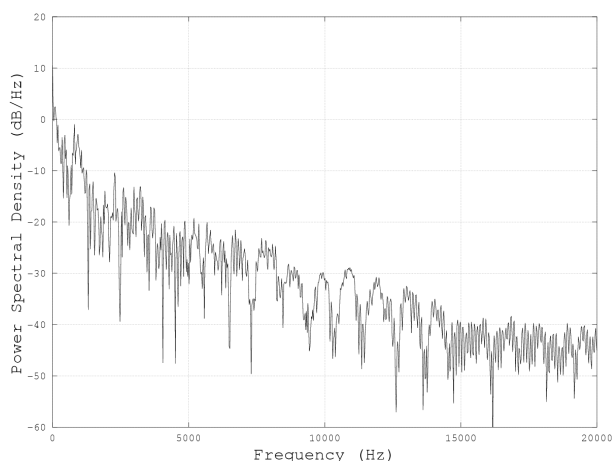
(c) Wide slot Flow field PSD
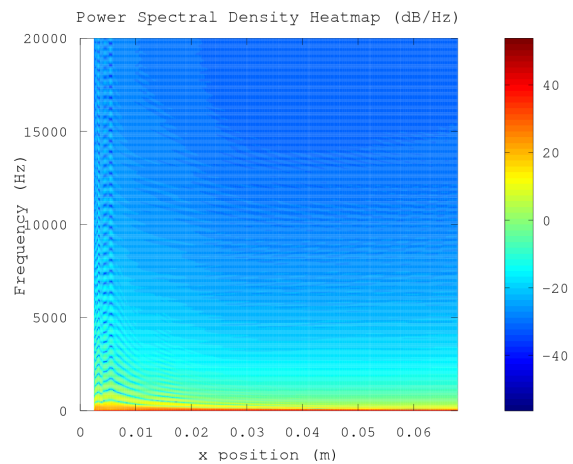
(d) Wide slot Wall Temp PSD
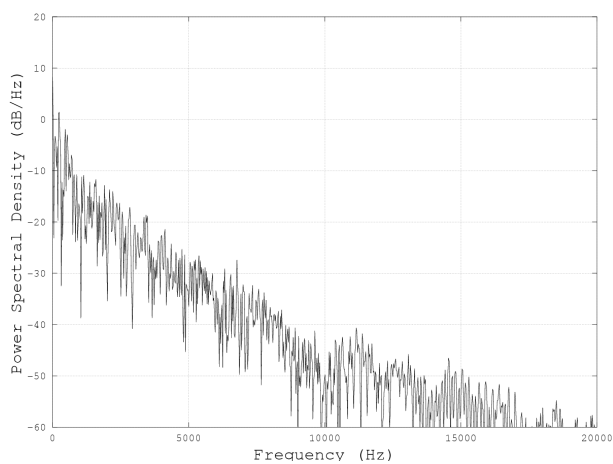
(e) Bent slot Flow field PSD
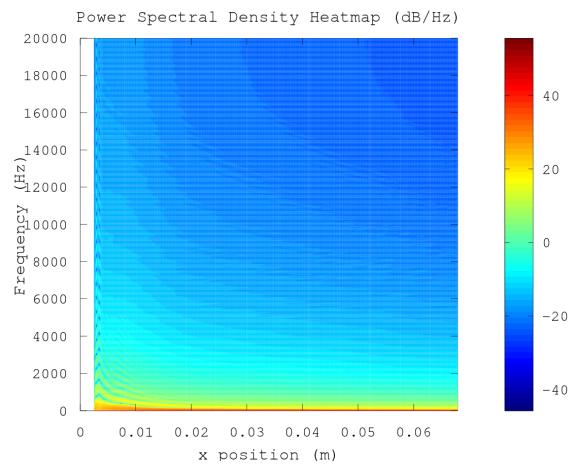
(f) Bent slot Wall Temp PSD

Figure 36. Power spectral density of flow field (left) and wall temperature (right) for the three cases.

These results do not have a strong driving frequency in either the flow field or the wall temperature. As a result, there is no clear Strouhal or Helmholtz number for these cases. They are unsteady flows, but not ones driven by one strong frequency; in the Wide slot, the unsteadiness is dictated by the recirculation region . The unsteadiness still has a strong impact on wall temperature, as seen in Figures 37 through 39.
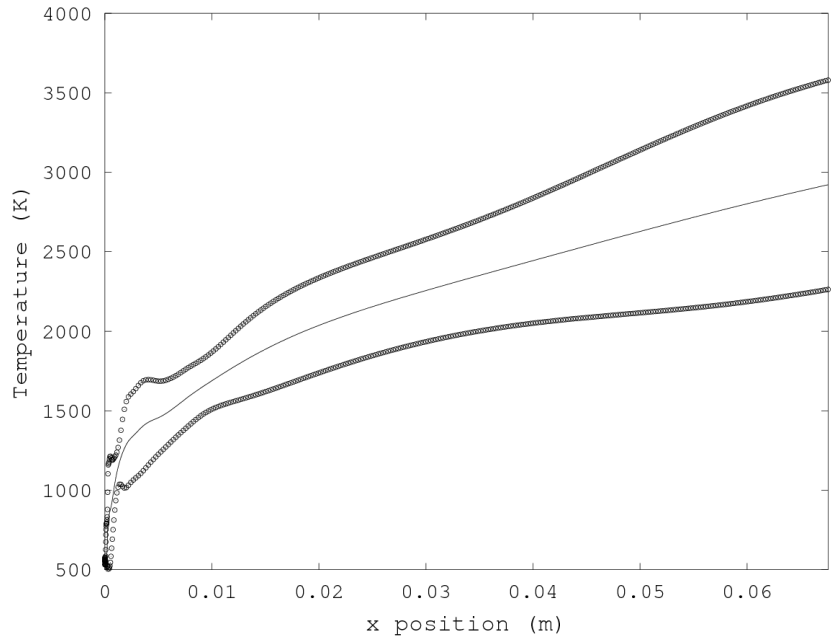
Figure 37. Average wall temperature in the Thin slot. The outer marks denote the amplitude of oscillation in wall temperature (one standard deviation in each direction).
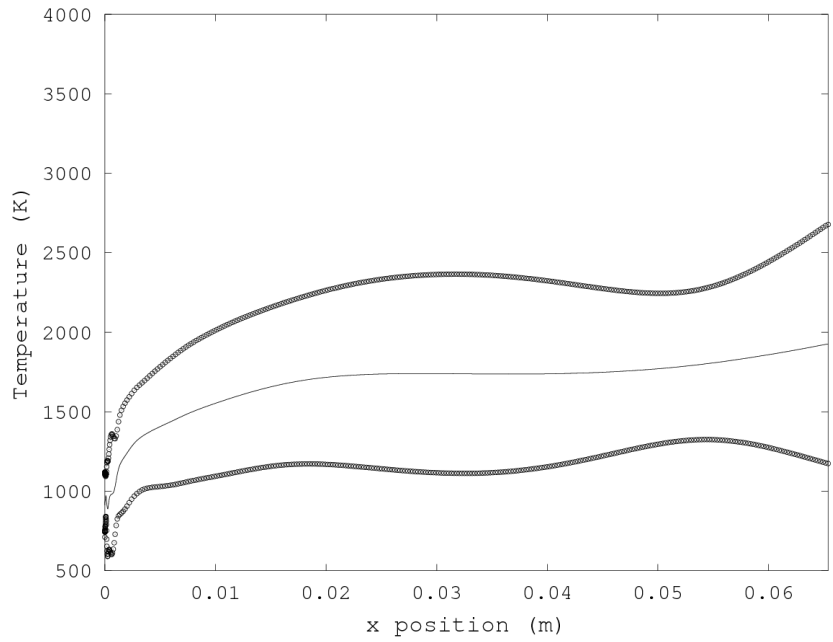
Figure 38. Average wall temperature in the Wide slot. The outer marks denote the amplitude of oscillation in wall temperature (one standard deviation in each direction).
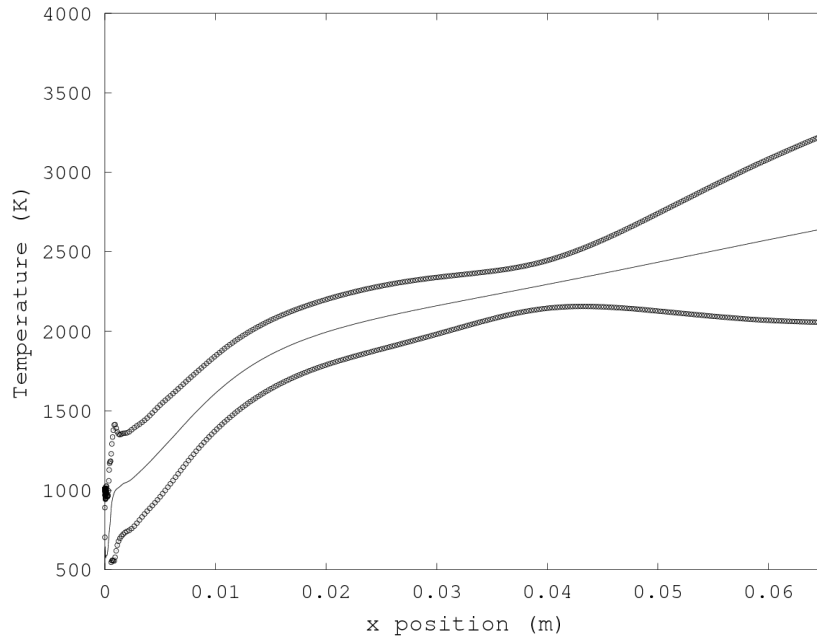
Figure 39. Average wall temperature in the Bent slot. The outer marks denote the amplitude of oscillation in wall temperature (one standard deviation in each direction).

These charts show a somewhat surprising result: the Wide slot had the highest adiabatic effectiveness of the three cases tested. This is of particular interest due to the recirculation region, as one could assume that a strong mixing region would heat up the fuel and react, breaking up the cooling layer before it even reaches the wall. However, it appears that the recirculation results in a much more diffuse film layer, which better shields the wall from hot exhaust gases.

It is worth mentioning that there is limited overlap with the experimental domain in these cases; due to the nature of the experimental hardware, there are limited data points in the same range as the computational domain. To address this fault, the bent slot geometry case is extended to have a much longer downstream region, covering the entirety of the experimental domain. Since this is a more costly simulation, it is only performed for the one case that most closely matches the experimental setup. Since the geometry of the FFC inlet is the same as the shorter case and frequency is not impacted by the far field, the frequency content is identical and omitted here. The time-averaged wall temperature profile is given in Figure 40.
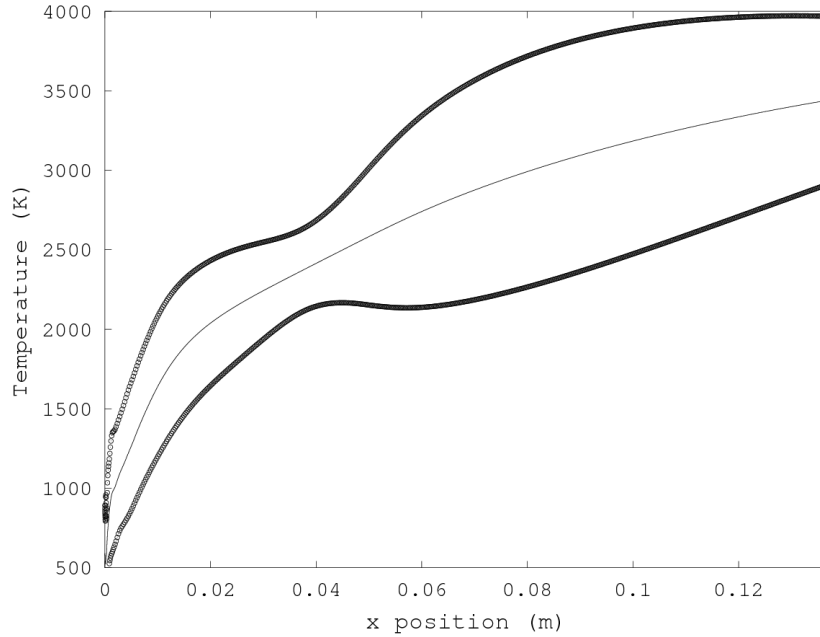
Figure 40. Average wall temperature in the extended version of the Bent slot. The outer marks denote the amplitude of oscillation in wall temperature (one standard deviation in each direction).

IV.G. Comparison to Experimental Results

Finally, we consider a comparison to experimental results. Because the walls in this simulation are adiabatic and the experimental setup from which the simulated conditions are drawn does not have adiabatic walls, a direct comparison is not possible. However, one can extrapolate a general trend in wall temperature data from the experimental results, and these can be compared to look at trends. Figure 41 shows how adiabatic efficiencies for all of the parametric studies compare to that one might expect from experimental results. Also included are some recent results from in-house experiments that more accurately record wall temperature, allowing for a better comparison to these results. This experiment used a chamber pressure of 700 psi, a mixture ratio of 2.8, and 2% FFC flow rate, which is almost identical to the baseline case simulated.

Experimental measurements of heat flux and wall temperature were used to estimate adiabatic wall temperature and adiabatic efficiency. The heat flux to a cooled wall q''_{FFC}, the film cooled wall temperature T_w, the heat flux to an uncooled wall q''_0, and the uncooled wall temperature $T_{w,0}$ can be used to estimate adiabatic wall temperature as follows:

$$q''_{FFC} = q''_0 \frac{T_{aw}-T_w}{T_\infty-T_{w,0}}$$
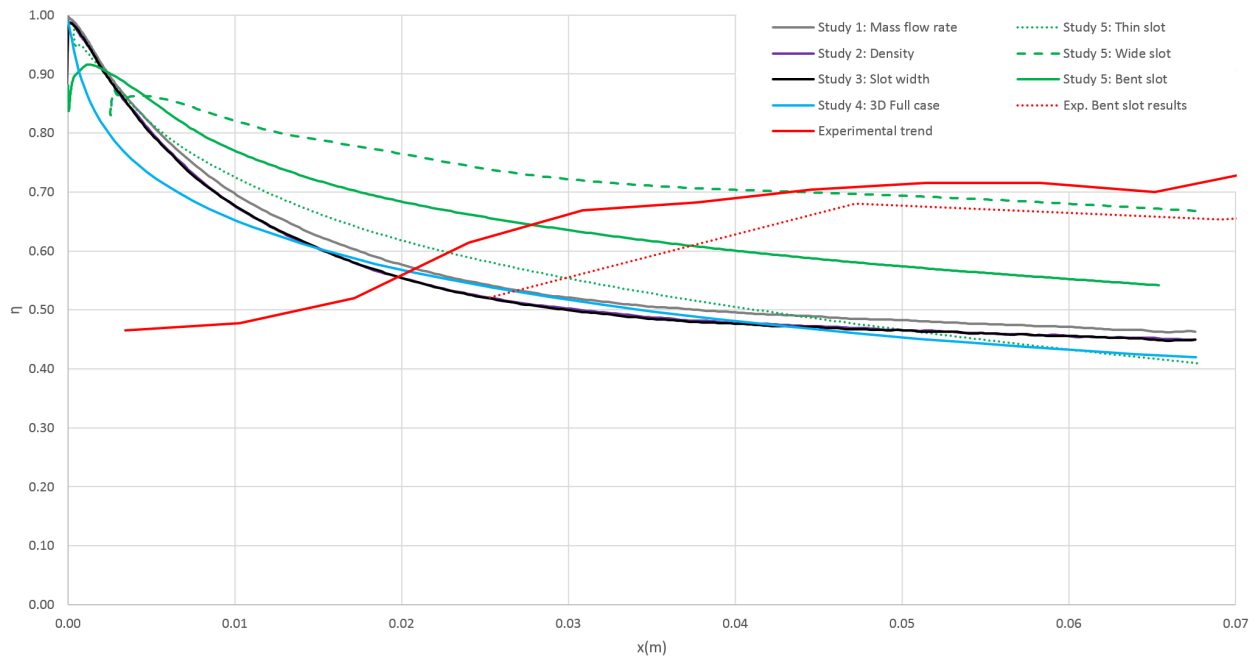
Figure 41. Experimental trend versus simulations for adiabatic effectiveness.

The extended bent slot case is show separately in Figure 42, to show how the adiabatic effectiveness compares against experimental results in the far field.
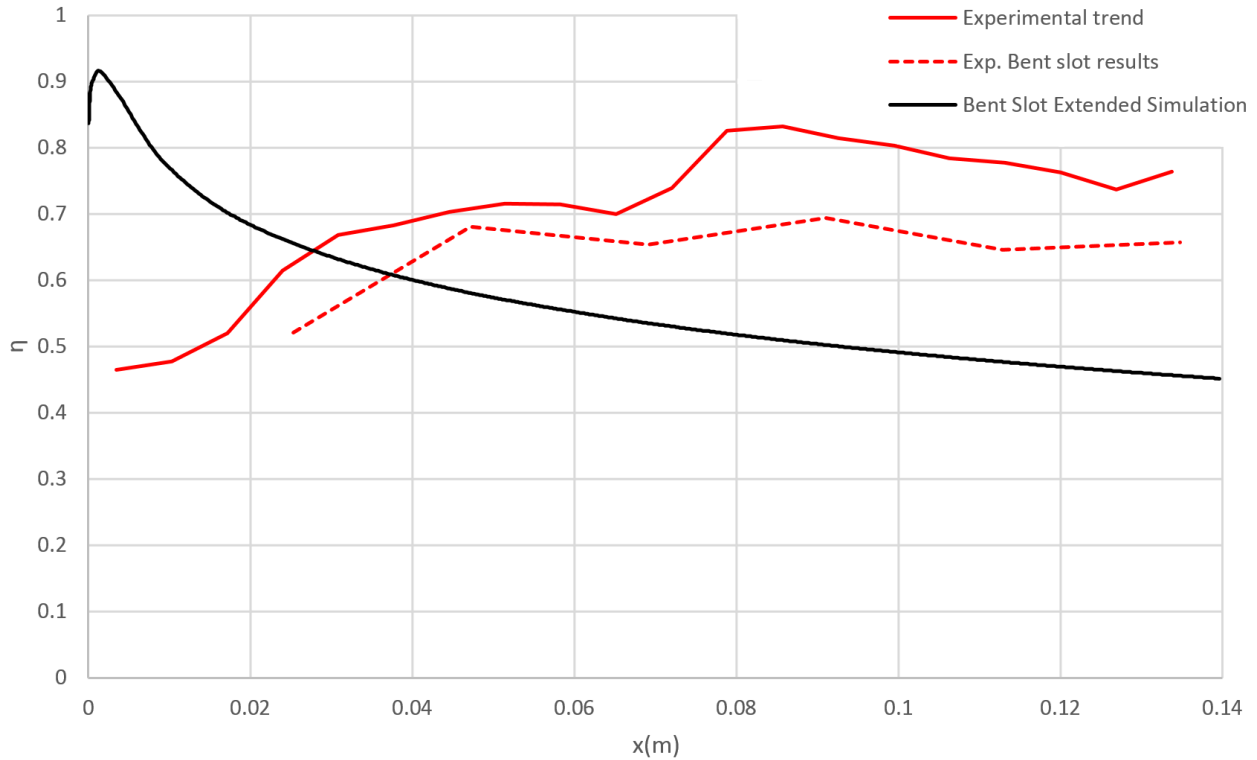
Figure 42. Experimental trend versus extended domain simulation for adiabatic effectiveness.

While the shorter domains appear to approach experimental results further downstream of the inlet, this

case shows that this does not necessarily remain true in the far downstream regions. While the experimental film cooling effectiveness increases with distance before tapering off as the fuel is consumed, simulations show a monotonic decrease throughout. It is clear from these results that, although simulations seem to point towards a definitive adiabatic effectiveness profile, all of the simulations follow a trend that is the inverse of that seen in the experimental results. Experiments have shown a higher heat flux close to the FFC inlet, with a lower heat flux being reported further downstream. By contrast, the simulations show the lowest heat flux adjacent to the FFC inlet, with the heat flux increasing monotonically and asymptotically as distance from the slot increases. This trend is observed in all the simulated cases. While there are several possible explanations for this discrepancy (to be expanded upon in the conclusions), the primary take away is that the fluid mechanical effects explored in these simulations are not sufficient in and of themselves to capture the effects of fuel film cooling on wall temperature.

V. Conclusions

By performing three parametric studies over a range of conditions, it was determined that the primary driver of adiabatic effectiveness for a given FFC geometry is the mass flow ratio of the fuel coolant to the main chamber. The effect of mass flow ratio on film cooling effectiveness was already known, but this work clarified that relationship by isolating other variables to study individual effects. Varying overall flow rates did not have a noticeable impact, and modifying the slot width also did not seem to have a large impact.

The predicted results indicate that the unsteadiness of the fuel film can be significant with the frequency of the oscillations being driven in the FFC inlet, which acts as an acoustic resonant cavity. The results show a switch from a lower frequency mode to a higher frequency, which seems to be related to the interactions of the cavity with the main flow. The assumption of an ideal gas equation of state for the FFC inlet means that the unsteady dynamics in these simulations may be significantly different from those at real LRE operating conditions.

The second parametric study, which was centered on varying fuel density, found that there was a small correlation between fuel density and film cooling effectiveness. This suggests that density, while not as strong a driver as mass flow ratio, still plays some role in the effectiveness of a given FFC scheme. While this cannot easily be changed experimentally, it does suggest that a more realistic modeled density will lead to more accurate FFC simulations. Introducing a real gas equation of state such as Peng-Robinson should yield more accurate wall temperatures.

Three-dimensional simulations show the presence of strong transverse waves, with are of a lower frequency than the acoustic resonator waves seen in 2D. These transverse waves prevent a strong resonance from forming, resulting in a less unsteady fuel film. However, when periodic walls are used in a 3D simulation, the acoustic resonance behavior is recovered, suggesting that these transverse waves may only dominate in FFC inlets that are not very wide. As a consequence, the 3D simulations may better model the experimental setup used, but are perhaps not representative of the long circumferential slots used in modern rocket engines.

The final parametric study, which focuses on inlet shapes, reveals that inlet shape plays a large role in overall cooling effectiveness. While the simple slot has a strong acoustic resonance, the wide cavity's strong recirculation zone prevents a strong wave from forming, resulting in a longer-lived fuel film that better shields the wall from hot gases. The bent slot geometry suggests that when such acoustic resonances do form, they are largely confined to the section of inlet closest to the injection point. This suggests that for a first approximation of unsteady behavior for a complex FFC inlet, internal geometries do not need to be modeled far upstream of the film-gas interface.

Discrepancies between experimental results and these simulations suggest that additional physics unaccounted for by these simulations may play a significant role in both increasing the heat flux neat the FFC inlet and decreasing the heat flux further downstream. One likely culprit is the deposition of soot on walls downstream of the FFC inlet. As the fuel film interacts with the hot freestream gases, it undergoes hydrocarbon cracking and soot particulates form, depositing on the wall and creating a thermal barrier coating. Soot deposition has been observed experimentally[5] to increase in thickness as it gets further downstream from the FFC inlet, with the area immediately downstream of the inlet having no soot deposits at all. This corresponds with the observed wall temperature profiles. However, this may be conflating cause and effect; it is also possible that lower wall temperatures lead to increased deposition due to thermophoresis.

VI. Future Work

With a large parametric study of the simple FFC geometry complete, there are several interesting directions this work can take. One would be to hone in on two or three cases of interest for a full three-dimensional study. Another would be the introduction of a real gas model, and comparisons of accuracy between different equations of state. A third direction would be to introduce additional physics such as a radiative heat transfer model to attempt to address the deficiencies between simulated and experimental wall temperature profiles. And finally, the geometry of the FFC inlet can be tailored to better match the inlet geometries used in actual LREs.

References

[1]Lawson, S., Barakos, G., "Review of Numerical simulations for high-speed, turbulent cavity flows," *Progress in Aerospace Sciences*, Vol. 47, pp. 186-216, February 2011.

[2]Colonius, T., "An Overview of Simulation, Modeling, and Active Control of Flow/Acoustic Resonance in Open Cavities," *39th AIAA Aerospace Sciences Meeting and Exhibit*, Reno, NV, 2001.

[3]Rowley, C., Colonius, T., Basu, A., "On Self-sustained Oscillations in Two-dimensional Compressible Flow Over Rectangular Cavities," *Journal of Fluid Mechanics*, Vol. 455, pp. 315-346, 2002.

[4]Himansu, A., Coy, E., Sankaran, V., and Danczyk, S., "Modeling of Fuel Film Cooling on Chamber Hot Wall," *50th AIAA/ASME/SAE/ASEE Joint Propulsion Conference*, Cleveland, OH, July 2014.

[5]Coy, E., and Danczyk, S., "Film Cooling of Combustion chambers with Liquid Hydrocarbon Fuels," *JANNAF 6th LPS Meeting*, Huntsville, AL, Dec. 2011.

[6]Yu, C.Y., Schuff, R.Z., Anderson, W.E., "Liquid Film Cooling Using Swirl in Rocket Combustors," *40th AIAA/ASME/SAE/ASEE Joint Propulsion Conference*, 2004.

[7]Shine, S.R., Kumar, S.S., Suresh, B.N., "A New Generalized Model for Liquid Film Cooling in Rocket Combustion Chambers," *International Journal of Heat and Mass Transfer*, 55, pp. 5065-5075, 2012.

[8]Zhang, H.W., Tao, W.Q., He, Y.L., Zhang, W., "Numerical Study of Liquid Film Cooling in a Rocket Combustion Chamber," *International Journal of Heat and Mass Transfer*, 49, pp. 349-358, 2006.

[9]Rutledge, J., King, P., Rivir, R., "CFD Predictions of the Frequency Dependence of Pulsed Film Cooling Heat Flux on a Turbine Blade Leading Edge," *47th AIAA Aerospace Sciences Meeting*, Orlando, FL, 2009.

[10]Li, D., Sankaran, V., Xia, G., Merkle, C., "Computational Framework for Complex Fluids Applications," *Computational Fluid Dynamics 2004*, pp. 619-624, Berlin, Springer Berlin Heidelberg, 2006.

[11]Xia, G., Sankaran, V., Li, D., Merkle, C., "Modeling of Turbulent Mixing Layer Dynamics in Ultra-High Pressure Flows," *36th AIAA Fluid Dynamics Conference and Exhibit*, San Francisco, CA, AIAA Paper No. 2006-3729, 2006.

[12]Lian, C., Xia, G., Merkle, C., "Impact of Source Terms on Reliability of CFD Algorithms," *Computers and Fluids*, Vol. 39, pp. 1909-1922, June 2010.

[13]Lian, C., Xia, G., Merkle, C., "Solution-Limited Time Stepping to Enhance Reliability in CFD Applications," *Journal of Computational Physics*, Vol. 228, pp. 4836-4857, 2009.

[14]Wilcox, D., "Formulation of the k-ω turbulence model revisited," *AIAA Journal*, Vol. 46, No. 11, pp. 2823-2838, January 2008.

[15]Travin, A., Shur, M., Spalart, P., "Physical and numerical upgrades in the detached-eddy simulation of complex turbulent flows," *Fluid Mechanics and Its Applications*, Vol. 65, pp. 239-254, 2002.

[16]Spalart, P., "Detached Eddy Simulations," *Annual Review of Fluid Mechanics*, Vol. 41, pp. 181-202, 2009.

[17]Westbrook, C., Dryer, F., "Simplified Reaction Mechanisms for the Oxidation of Hydrocarbon Fuels in Flames," *Combustion Science and Technology*, Vol. 27, pp. 31-43, 1981.

[18]Salazar, D., Forliti, D., Kuzmich, K., and Coy, E., "Near-Wall Velocity Field Measurements of a Very Low Momentum Flux Transverse Jet," *50th AIAA/ASME/SAE/ASEE Joint Propulsion Conference*, Cleveland, OH, July 2014.

[19]Sarohia, V., Massier, P., "Control of Cavity Noise," *AIAA Journal of Aircraft*, Vol. 14, No. 9, pp. 833-837, September 1977.

[20]Dimotakis, P.E. "Two-dimensional shear-layer entrainment," *AIAA Journal*, Vol. 24, No. 11, pp. 1791-1796, 1986.

[21]Wegener, J.L., Forliti, D.J., Leyva, I.A., Talley, D.G, "Receptivity of a Cryogenic Coaxial Gas-Liquid Jet to Acoustic Disturbances," *50th AIAA/ASME/SAE/ASEE Joint Propulsion Conference*, Cleveland, OH, July 2014.

[22]Goldstein, R.J., "Film Cooling," *Advances in Heat Transfer*, Vol. 7 pp. 321-379, 1971.

[23]Brown, K., Coy, E., Harvazinski, M., and Sankaran, V. "Modeling of Fuel film Cooling Using Steady State RANS and Unsteady DES Approaches," *52nd AIAA/ASME/SAE/ASEE Joint Propulsion Conference*, Salt Lake City, UT, 2016.

[24]Eckert, E.R.G., Drake, R.M., "Analysis of Heat and Mass Transfer," McGraw Hill, 1972.

2D and 3D Modeling Efforts in Fuel Film Cooling of Liquid Rocket Engines

15 November 2016

Kevin Brown

Edward Coy

Venkateswaran Sankaran

Integrity ★ Service ★ Excellence

Overview

- **Introduction**

- **Numerical Models**

- **Parametric Studies**

- **Results**
  - 2D
  - 3D
  - Varying inlet geometry

- **Comparison with experiments**

- **Conclusions and Future Work**

Introduction

- **Fuel film cooling (FFC) is a required technology for modern rocket engines**

- **Too little cooling = exceed wall temperature limit**

- **Too much cooling = I_{sp} decrease**

- **Difficult to model computationally**

- **Supercritical conditions**

- **Complex chemistry**

- **Soot buildup**

- **Radiative heat transfer**
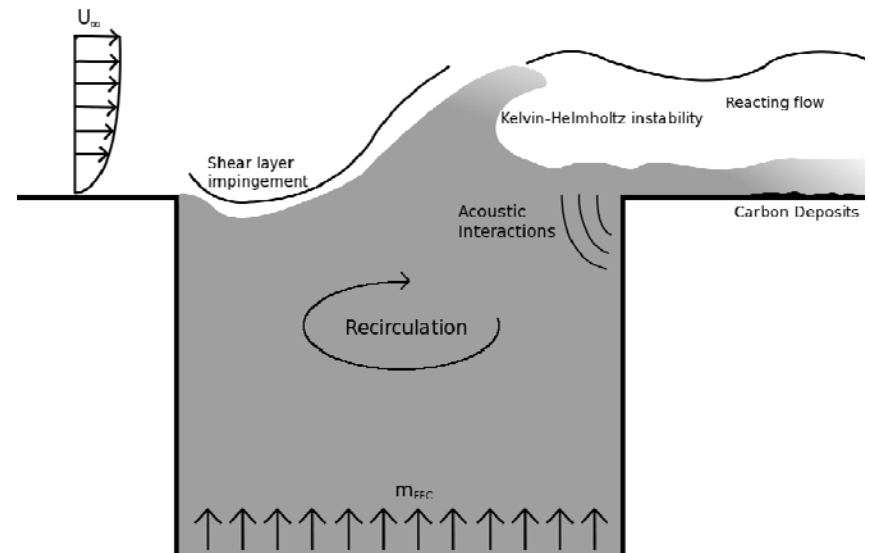
Introduction

- **New additions to fluid model:**
  - Time-accurate unsteady flow simulations
  - Detached Eddy Simulations (DES)
  - Can modify molecular weight to change density
- **Limitations of fluid model:**
  - Does not include soot deposition
  - Does not include Radiative heat transfer
  - Does not include real gas EOS
- **As a result, experimental trends could not be replicated**

Introduction

- **Previous work was steady state, failed to predict heat fluxes**

- **Objectives:**
  - **Determine if unsteady fluid mechanics drive effectiveness**
  - **Determine differences between 2D and 3D simulations**
  - **Determine impact of inlet geometry on effectiveness**

Numerical Models

- Using GEMS – finite volume code developed by Purdue

- Ideal gas law used

- RANS used for setting up initial condition

- Detached Eddy Simulations (DES) used for main computation
  - k-ω turbulence model

- Simplified chemical kinetics used

- Conjugate heat transfer not used – adiabatic walls used instead to decrease computational cost

Parametric Studies

- **5 Parametric studies:**
  - Varying mass flow rates
  - Varying fuel density
  - Varying FFC inlet slot width
  - 3D study
  - Inlet geometry effects

- **All vary around a baseline case for comparison**

Baseline Case

Pressure (MPa)	5.2	Slot width (m)	5.6×10^{-4}
FFC temperature (K)	350	Main chamber temperature (K)	3680
FFC mass flow rate (kg/s)	0.41	Main chamber mass flow rate (kg/s)	25.64
FFC density (kg/m^3)	638	Main chamber density (kg/m^3)	4.4
Density ratio	145	Momentum ratio	7.9×10^{-5}
Mass flow ratio	0.015	Main chamber Mach number	0.2

Baseline Case
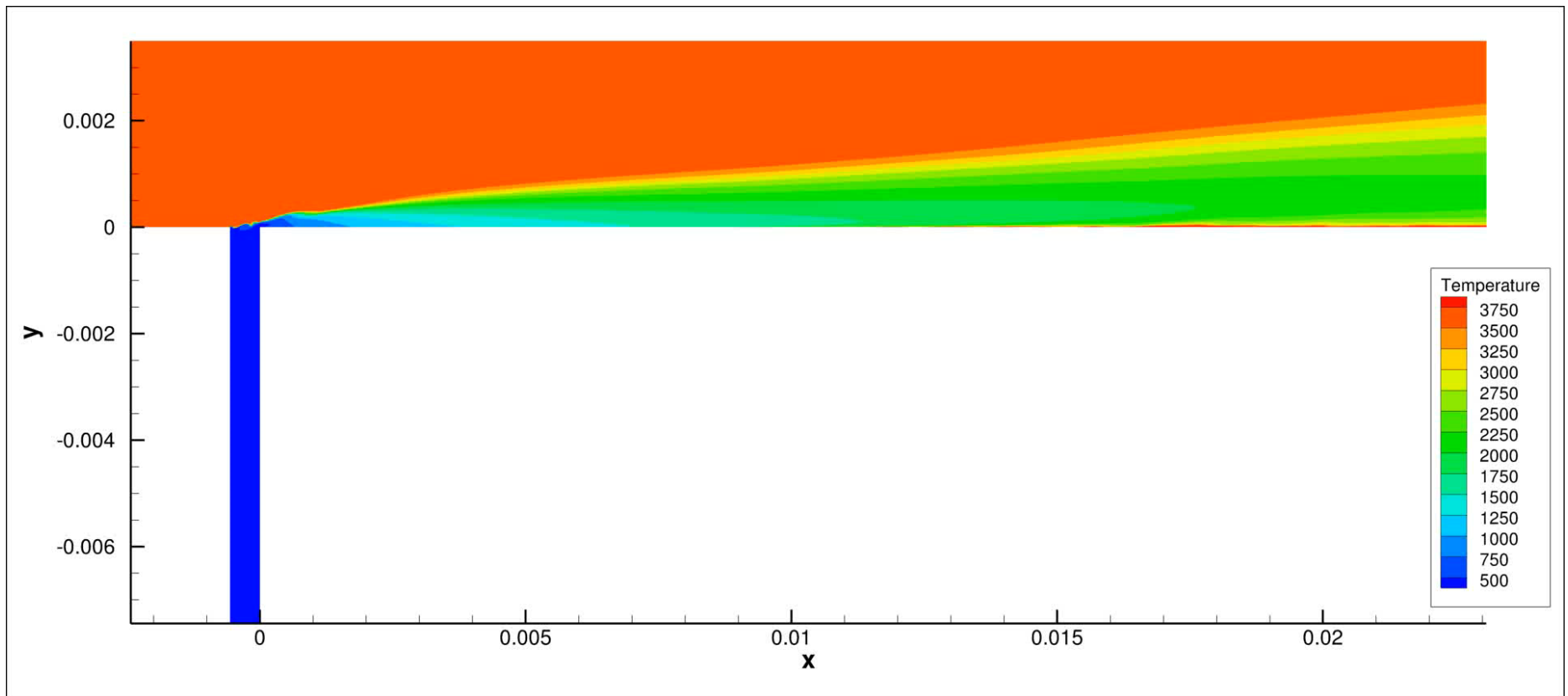
Baseline Case

Study 1: Varying Mass Flow Rates

- **Varied main chamber mass flow rate, FFC mass flow rate, or both**

- **Same geometry for all cases in this study**

- **Total of 21 cases**

Main Chamber Inlet
(hot combustion products)

Outlet

FFC Inlet
(cold fuel)
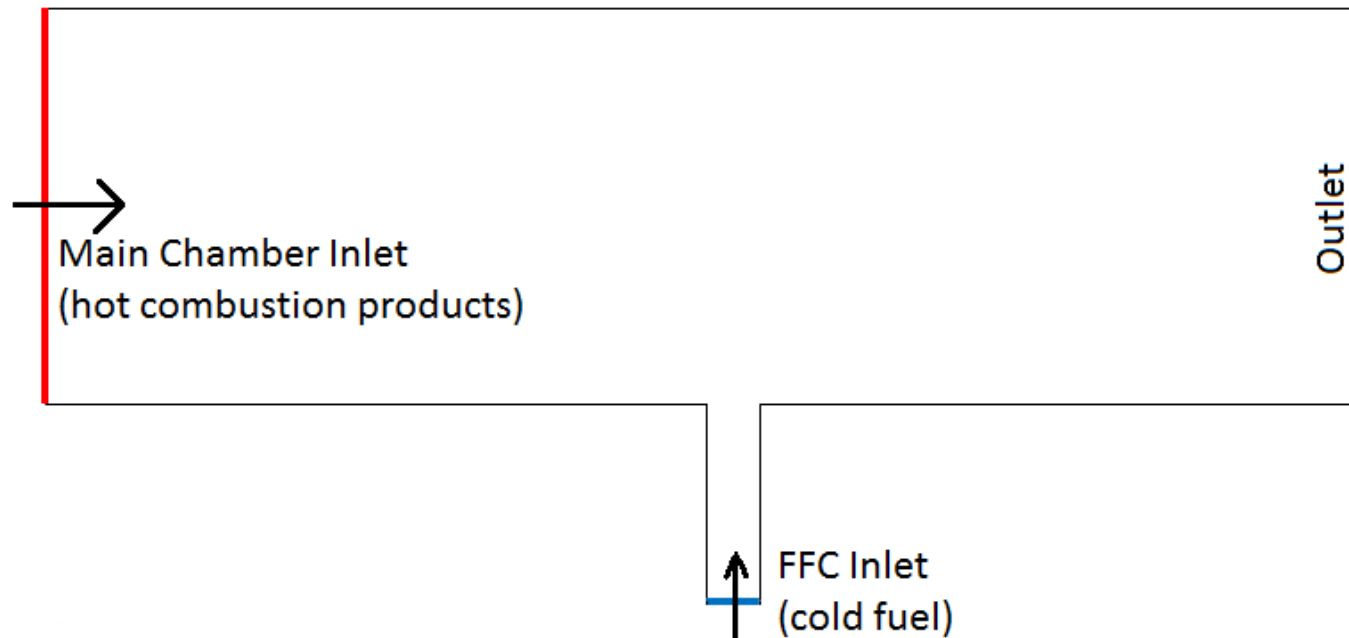
Study 1: Varying Mass Flow Rates

Mass flow rates vary, constant density/slot width

FFC Velocity (m/s)	0.7 - 5.4	Main Velocity	50 - 371	Main Mach	0.05 - 0.32
FFC Density (kg/m^3)	638	Main Density	4.41	Density Ratio	145
M	1.0E-02 - 7.5E-02	J	3.0E-05 - 1.7E-03	Slot width (m)	5.59E-04

Study 1: Varying Mass Flow Rates
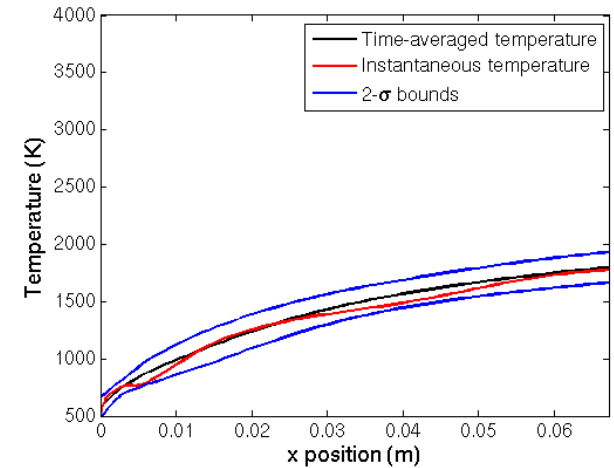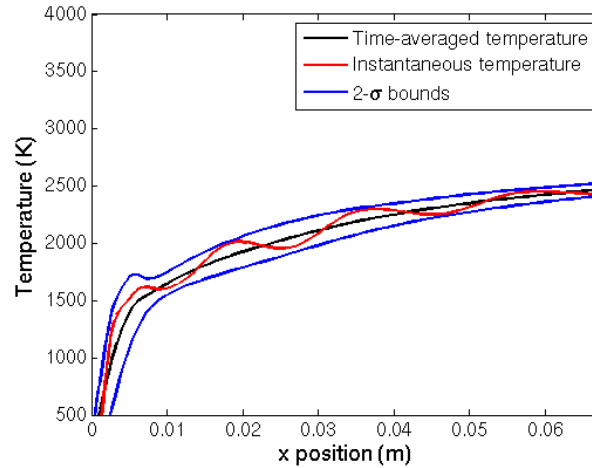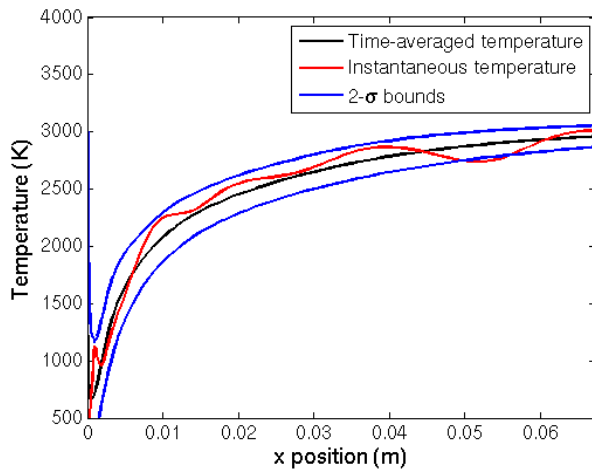
↑ Temperature ↑

→ Increasing mass flow ratio →

↓ PSD ↓
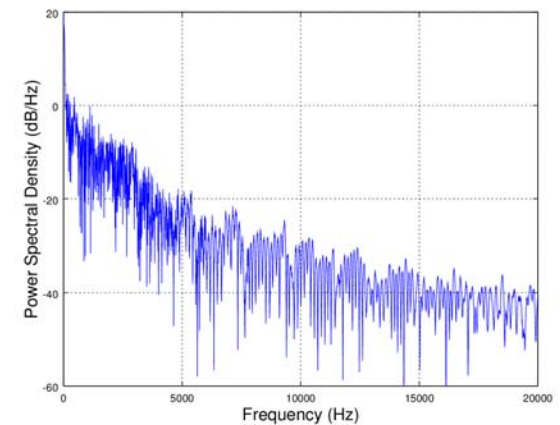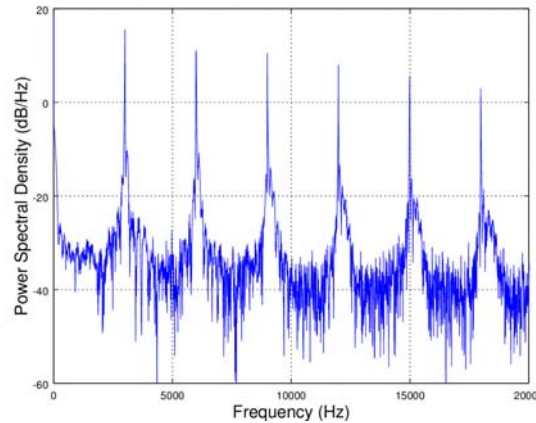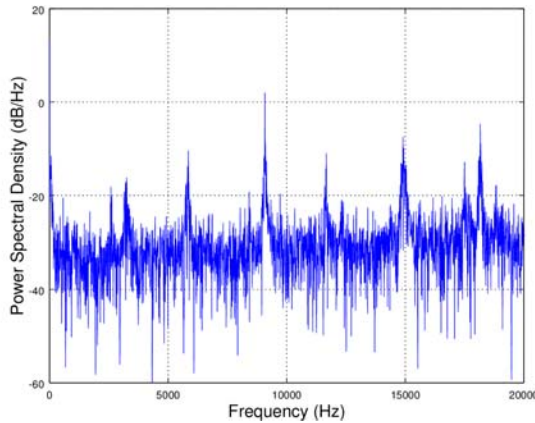
Study 2: Varying Density

- **Mass flow rates held constant, density varied**
- **Slot width also varied to preserve momentum ratio**

$d \, (\mathrm{m} \times 10^{-4})$	$\rho \, (\mathrm{kg/m^3})$
11.4	145.02
7.46	221.45
5.59	295.45
4.79	344.72
3.83	430.95
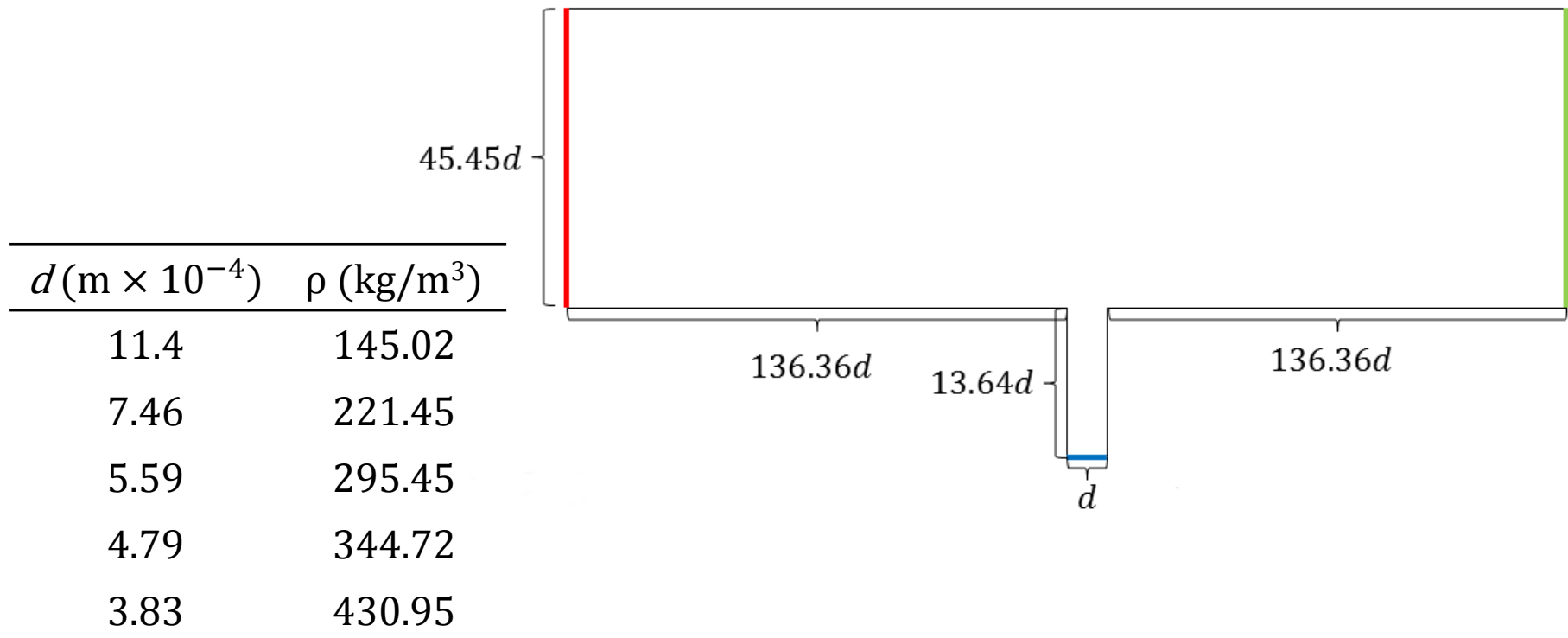
Study 2: Varying Density

Density varies, slot width varies, constant mass flow/momentum

FFC Velocity (m/s)	2.12	Main Velocity	233.4	Main Mach	0.2
FFC Density (kg/m^3)	145 - 430	Main Density	4.411	Density Ratio	33-98
M	1.40E-02	J	1.20E-04	Slot width (m)	3.8E-04 - 1.1E-03

Study 2: Varying Density
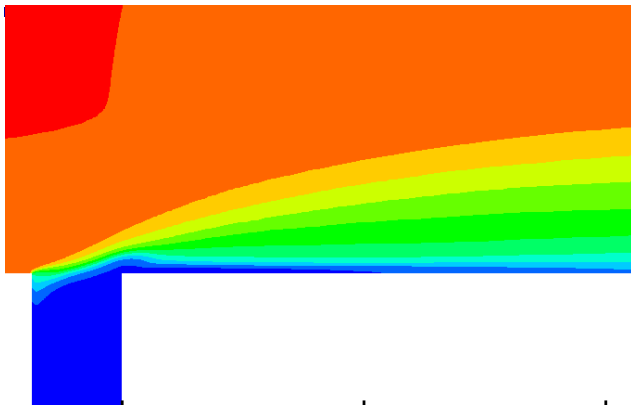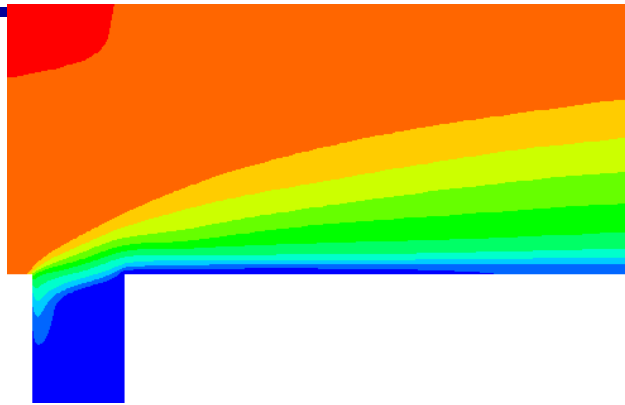
75% Density   100% Density   125% Density
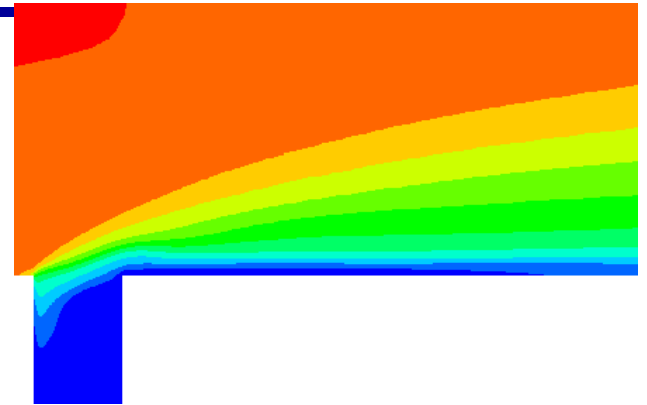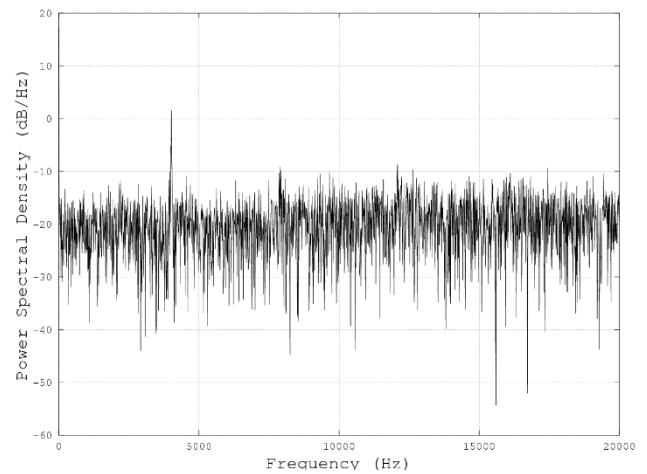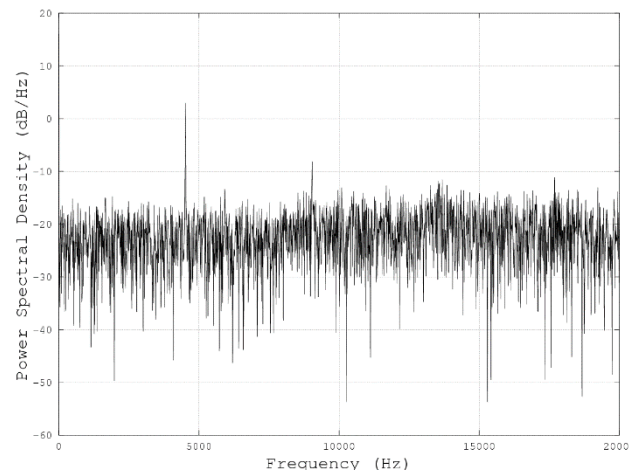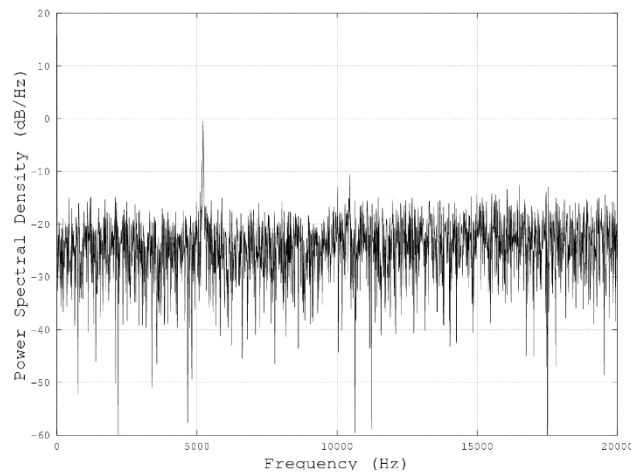
Study 3: Varying slot width

- **Same grids as study 2, density constant**
- **Mass flow ratio constant, momentum ratio varies**
- **Same temperature profiles as study 2**
- **Frequency steady**
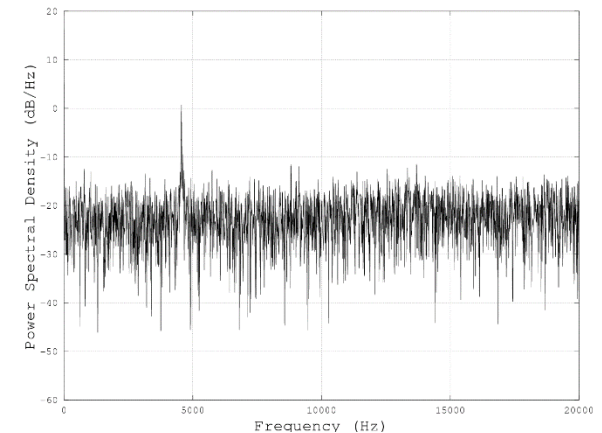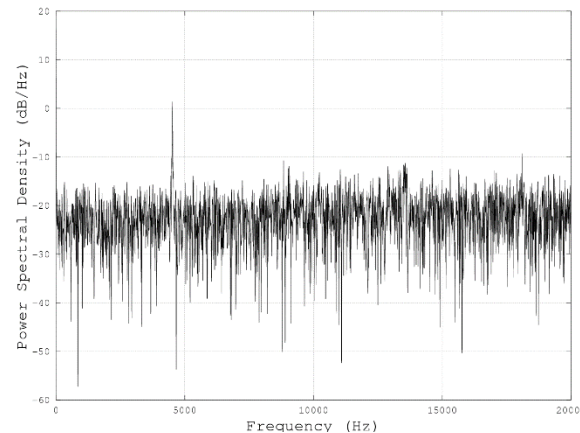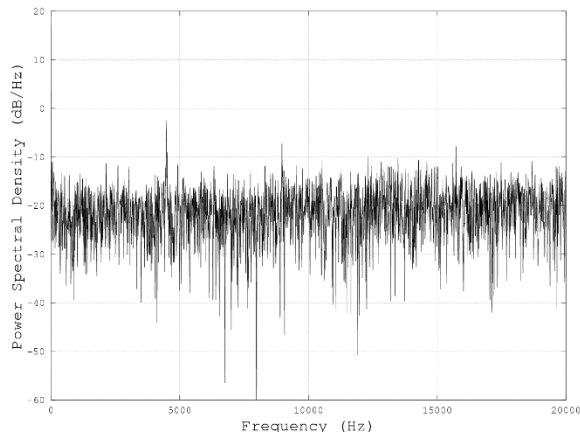
Increasing slot width

Study 3: Varying slot width

				Slot width varies, constant density/mass flow			
FFC Velocity (m/s)	1.04 - 3.09	Main Velocity	233.4	Main Mach	0.2
FFC Density (kg/m^3)	295.45	Main Density	4.411	Density Ratio	67
M	1.40E-02	J	6.1E-05 - 1.8E-04	Slot width (m)	3.8E-04 - 1.1E-03

Studies 1-3: Comparing Results

- **Can characterize unsteadiness using Strouhal number and Helmholtz numbers:**

$$\text{St}_c = \frac{fd}{U_c} \quad \text{He} = \frac{2\pi f}{c} L \quad U_c = \frac{U_1 \rho_1^{1/2} + U_2 \rho_2^{1/2}}{\rho_1^{1/2} + \rho_2^{1/2}}$$

f = frequency   c = speed of sound

d = slot width   L = slot depth

U_c = convection velocity U_1 = main chamber velocity, U_2=FFC velocity

- **Can nondimensionalize temperature profiles as η :**

$$\eta = \frac{T_\infty - T_{aw}}{T_\infty - T_f}$$

T_∞ = freestream temperature T_{aw} = adiabatic wall temperature

T_f = FFC inlet temperature

Study 1: Varying Main mass flow
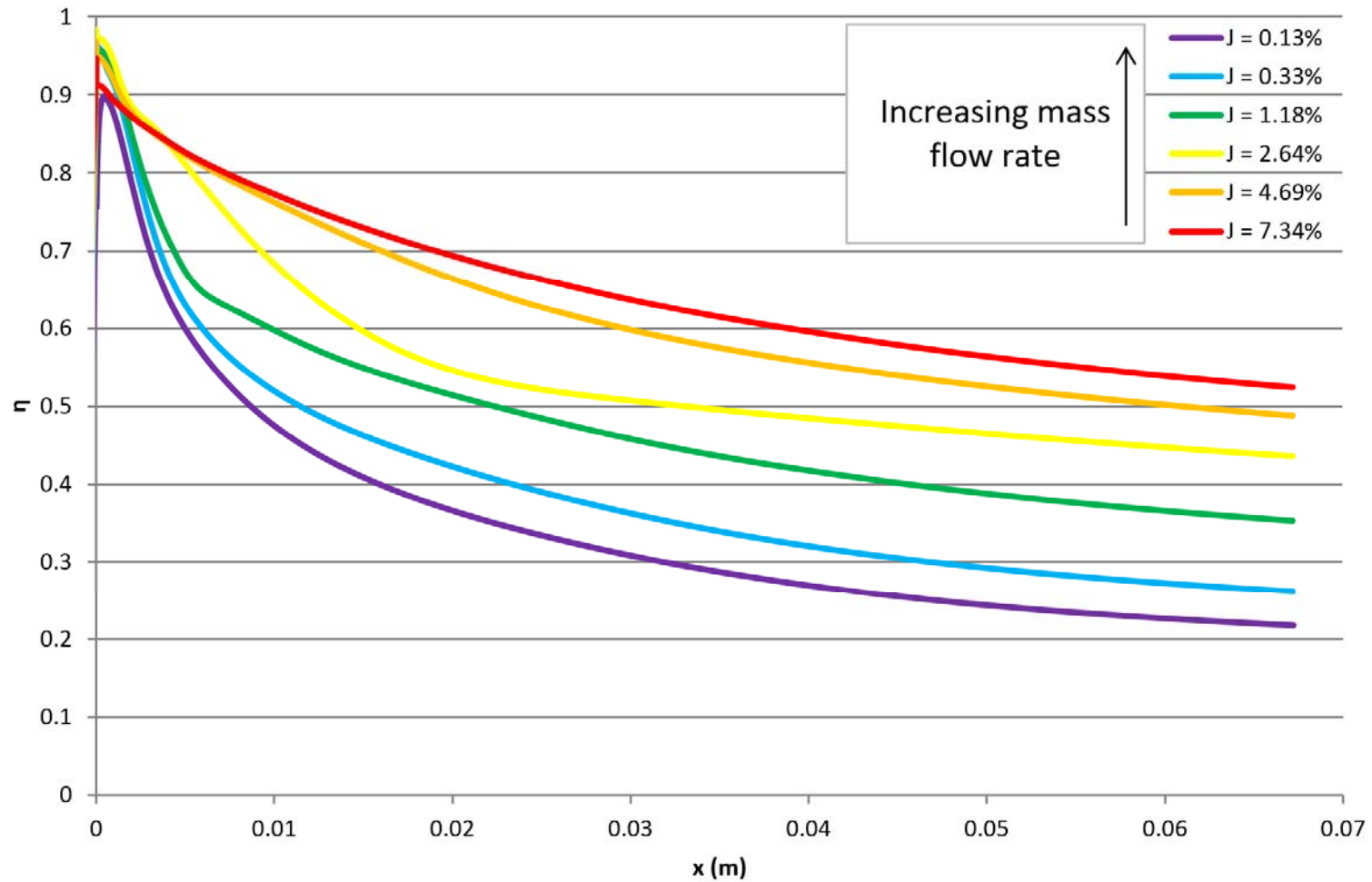
Study 2: Varying density
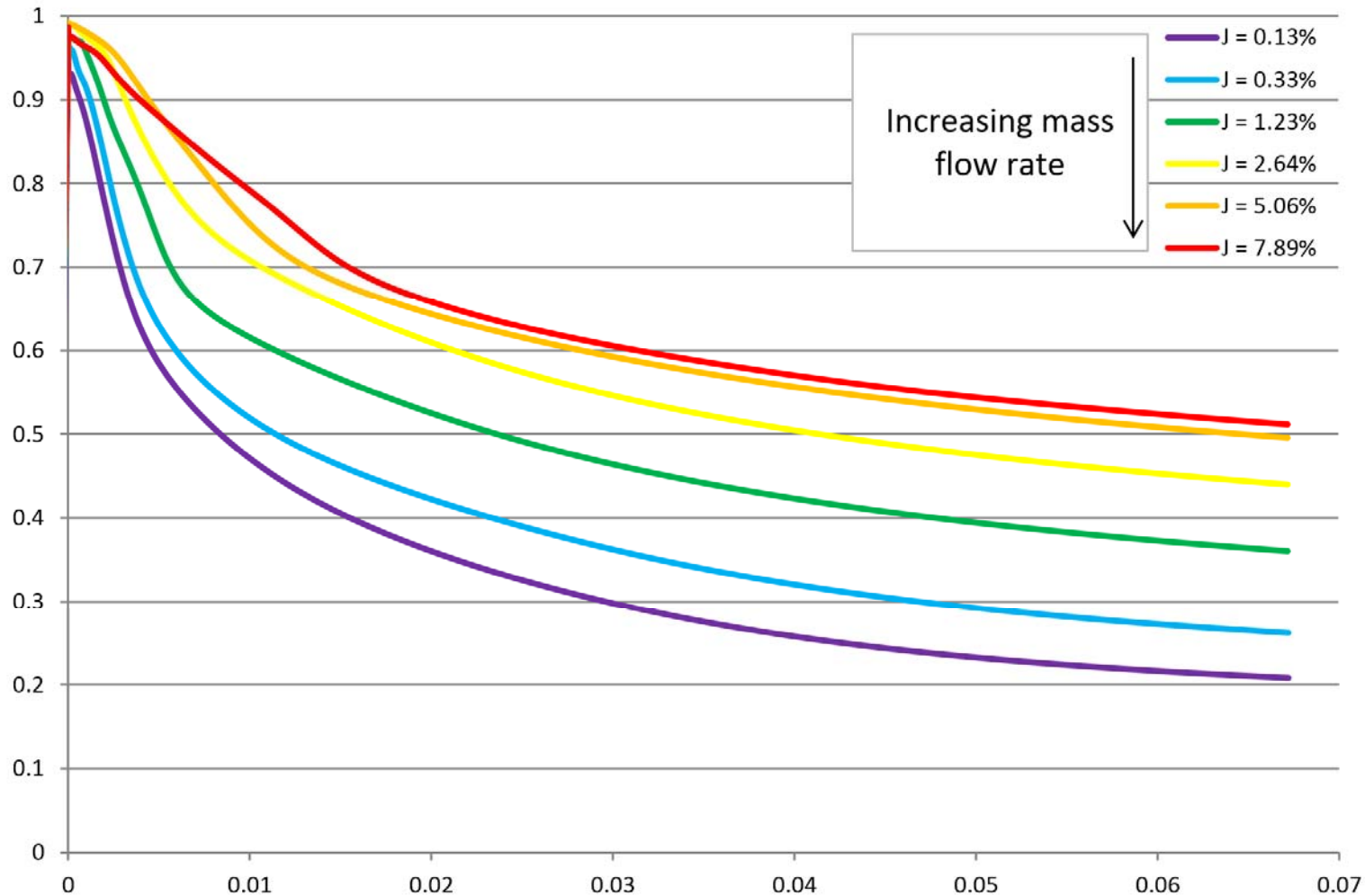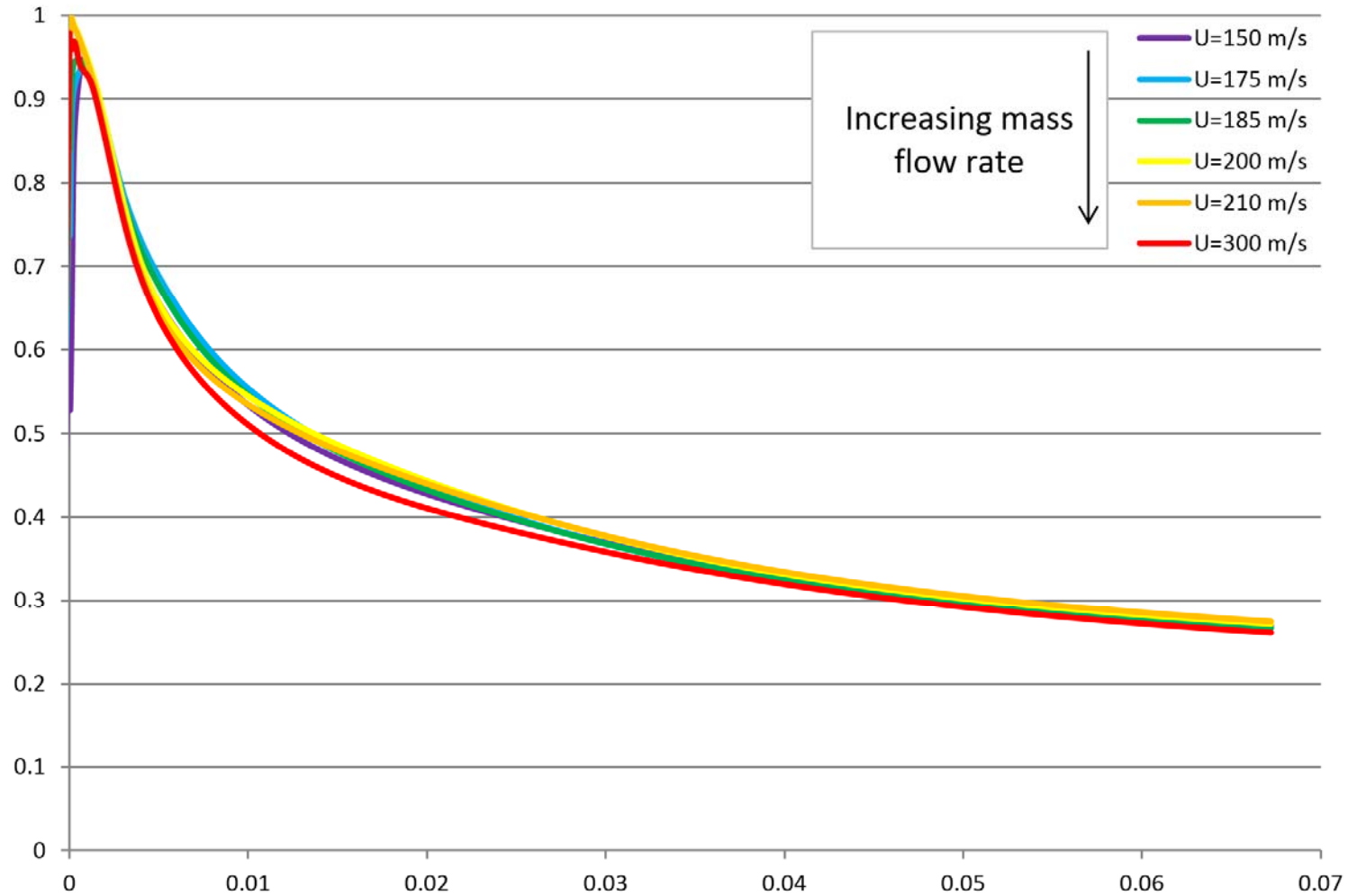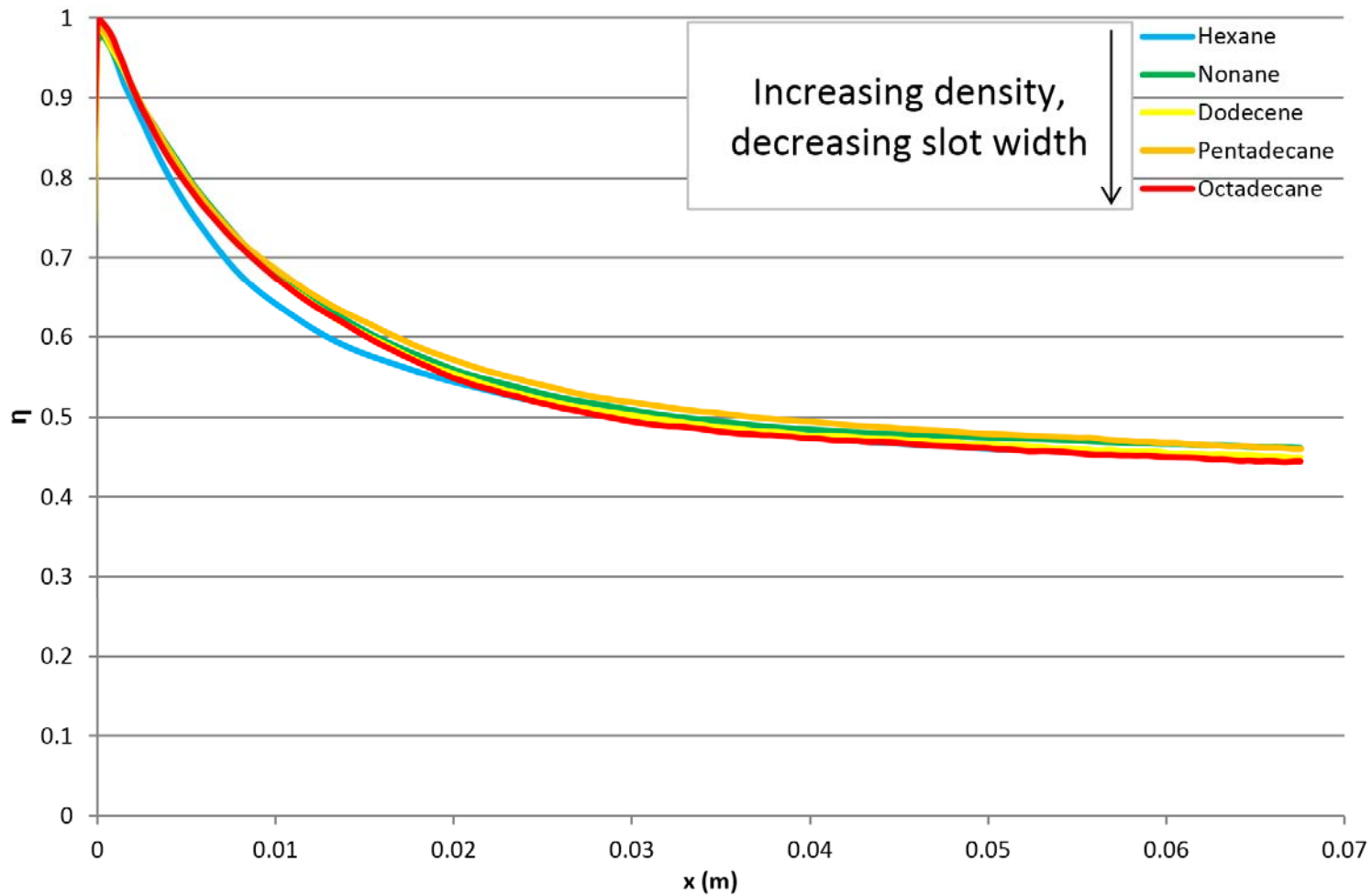
Study 3: Varying slot width
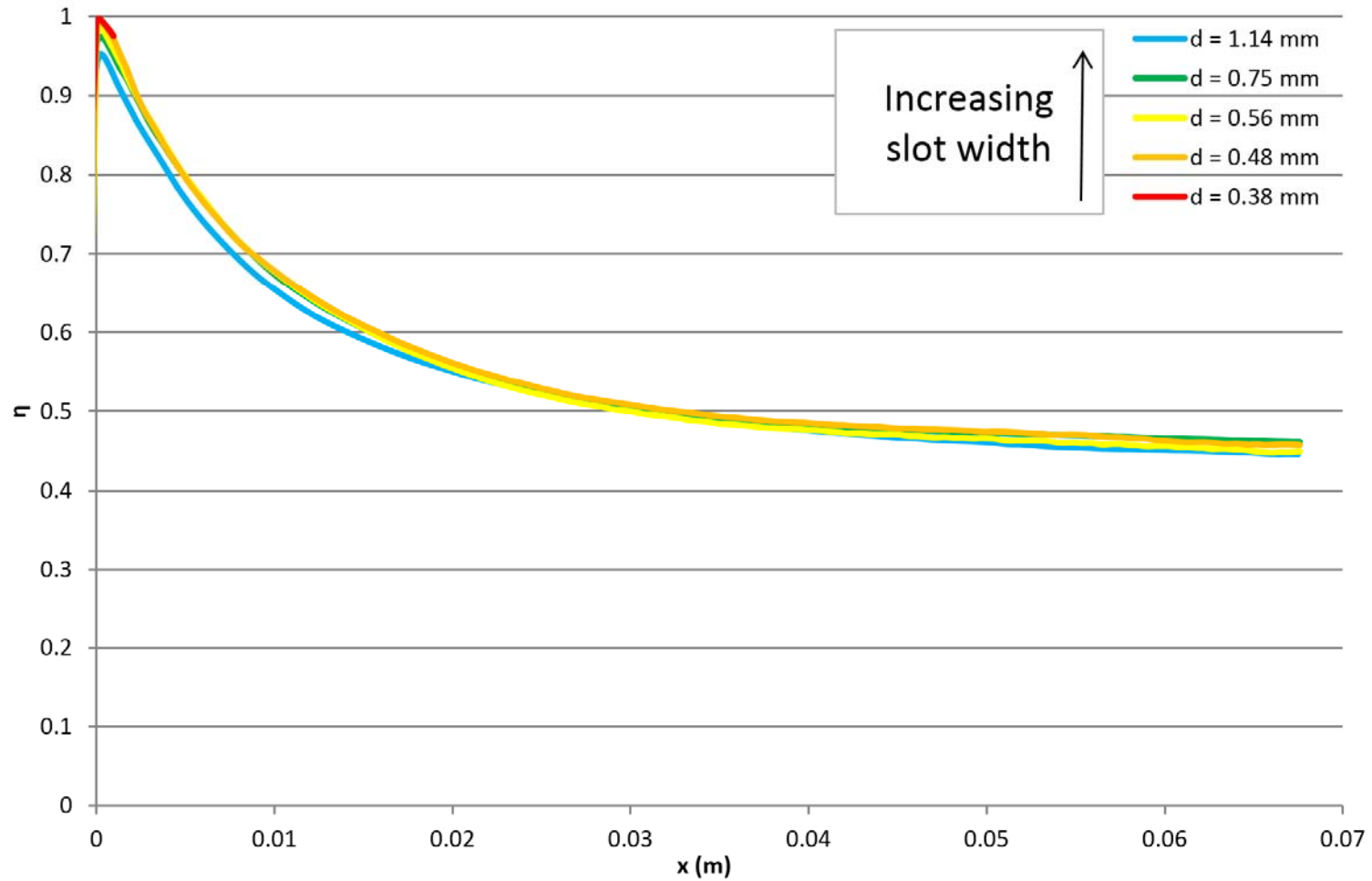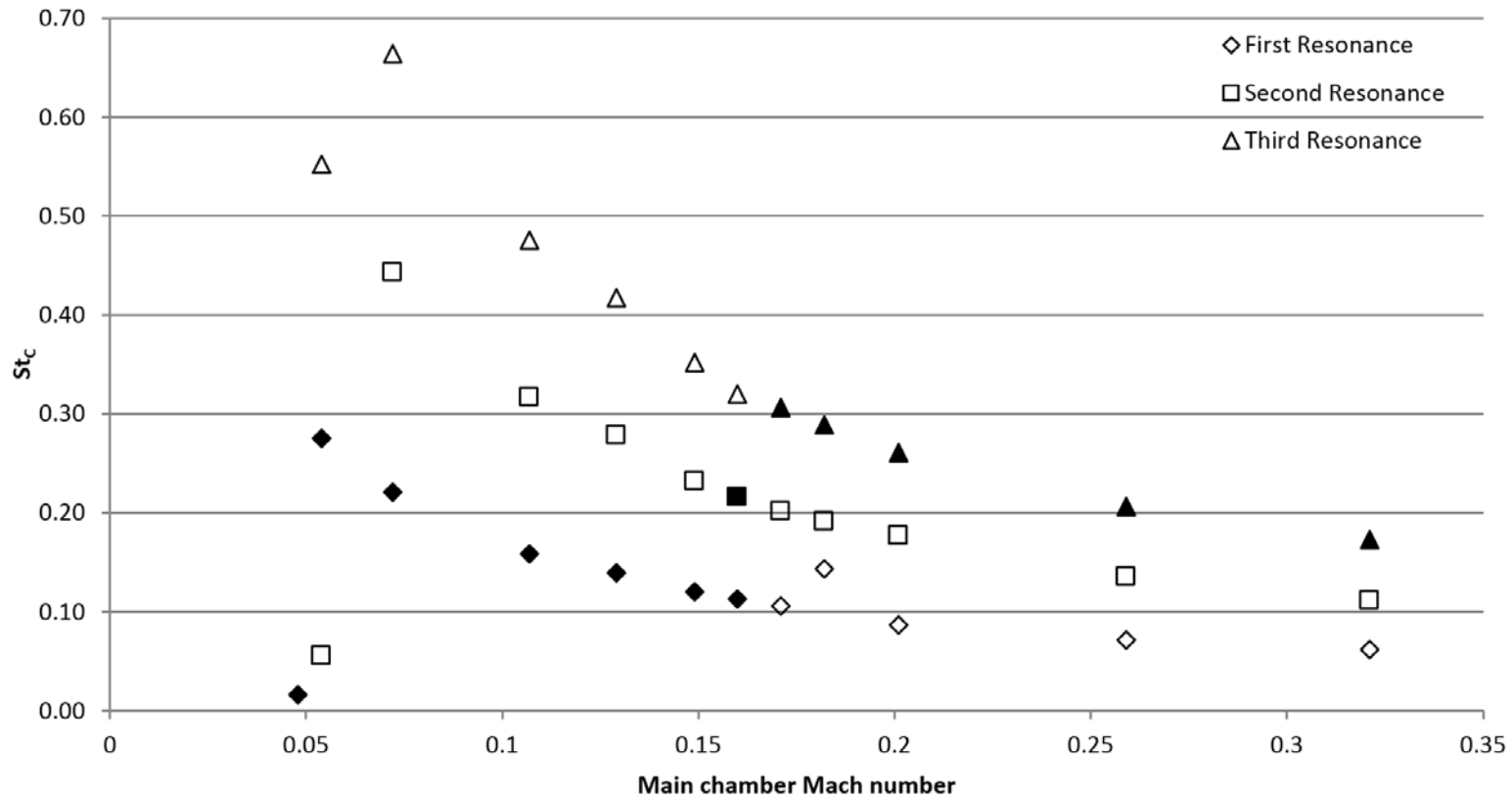
- **Each line represents a resonant frequency**
- **Filled in dots correspond to dominant frequency**

Study 1: Varying Mass Flow Rates
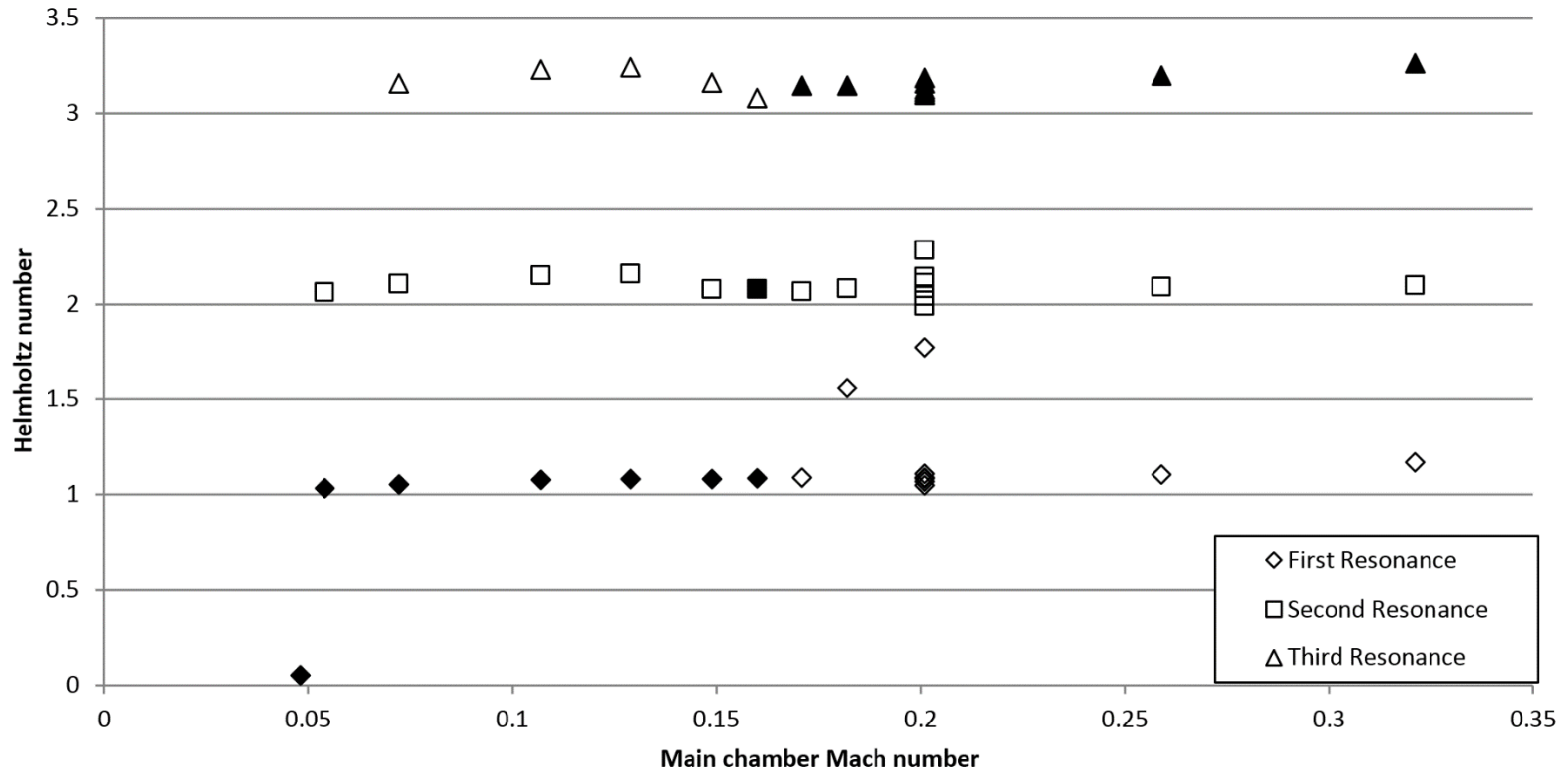
- **FFC inlet is functioning as Helmholtz resonator**
- **Changes in mode driven by main chamber flow rate**

Study 4: 3D

- Same conditions and geometry as baseline case, extended to 3D
- 9M cell case which matched experimental setup
- Also performed case with periodic walls
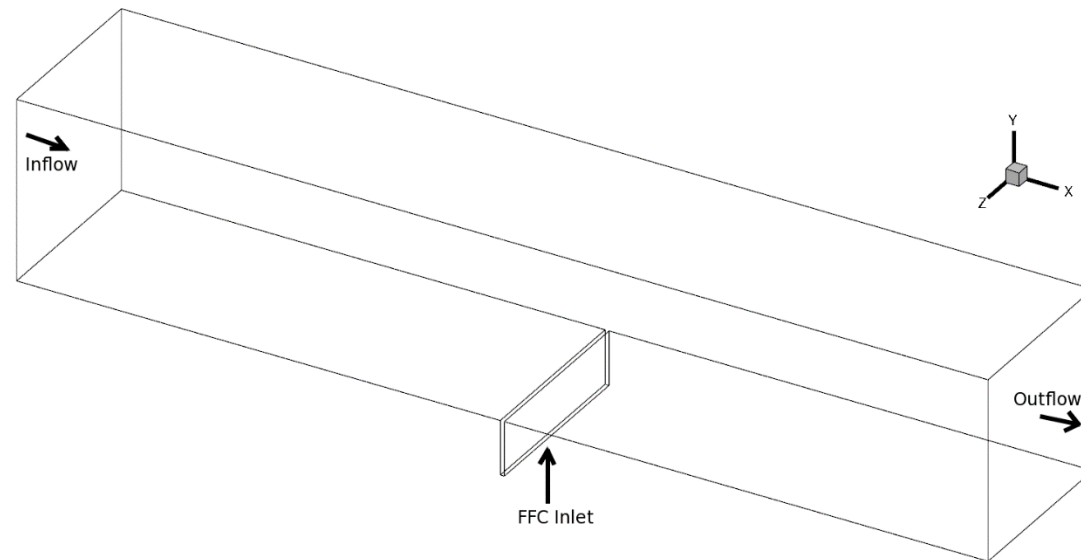
Study 4: 3D

3D Case					
FFC Velocity (m/s)	3.1	Main Velocity	224	Main Mach	0.19
FFC Density (kg/m^3)	281	Main Density	4.41	Density Ratio	64
M	1.6E-02	J	5.6E-04	Slot width (m)	5.59E-04

Study 4: 3D with Walls
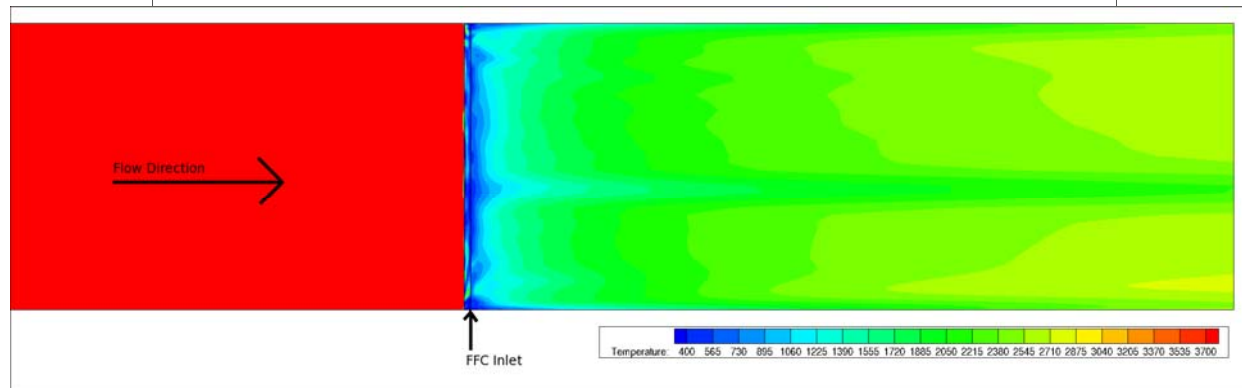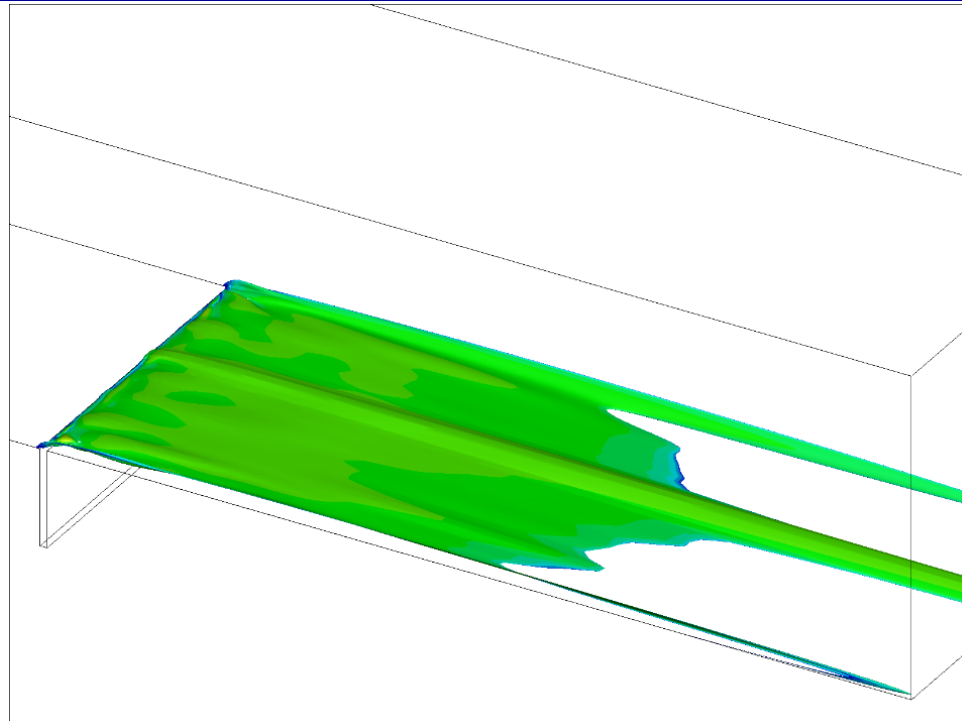
Flow Direction →

FFC Inlet

Temperature: 400 565 730 895 1060 1225 1390 1555 1720 1885 2050 2215 2380 2545 2710 2875 3040 3205 3370 3535 3700
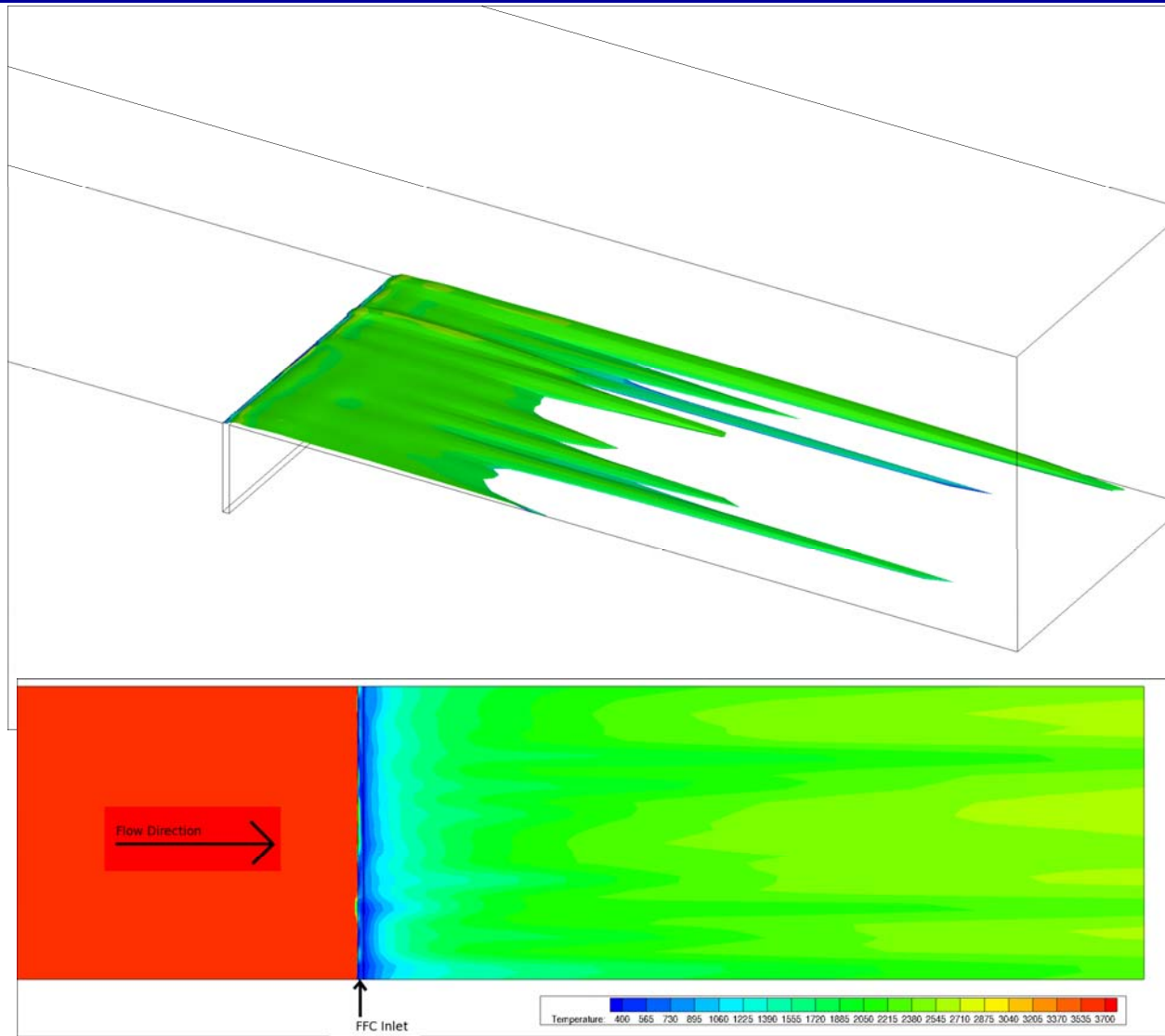
Study 4: 3D Periodic
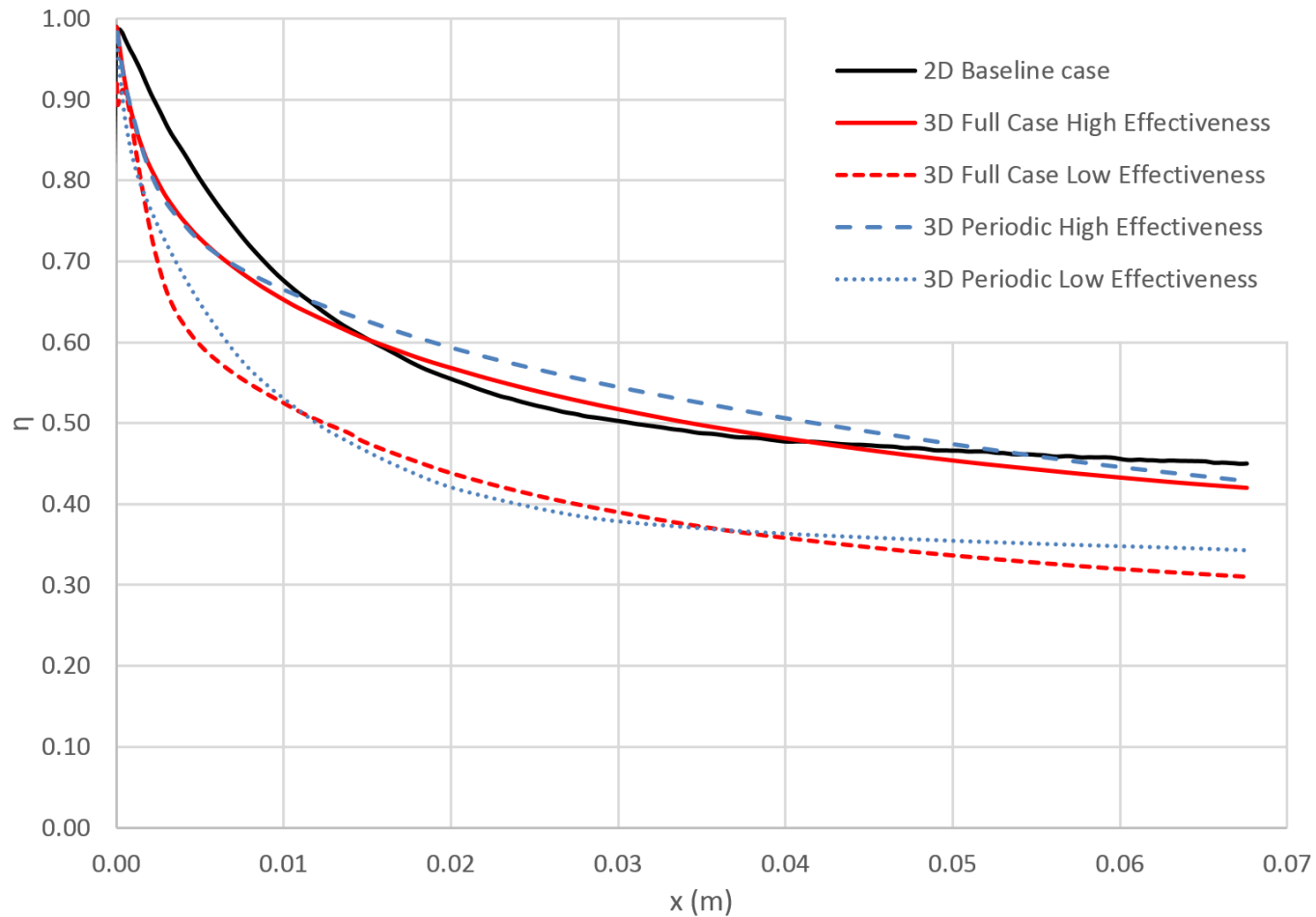
Study 4: 3D

Study 4: 3D

- 3D simulation introduces a rich mix of oscillatory modes rather than just the longitudinal mode observed in 2D

- Periodic wall case tests if transverse modes disappear in infinitely long inlet (they do)

- Helmholtz resonation reappears in periodic case, but much weaker than 2D results

Baseline case

With periodic walls
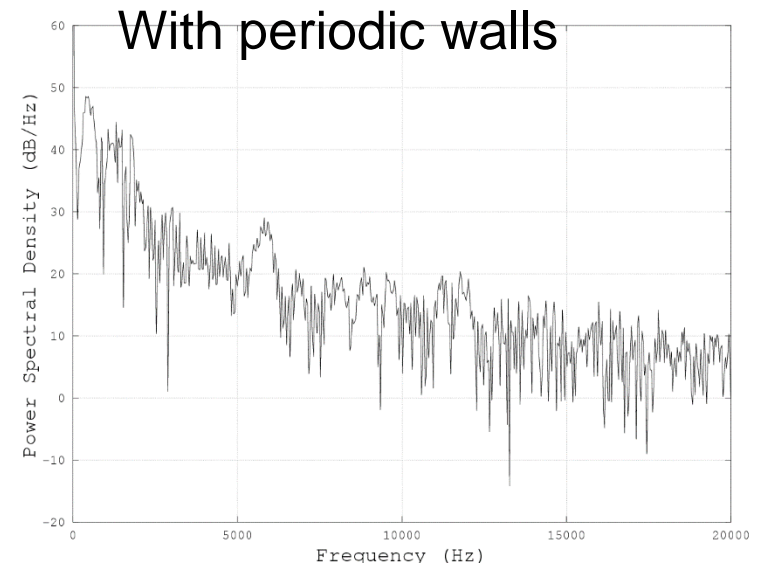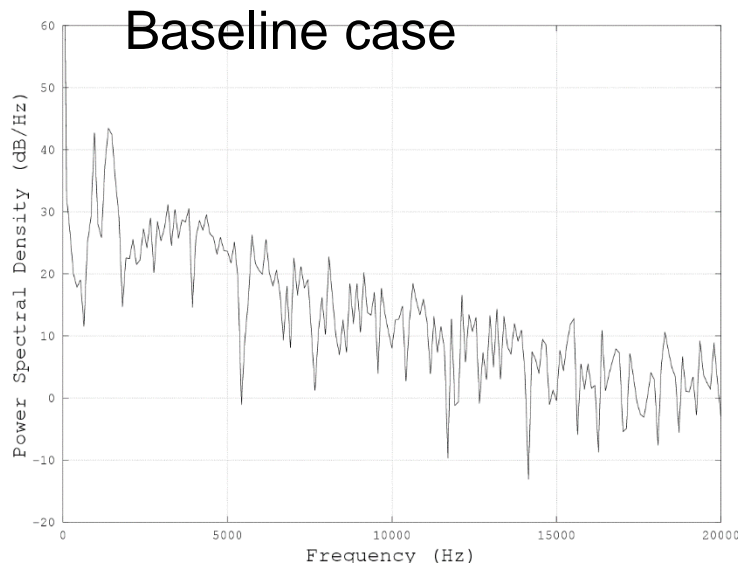
Study 5: Varying Inlet shape

- **Vary Inlet geometry to test impact on film cooling effectiveness**
- **Three different geometries are used:**
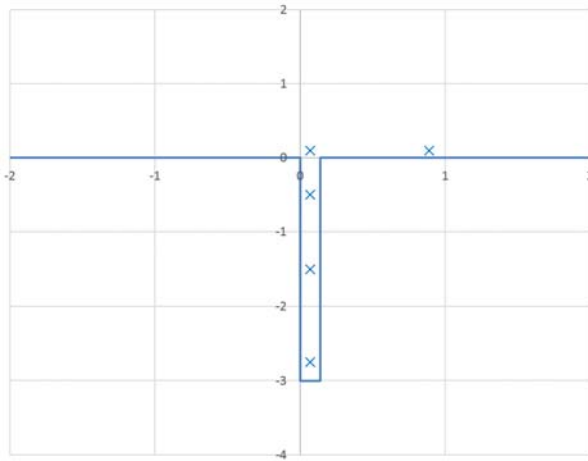
Thin Slot
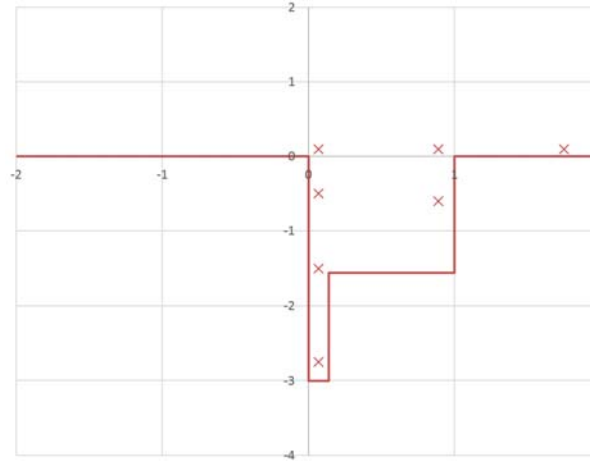
Wide Slot
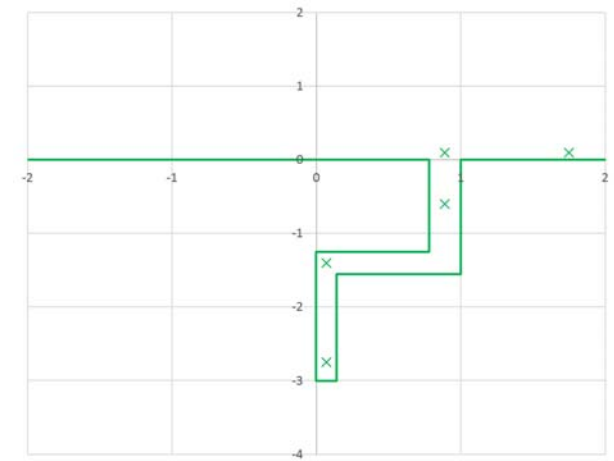
Bent Slot

Study 5: Varying inlet shape

Varying Inlet Geometry				
FFC Velocity (m/s)	3.5	Main Velocity	230	Main Mach	0.199
FFC Density (kg/m^3)	285	Main Density	4.41	Density Ratio	65
M	1.6E-02	J	2.50E-04	Slot width (m)	3.6E-04 - 2.5E-03

Study 5: Varying Inlet shape
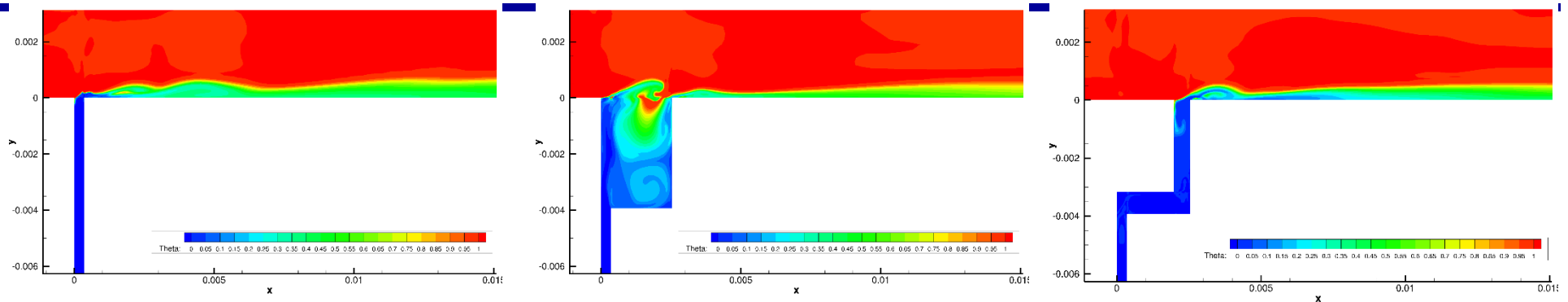
All cases are unsteady, but with very low frequency of oscillation.

↑ Temperature ↑

↓ Adiabatic effectiveness ↓
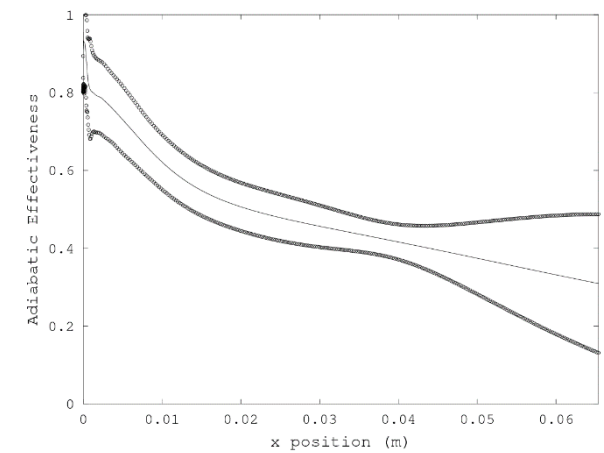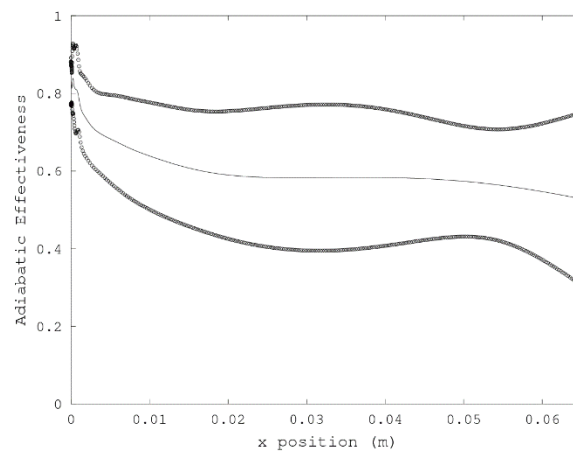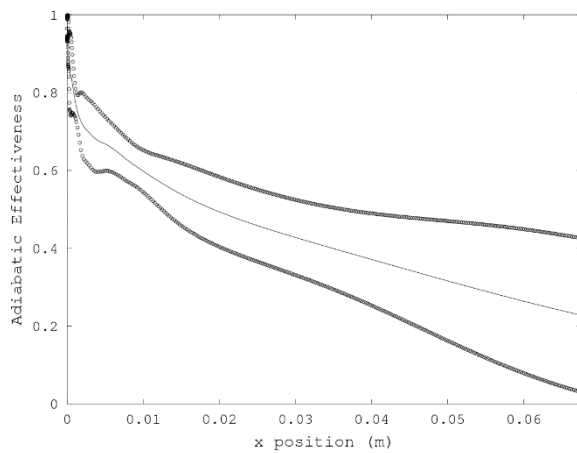
Study 5: Varying Inlet shape

- **No strong, high frequency oscillations in either FFC inlet or fuel film**
  - Thin slot results consistent with thinnest slot in study .
  - Unsteadiness in wide slot driven by recirculation.
  - Bent slot has low frequency resonance before first bend.
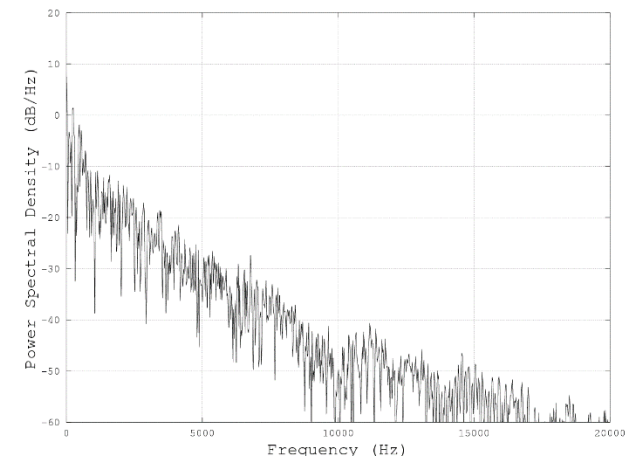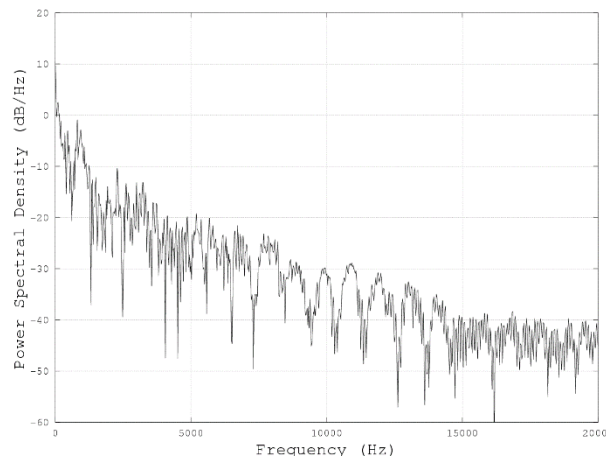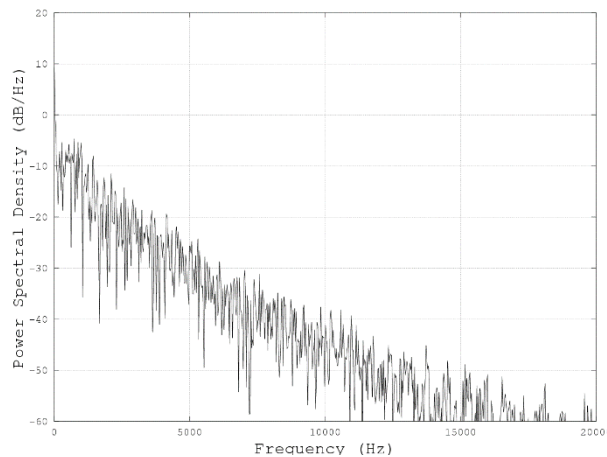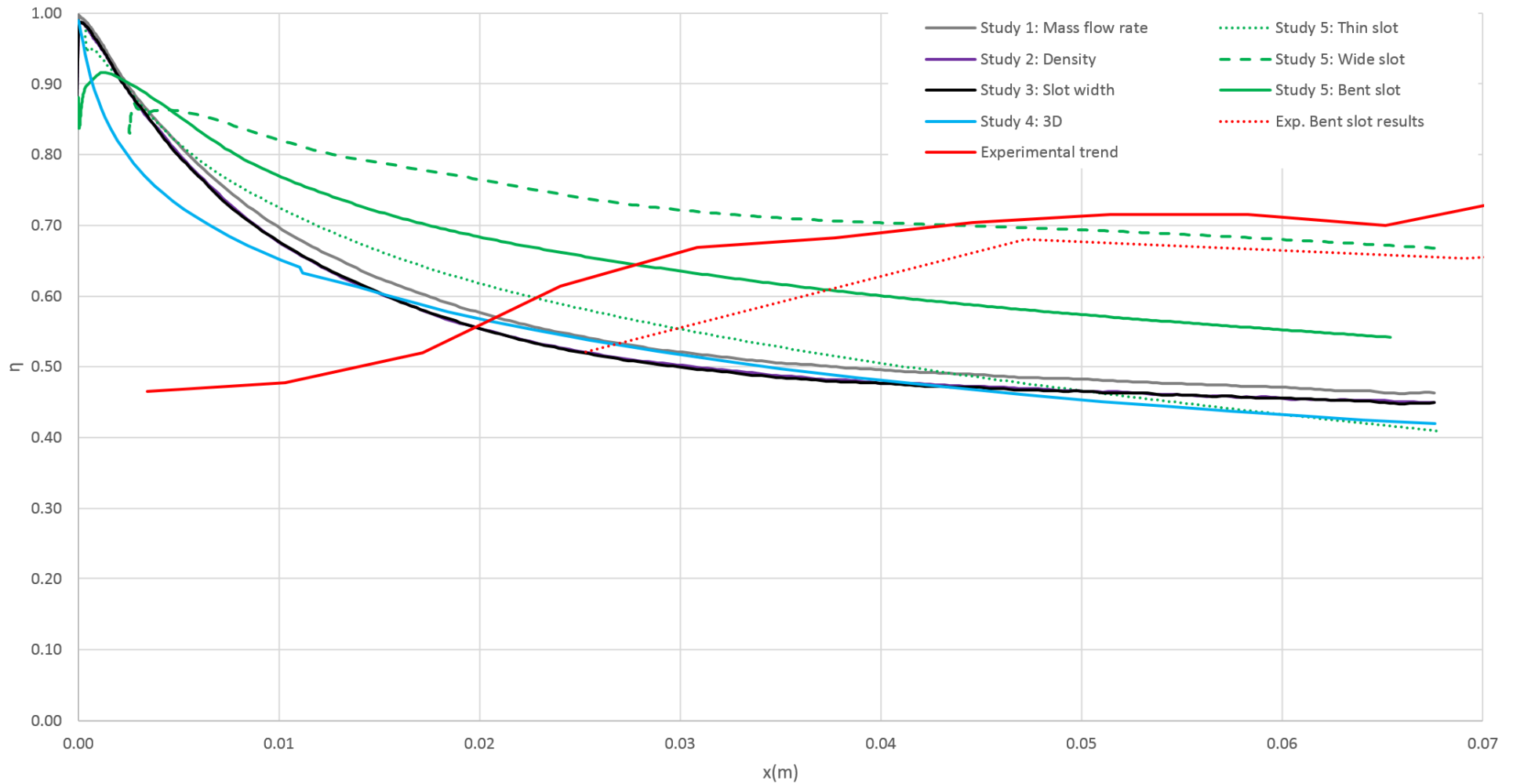
Comparison with experiments
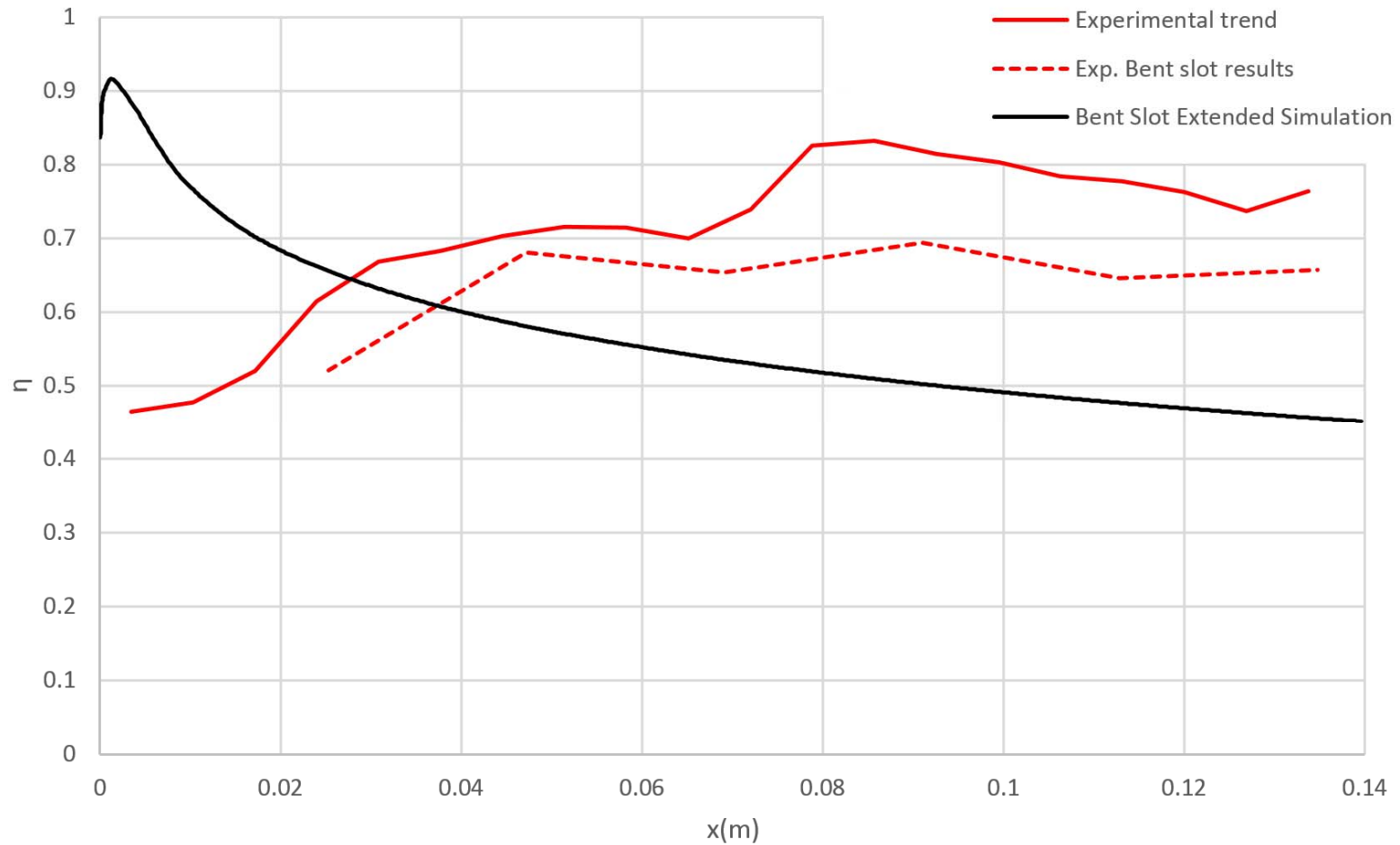
Conclusions

- **FFC effectiveness appears to be linked to mass flow ratio**
  - Momentum ratio and slot width are not correlated
- **Fuel density has small effect on frequency, wall temperatures**
- **Most cases tested had unsteady fuel films**
  - Unsteadiness is determined by inlet geometry and main chamber mass flow rate
- **3D effects not fully captured by 2D**
  - May still capture effects in wide/circumferential inlets
- **Inlet shape has large impact on fuel film profile and effectiveness**
- **Future work aims to better capture experimental trends**

Future Work

- **Fluid mechanics do not appear to be the cause of difference between CFD models and experiments. Need to include other elements:**
  - **Radiative heat transfer model**
  - **Soot formation/deposition models**
  - **Better modeling of FFC inlet**
  - **More expansive 3D study**
  - **Real gas equation of state**